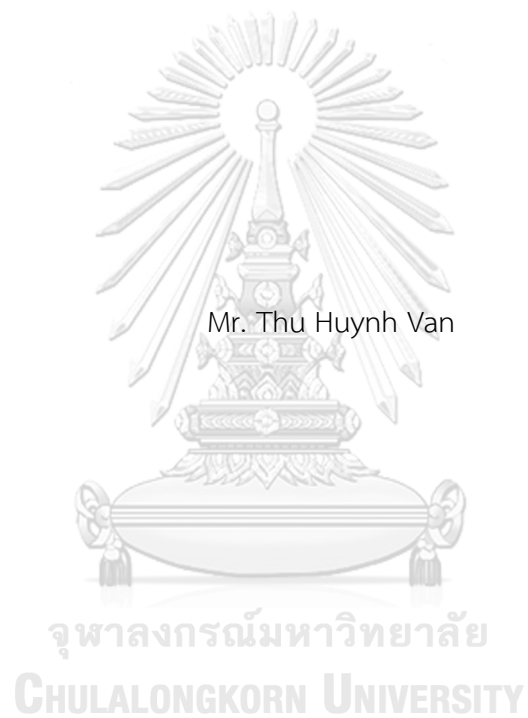


ANALYSIS AND OPTIMUM DESIGN OF COLD-FORMED STEEL ARCH STRUCTURES



A Thesis Submitted in Partial Fulfillment of the Requirements
for the Degree of Master of Engineering in Civil Engineering

Department of Civil Engineering

Faculty of Engineering

Chulalongkorn University

Academic Year 2018

Copyright of Chulalongkorn University

การวิเคราะห์และออกแบบอย่างเหมาะสมที่สุดของโครงสร้างโค้งเหล็กขึ้นรูปเย็น



วิทยานิพนธ์นี้เป็นส่วนหนึ่งของการศึกษาตามหลักสูตรปริญญาวิศวกรรมศาสตรมหาบัณฑิต

สาขาวิชาวิศวกรรมโยธา ภาควิชาวิศวกรรมโยธา

คณะวิศวกรรมศาสตร์ จุฬาลงกรณ์มหาวิทยาลัย

ปีการศึกษา 2561

ลิขสิทธิ์ของจุฬาลงกรณ์มหาวิทยาลัย

Thesis Title ANALYSIS AND OPTIMUM DESIGN OF COLD-FORMED
STEEL ARCH STRUCTURES
By Mr. {Thu Huynh Van
Field of Study Civil Engineering
Thesis Advisor Sawekchai Tangaramvong, Ph.D.

Accepted by the Faculty of Engineering, Chulalongkorn University in Partial
Fulfillment of the Requirement for the Master of Engineering

..... Dean of the Faculty of Engineering
(Professor Supot Teachavorasinskun, D.Eng.)

THESIS COMMITTEE

..... Chairman
(Associate Professor Akhrawat Lenwari)

..... Thesis Advisor
(Sawekchai Tangaramvong, Ph.D.)

..... External Examiner
(Professor Thaksin Thepchatri)

จุฬาลงกรณ์มหาวิทยาลัย
CHULALONGKORN UNIVERSITY

ทู ฮีน แวน : การวิเคราะห์และออกแบบอย่างเหมาะสมที่สุดของโครงสร้างโค้งเหล็กขึ้นรูปเย็น. (ANALYSIS AND OPTIMUM DESIGN OF COLD-FORMED STEEL ARCH STRUCTURES) อ.ที่ปรึกษาหลัก : เสวกชัย ตั้งอร่ามวงศ์

-



สาขาวิชา วิศวกรรมโยธา

ปีการศึกษา 2561

ลายมือชื่อนิสิต

ลายมือชื่อ อ.ที่ปรึกษาหลัก

5970477421 : MAJOR CIVIL ENGINEERING

KEYWORD: Evolutionary structural optimization, Application programming interface, Particle swarm optimization, Visual Basic Application

Thu Huynh Van : ANALYSIS AND OPTIMUM DESIGN OF COLD-FORMED STEEL ARCH STRUCTURES. Advisor: Sawekchai Tangaramvong, Ph.D.

This research presents the development of a unified framework for cold-formed steel warehouse design at variations of clear roof spans. The work involves the advanced finite element analyses of nonlinear arch-shape warehouse structures, namely one that considers 2nd-order nonlinear geometry effects-sufficiently accurate approximation of large deformation responses. An optimum design procedure of 3D arch steel warehouse structures is conducted with the help of a novel algorithm, called mixed ESO-PSO approach. The generic idea is based on the implementation of a well-known evolutionary structural optimization algorithm (ESO), and further integrates a mapping, underpinning particle swarm optimization (PSO), technique of design variables to the closest upper or lower integer numbers listed in the available steel sections. In essence, the use of ESO algorithm during the preliminary design provides good initial points by eliminating those ineffective or even infeasible design domains, and hence reduces the sizes of discrete variable entries prior to performing the PSO searches in the final step. The objective function is to minimize suitable arch geometry that yields minimum cold-formed steel hollow sections employed specifically in warehouse applications. Both ultimate strength and serviceability criteria of designed structures comply with AISC-LRFD and AISI-LRFD specifications. The algorithm and various constraints were coded within a Microsoft Visual Basic environment

Field of Study: Civil Engineering

Student's Signature

Academic Year: 2018

Advisor's Signature

ACKNOWLEDGEMENTS

First of all, I would like to express my deepest gratitude to my advisor, Doctor Sawekchai Tangaramvong, for his invaluable advice. In addition to his great academic contribution, his positive personalities exceptionally inspire my life as well as my future academic. I could not finish my study without his strong support.

My profound thanks and gratitude go to all committee members for giving constructive comments.

I thank my friends for their continuous motivation and inspiration.

My grateful thanks to all administrative staffs working at the International School of Engineering and the Department of Civil Engineering for their helpfulness and kind facilitation. I honestly thank Chulalongkorn University for offering the scholarship for my Master's degree. I also acknowledge all scholarship coordinators, assisting and encouraging me during my study.

Thu Huynh Van

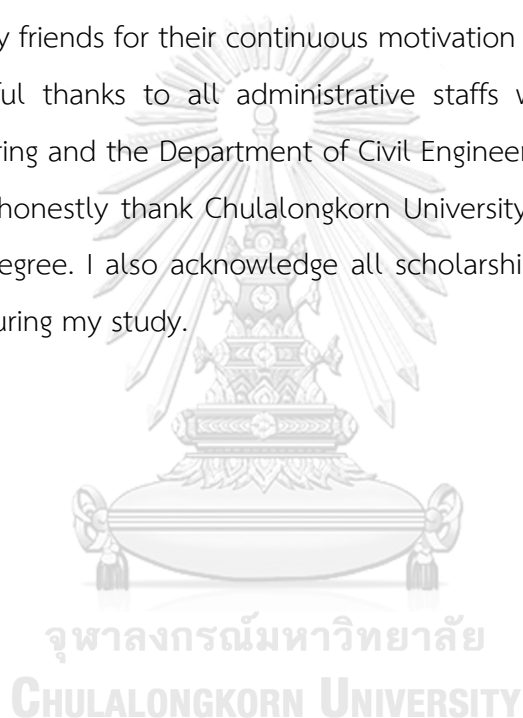


TABLE OF CONTENTS

	Page
ABSTRACT (THAI)	iii
ABSTRACT (ENGLISH)	iv
ACKNOWLEDGEMENTS	v
TABLE OF CONTENTS	vi
LIST OF FIGURES	1
LIST OF TABLES	4
CHAPTER 1 INTRODUCTION	5
1.1 Background	5
1.2 Research Objective	9
1.3 Scope of Research	9
1.4 Methodology	10
CHAPTER 2 LITERATURE REVIEW	11
2.1 Steel Warehouse	11
2.2 Arches	11
2.2.1 Application of Arch Structures	11
2.2.2 Configuration of Arch	12
2.3 Finite Element Method Reviews	12
2.3.1 General	12
2.3.2 Stiffness Analysis Method	13
2.3.3 Influences of Second-Order Geometry Effects	18
2.4 Structural Optimization	20

2.4.1 Overview of Structural Optimization Problems.....	20
2.4.2 Structural Optimization Methods for Steel Frame Problems	21
2.4.2.1 Deterministic Techniques for Steel Frame Optimization Problems.....	21
2.4.2.2 Stochastic Search Methods	23
2.4.3 Application of Optimum Steel Structures	24
2.4.3.1 Application of Meta-Heuristic Algorithms for Steel Frame Design	25
2.4.3.2 Application of PSO Algorithms for Steel Frame Design.....	26
CHAPTER 3 STATE FORMULATIONS AND OPTIMIZATION PROBLEMS.....	29
3.1 Finite Element Modelling	29
3.1.1 Finite Element Type and Discretization	29
3.1.2 Boundary Conditions.....	30
3.1.3 Dimensions and Configuration of Arch Warehouse Structures.....	31
3.1.4 Finite Element Analysis.....	32
3.1.5 Material Properties and Profiles.....	32
3.1.6 Loading Conditions.....	33
3.1.6.1 Dead Load.....	33
3.1.6.2 Live Load.....	33
3.1.6.3 Wind Load.....	33
3.1.6.4 Crane Load.....	36
3.1.6.5 Combination Loads.....	39
3.2 Advanced Analysis of 3D Steel Arch Structures.....	40
3.3 Formulation of the Optimum Design Problem	41

3.3.1 Design Variables	41
3.3.2 Objective Function	41
3.3.3 Constraints.....	42
3.3.3.1 Strength Constraints.....	42
3.3.3.2 Serviceability Constraints	43
CHAPTER 4 SOLUTION ALGORITHM	44
4.1 Evolutionary Structural Optimization (ESO).....	44
4.1.1 Algorithm Overview	44
4.1.2 Basic of Evolutionary Optimization Algorithm	45
4.1.2.1 Uniform Scaling and Critical Scale Factor	45
4.1.2.2 Element Sensitivity Number for Resizing.....	45
4.1.2.3 Termination Criteria.....	50
4.1.3 Procedure of ESO algorithm	50
4.1.4 Test on BenchMark Steel Frame	53
4.1.4.1 Optimization of two-bay, three storey Steel Framed Structure....	54
4.1.4.2 Optimization of one-bay, ten-storey steel frame.....	58
4.1.5 Concluding Remarks.....	64
4.2 Particle Swarm Optimization (PSO).....	65
4.2.1 Algorithm Overview	65
4.2.2 Basic of Particle Swarm Optimization.....	66
4.2.2.1 Mathematical Formulation of PSO Algorithm.....	66
4.2.2.2 Initial Swarm	66
4.2.2.3 Inertial Weight Update.....	67
4.2.2.4 Design Variable Bounds Handling.....	68

4.2.2.5 Main PSO Parameters	68
4.2.2.6 Constraint Handling Techniques.....	69
4.2.2.7 Termination Criteria.....	69
4.2.3 Strategy in PSO for Tackling Discrete Structural Optimization Problems..	70
4.2.4 Pseudo Code of PSO algorithm	71
4.2.5 BenchMark Test Function.....	73
4.3 A Mixed ESO-PSO Approach for Optimum Design.....	75
4.3.1 The procedure of the Mixed ESO-PSO Approach	75
4.3.2 Test on BenchMark Steel Frame	76
CHAPTER 5 OPTIMUM DESIGN OF COLD-FORMED STEEL ARCH WAREHOUSE STRUCTURES	81
5.1 Optimization Scheme of Arch Steel Warehouse Structures.....	81
5.2 Optimization Results and Discussion	82
CHAPTER 6 CONCLUSIONS AND FUTURE RESEARCH	90
6.1 Conclusions	90
6.2 Future Researchs.....	91
REFERENCES	92
VITA.....	98

LIST OF FIGURES

Fig . 1.1 Cost breakdown of structural steel.....	5
Fig . 1.2 PEB clear span.....	6
Fig . 1.3 PEB arched clear span.....	6
Fig . 1.4 The simple arch warehouse structures (Pacific Pipe Public CoMPany Limited).....	7
Fig . 2.1 Sydney Harbor Bridge (503 m, year of completion 1932), Sydney.	11
Fig . 2.2 Urban Loritz Platz (130 m, year of completion 2000) , Vienna, Austria.....	12
Fig . 2.3 The Uniform Distribution of Bending Moments (Kostina, 2017).....	12
Fig . 2.4 Motion of beam-column element based on the Updated Lagrangian formualtion (Conci, 1992)	14
Fig . 2.5 Force and displacement components of a beam-column element (Yang & Kuo, 1994)	15
Fig . 2.6 Behavior of Beam with Rigid Body Motion (a) Initial Forces $\{^1f\}$ at C_1 , (b) Initial Forces $\{^1f\}$ at C_2 , (c) Forces Generated by $[k_g]$, (d) Final Forces $\{^2f\}$ at C_2 (Yang & Chiou, 1987).....	17
Fig . 2.7 Predictions of structural analyses (White & Hajjar, 1991).....	19
Fig . 2.8 Second-order P- δ and P- Δ moment (Ziemian, 2010).	19
Fig . 2.9 Three main categories of structural optimization problems.....	20
Fig . 2.10 A few important motivations for choosing a suitable algorithm.....	21
Fig . 3.1 Straigth-Beam Approximation (Yang, Kuo, & Yau, 1991).....	29
Fig . 3.2 The meshed line element model of arch structures	30
Fig . 3.3 The restraint conditions in the major direction of arch frame	30
Fig . 3.4 The restraint conditions in the minor direction of arch frame	31

Fig . 3.5 The entire configuration of long-spanned arch warehouse.	31
Fig . 3.6 The typical dimensions of a crane bridge	36
Fig . 3.7 Plane view of a crane aisle (MBMA 2012)	36
Fig . 3.8 The influence line due to the movement of crane on runway beam	37
Fig . 3.9 The crane loading conditions (MBMA-2012)	38
Fig . 3.10 Deflection limit ratios for structures under horizontal load according to AISC.....	40
Fig . 4.1 The Qatar National Convention Centre (http://www.amlak.com.qa).....	44
Fig . 4.2 Flowchart of the ESO algorithm (continued).....	53
Fig . 4.3 Two-bay, three storey planar steel frame (Degertekin, 2008).....	54
Fig . 4.4 Optimum design coMParison for two-bay, three storey steel frame	56
Fig . 4.5 Convergence history of two-bay three-storey frame design (Case 1)	56
Fig . 4.6 Stress ratio for members of two-bay three storey frame (Case 1).....	57
Fig . 4.7 Convergence history of two-bay three-storey frame design (Case 2)	57
Fig . 4.8 Stress ratio for members of two-bay three storey frame (Case 2).....	57
Fig . 4.9 Convergence history of two-bay three-storey frame design (Case 3)	58
Fig . 4.10 Stress ratio for members of two-bay three storey frame (Case 3)	58
Fig . 4.11 One-bay ten-storey frame (Degertekin, 2008)	59
Fig . 4.12 Optimum design coMParison for one bay, ten-storey steel frame.....	62
Fig . 4.13 Convergence history of one-bay ten-storey frame design	63
Fig . 4.14 stress ratio for members of one-bay ten storey frame.....	64
Fig . 4.15 Interstorey drift for one-bay ten-storey frame.....	64
Fig . 4.16 PSO position and velocity update (Perez & Behdinan, 2007).....	66
Fig . 4.17 Flowchart of PSO algorithm	72

Fig . 4.18 Rosenbrock function.....	73
Fig . 4.19 Convergence history of Rosenbrock function using the PSO algorithm	74
Fig . 4.20 Flowchart of the mixed ESO-PSO approach.....	75
Fig . 4.21 Two-bay, three storey planar steel frame (Degertekin, 2008)	76
Fig . 4.22 Optimum design coMParison for the two-bay, three-storey steel frame.....	78
Fig . 4.23 Convergence history of two-bay three-storey frame design (Case 1)	78
Fig . 4.24 Stress ratio for members of two-bay three storey frame (Case 1)	79
Fig . 4.25 Convergence history of two-bay three-storey frame design (Case 2)	79
Fig . 4.26 Stress ratio for members of two-bay three storey frame (Case 2)	80
Fig . 5.1 Optimization scheme of arch steel warehouse structures.....	81
Fig . 5.2 The main components of optimum design arch warehouse structures.....	82
Fig . 5.3 Convergence history with a 20-m span	83
Fig . 5.4 Stress ratio for members with a 20-m span.....	84
Fig . 5.5 Material distributed over an arch warehouse structure with a 20-m span....	84
Fig . 5.6 Convergence history of arch warehouse structure with a 25-m span.....	85
Fig . 5.7 Stress ratio for members with a 25-m span.....	86
Fig . 5.8 Material distributed over an arch warehouse structure with a 25-m span	86
Fig . 5.9 Convergence history of arch steel warehouse with a 30-m span.....	87
Fig . 5.10 Stress ratio for members with a 30-m span	88
Fig . 5.11 Material distributed over an arch warehouse structure with a 30-m span...	88

LIST OF TABLES

Table 2.1 Timeline of main meta-heuristic algorithms (Gandomi et al., 2013).....	24
Table 3.1 Material properties.....	32
Table 3.2 Parameters of velocity pressure.....	34
Table 3.3 Parameters of crane bridge (16Tons)	36
Table 3.4 Load combinations for strength conditions (Thompson, 2007).....	39
Table 3.5 Load combinations for serviceability conditions	39
Table 4.1 Optimization results obtained for the two-bay, three storey steel frame...	55
Table 4.2 Optimization results obtained for the one-bay, ten-storey steel frame	60
Table 4.3 Main PSO parameters	68
Table 4.4 Results of the objective function value	74
Table 4.5 Optimization results obtained for the two-bay, three storey steel frame...	77
Table 5.1 Optimum sections obtained for arch warehouse structure with a 20-m span.....	83
Table 5.2 Optimum sections obtained for arch warehouse structure with a 25-m span.....	85
Table 5.3 Optimum sections obtained for arch steel warehouse with a 30-m span...	87

CHAPTER 1

INTRODUCTION

1.1 Background

Economical design of industrial buildings normally depends on selections of steel sections with respect to material cost. In addition, a simple configuration of structures accounts for large percentages in the total construction cost relating to fabrication cost and erection cost as shown in Figure 1.1. Therefore, a simple structure not only gives the lowest material but also gives an economical solution in terms of fabrication and erection cost.

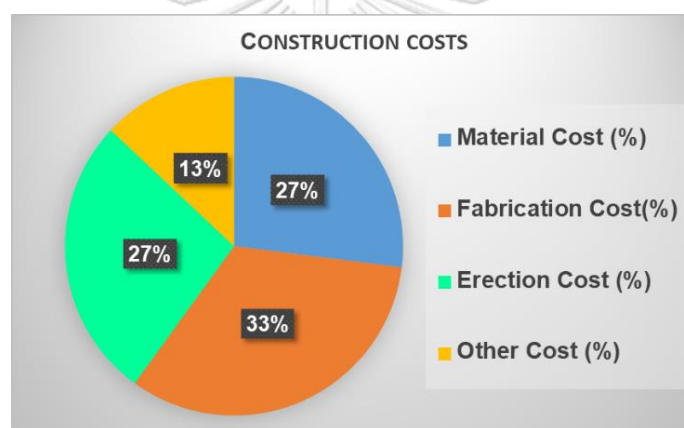


Fig . 1.1 Cost breakdown of structural steel.

In recent years, steel frames are popularly used in industrial buildings. Pre-Engineered Building (PEB) is one of a typical solution in the construction market. Base on the advantage of PEB, clear long span of PEB can reach up to 100 m. In addition, PEB fulfills this requirement along with reduced time and cost. Figures 1.2 and 1.3 show PEB clear span and PEB arched clear span popularly using in the industrial buildings. They are often composed of hot-rolled steel sections, or alternatively can be constructed from cold-formed steel sections.



Fig . 1.2 PEB clear span



Fig . 1.3 PEB arched clear span.

In the past, arches are less used. However, arches should not be underestimated because they are good alternatives to achieve very long span (Farreyre & Journot, 2005). Moreover, from an aesthetical point of view, arches are thin and slender structures and provide economical solutions for crossing large spans and carry higher loads for a given volume of material when properly shaped compared with other long-span building.

Nowadays, the use of cold-formed steel members for low-rise building construction have been a popular form of construction. In Australia and the UK more than 70% of all steel building construction is expected to be cold-formed in the near future (Phan, Lim, Tanyimboh, & Sha, 2017). Compared to hot-rolled steel sections,

cold-formed members are often more economical and efficient, due to inherent advantages such as lightweight, ease and speed of erection and a greater flexibility in manufacturing cross-sectional profiles and sizes. The utilization of cold-formed steel sections furnishes green structures demanding less material and cost while providing high strength. However, the drawbacks of cold-formed members are easy to buckling before the stresses reach to yield stress due to their relatively thin steel walls. This leads to failure of the whole structures. Normally, the application of cold-formed sections include channel-sections are used for the column and rafter members, and Z-sections are used for purlins and side rails. In the current construction market, besides using Z and C sections, hollow steel sections have also become common in the application of structural design. There are several reasons which had led to this and one of the most significant is the excellent mechanical properties of hollow members. Hollow sections have high bending and torsional rigidity compared to their weight and they are suitable for compressed members.

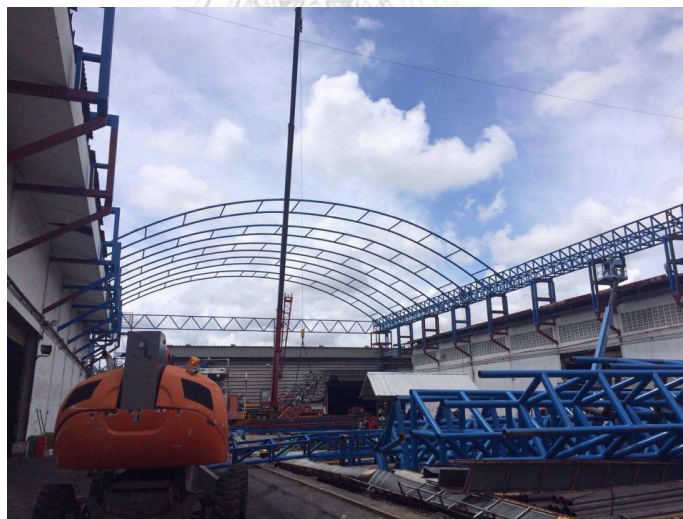


Fig . 1.4 The simple arch warehouse structures (Pacific Pipe Public CoMPany Limited).

Over the past years, optimum designs of steel frames is a challenging task for structural designers. Generally, the main objective in design optimization of frame structures is to achieve the lowest weight or cost of structures, since material consumption is one of the most important factors influencing on the construction costs. The standard formulation is set to contain an objective function under the

constraints describing intrinsic structural behavior with some design criteria. Traditionally, various mathematical programming methods and optimality criteria methods of deterministic techniques have been applied for structural design optimizations. However, most mathematical optimization applications are suited for continuous design variables. While almost structural optimization problems as well as in the optimum design steel frames are non-smooth and non-convex optimization problems which can not be efficiently solved by using deterministic methods. The recent developments of meta-heuristic algorithms in the stochastic search techniques of numerical optimization problems have been used as an innovative tendency to obtain the optimum solution by using special strategies. The main idea behind these techniques is to simulate natural phenomena, such as survival of the fittest, immune system, swarm intelligence and the musical performance process into a numerical algorithm (Saka & Geem, 2013). These methods became suitable and effective to handle the solution of discrete structural optimization problems and more attractive than the deterministic methods. However, the drawbacks of meta-heuristic algorithms are approximate and non-deterministic, they do not guarantee for (leaving alone global one) optimum solution in views of the intrinsic non-convex and non-smooth optimization problems. Numerous alternative meta-heuristic techniques have employed for solving the optimization of steel frames, some of the well-known methods being a genetic algorithm (GA) (Pezeshk, Camp, & Chen, 2000), ant colony optimization (ACO) (C. V. Camp, Bichon, & Stovall, 2005), harmony search (HS) algorithm (Degertekin, 2008), teaching learning-based optimization (TLBO) (Toğan, 2012), particle swarm optimization (PSO) (Doğan & Saka, 2012), charge system search (A Kaveh & Talatahari, 2012), cuckoo search (CS) algorithm (A Kaveh & Bakhshpoori, 2013), firefly algorithm (FFA) (Carbas, 2016), search group algorithm (SGA) (Carraro, Lopez, & Miguel, 2017), a school-based optimization (SBO) (Farshchin, Maniat, Camp, & Pezeshk, 2018).

Based on the above-mentioned background, this study proposes the development of a unified design framework for simple arch steel warehouse having variations of span length between 20 to 30 m, bay length of 6 m, eave height of 8 m. The work involves the advanced analyses of non-linear arch-shape warehouse

structures and the optimum design is performed with a series of cold-formed steel hollow sections, namely circular hollow steel (CHS), rectangular hollow steel (RHS) and square hollow steel (SHS). The aim of work is to minimize the total weight of material distribution over an arch steel warehouse structure.

1.2 Research Objective

The three main objectives are:

- (1) To perform nonlinear finite element analyses of arch steel warehouse structures under applied forces. Namely, second-order nonlinear geometry effects-sufficiently accurate approximation of large deformation responses are considered.
- (2) To furnish an efficient algorithm solution for structural design optimization.
- (3) To implement the optimum design with cold-formed hollow steel members complying with AISI S100-2016 & ANSI/AISC 360-16 specifications. The main objective is to optimize suitable arch geometry that yields minimum steel hollow sections employed specifically in warehouse applications.

1.3 Scope of Research

- (1) The designs comply with American Institute of Steel Construction (AISC-LRFD) 360-16, American Iron and Steel Institute (AISI-LRFD) S100-16 specifications for structural steel buildings.
- (2) The design loads and load combinations comply with Metal Building Systems Manual (MBMA-2012) that based on Minimum Design Loads for Buildings and Other Structures ASCE 07-10 specification.
- (3) The 3D advanced analysis of steel arch structures assumes elastic material with second-order nonlinear geometry effects.
- (4) The effects of residual stress and initial crookedness are ignored.
- (5) The whole arched roof is fully laterally braced.
- (6) The effects of shearing and torsion deformations are minimal and can be negligible.

1.4 Methodology

For modeling of 3D steel arch warehouse structures, the entire curvature of arches is broken down into a number of straight-line elements. Non-linear advanced analyses are directly performed in SAP2000 under applied forces. Namely, one that considers 2nd-order nonlinear geometry effects—efficiently accurate approximation of large deformations responses. Material assumes elastic with non-linear analyses.

A novel algorithm called mixed ESO-PSO approach is proposed. The generic idea is based on the implementation of well-known evolutionary structural optimization (ESO), and further integrates a mapping, underpinning particle swarm optimization (PSO). The algorithm is tested on several well-known benchmark problems. The results were compared to those of some well-known meta-heuristics which successfully solved benchmarks highlighted efficiency and accuracy of the discrete optimization problems in practical steel structure applications.

An optimum procedure of 3D arch warehouse steel structures is conducted with a range of span length between 20-30 m, bay length of 6 m and eave height of 8 m. The aim of work is to minimize the total weight of material distributed over an arch steel warehouse structure considering simultaneously ultimate strength and serviceability conditions complying with AISC-LRFD and AISI-LRFD specifications under the load combinations. The mixed ESO-PSO algorithm and various constraints are coded directly using a post-processing Microsoft Visual Basic Application environment, whilst the respond of a structure with assigned specific cold-formed steel hollow sections is computed using a commercial analysis software (SAP2000). The transparent interface between the two computer programming environment is enabled through a so-called Open Application Programming Interface (OAPI). The optimum procedure is automatically performed as an iterative process and incorporated advanced analysis, namely large (i.e., second-order nonlinear geometry) deformations are considered. The optimum procedure terminates when the minimum cross-sections are obtained without violating its given constraints.

CHAPTER 2

LITERATURE REVIEW

2.1 Steel Warehouse

Warehouses are used for industrial purposes to furnish an adequate environment to store farming, equipment, and products that require protection from environmental factors. When designing a warehouse, many factors should be taken into accounts such as the storing capacity of the required materials and the lifting capacity of the related trucks and trailers.

The reasonable design of warehouses can provide economic benefits of construction costs at the beginning and later on. There are many structural solutions in the construction market. The current warehouses have been design popularly using steel structures such as CSB (Conventional Steel Building) and PEB (Pre-Engineering Building). The components are designed by adopting hot-rolled steel or cold-formed steel with various shapes.

2.2 Arches

2.2.1 Application of Arch Structures

Nowadays, the applications of arch structures are widely used in many kinds of architectures. Arch structures have been used for different purposes such as complex roofing, vaults, shops, exhibition halls, airports, hangars and bridge. The examples of typical long-span arch structures are shown in Figures 2.1-2.2.



Fig . 2.1 Sydney Harbor Bridge (503 m, year of completion 1932), Sydney.



Fig . 2.2 Urban Loritz Platz (130 m, year of completion 2000) , Vienna, Austria.

2.2.2 Configuration of Arch

It is obvious from Figure 2.3 that the arch configurations of span (l) and rise arch (f) are usually determined through the technological and architectural requirements for three hinged, two hinged and fixed supports (Kostina, 2017).

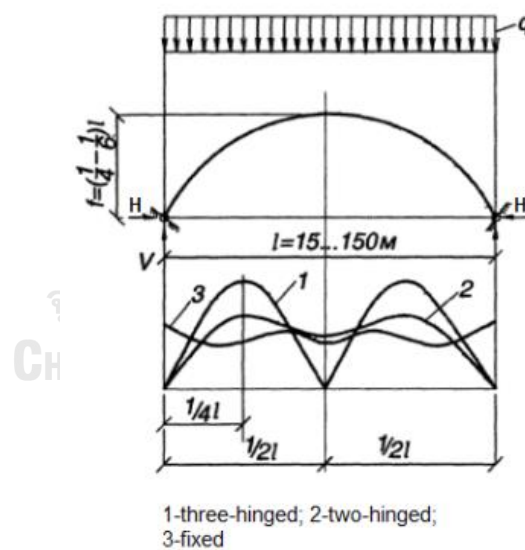


Fig . 2.3 The Uniform Distribution of Bending Moments (Kostina, 2017).

2.3 Finite Element Method Reviews

2.3.1 General

Almost all modern forms of structural analysis are typically variants of the matrix stiffness approach describing the response of the structure. Conventionally, two

approaches used in an incremental nonlinear finite element analysis are the updated Lagrangian (UL) and total Lagrangian (TL) formulations. When consistently developed, the two formulations yield identical global stiffness matrices and nodal point force vectors. Both the TL and UL formulations were reviewed by (Bathe, Ramm, & Wilson, 1975). Bathe and Bolourchi (1979) found the UL formulation to be computationally more effective when the geometric nonlinear stiffness matrix is evaluated by numerical integration.

Use of three-dimensional nonlinear analysis in the design of steel structures requires a stiffness method formulation of the analysis that has a rigorous base, has been developed along logical, clearly discernible lines, and is suitable for practice. To satisfy this need, the result is an elastic and a geometric stiffness matrix for use in an updated Lagrangian nonlinear elastic analysis (Al-Bermani & Kitipornchai, 1990; Conci, 1992; Yang & McGuire, 1986), presented a comprehensive formulation of the thin-walled beam element starting from the principle virtual displacements to analyze large deflection and buckling behavior of three-dimensional thin-walled frames.

2.3.2 Stiffness Analysis Method

A stiffness matrix for the analysis of thin-walled beam-column element is derived. Starting from the principle of virtual displacements, an updated Lagrangian procedure for nonlinear analysis is developed. In a finite element approach employing the principle of virtual displacements, they can only be included through a rigorous account of the virtual work done by nodal forces. The nonlinear deformation behavior of a solid body can be described by three typical configurations, the initial undeformed configuration C_0 , the last calculated configuration C_1 and the current unknown configuration C_2 . All three configurations in Figure 2.4 are assumed to be in equilibrium with the updated Lagrangian formulation, the equilibrium of a solid body at the C_2 configuration (at time $t+\Delta t$) can be expressed with reference to the C_1 configuration (at time t), according to Yang and McGuire (1986) and Yang and Kuo (1994).

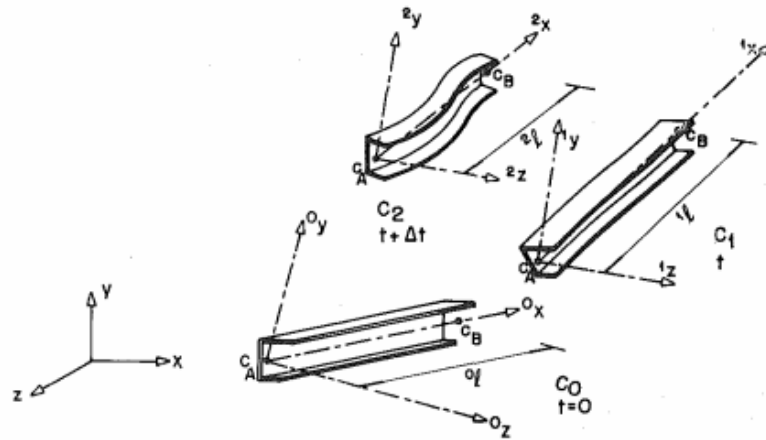


Fig . 2.4 Motion of beam-column element based on the Updated Lagrangian formulation (Conci, 1992)

Using the updated Lagrangian formulation, all variables are referred to the configuration C_1 at time t , and then linearized, yielding (Bathe & Bolourchi, 1979).

$$\int_{1V} {}^1C_{ijkl} e_{kl} \delta_1 e_{ij} {}^1dV + \int_{1V} {}^1\tau_{ij} \delta_1 \eta_{ij} {}^1dV = {}^2R - {}^1R \quad (1)$$

Or the virtual work equation of equilibrium can be written for the element at the deformed configuration C_2 , but with reference to C_1 (Yang & Kuo, 1994; Yang, Yau, & Leu, 2003) as follows:

$$\delta U + \delta V = {}^2R - {}^1R \quad (2)$$

In which ${}^2R = \int_{1S} {}^2t_i \delta u_i {}^1dS$; ${}^1R = \int_{1S} {}^1t_i \delta e_{ij} {}^1dS$; δ denotes the variational operator, C_{ijkl} represents the components of the constitutive tensor; ${}^1\tau_{ij}$ denotes the Cauchy stresses tensor existing at C_1 ; e_{ij} the linear components of the updated Green-Lagrange strains increments; 1t_i and 2t_i the surface tractions, acting on the body at C_1 and C_2 , respectively; u_i the displacement components; η_{ij} the nonlinear components of the corresponding strain increment; strain energy (δU) is the linear components, potential energy (δV) is the nonlinear components and 1V and 1S denote the volume and surface area respectively of the body at C_1 .

The incremental virtual work for three dimensional beam is expressed by Eq. (3).

$$\delta U + \delta V = \{\delta u\}^T \left(\{ {}^2f \} - \{ {}^1f \} \right) \quad (3)$$

Equation (3) consists of three translations and three rotations at each node. Correspondingly, the nodal forces $\{^1f\}$ and $\{^2f\}$ acting on the element at C_1 and C_2 are those depicted in Figure 2.5.

$$\begin{aligned} \{^1f\}^T &= \{^1F_{xa} \ ^1F_{ya} \ ^1F_{za} \ ^1M_{xa} \ ^1M_{ya} \ ^1M_{za} \ ^1F_{xb} \ ^1F_{yb} \ ^1F_{zb} \ ^1M_{xb} \ ^1M_{yb} \ ^1M_{zb}\} \\ \{^2f\}^T &= \{^2F_{xa} \ ^2F_{ya} \ ^2F_{za} \ ^2M_{xa} \ ^2M_{ya} \ ^2M_{za} \ ^2F_{xb} \ ^2F_{yb} \ ^2F_{zb} \ ^2M_{xb} \ ^2M_{yb} \ ^2M_{zb}\} \end{aligned} \quad (4)$$

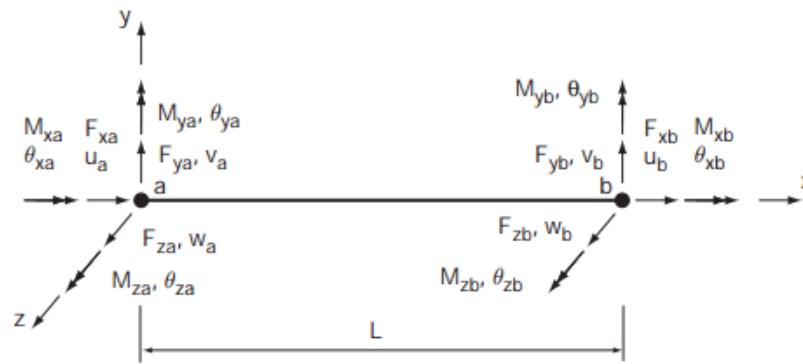


Fig . 2.5 Force and displacement components of a beam-column element (Yang & Kuo, 1994)

The displacement vector $\{u\}$ for the three-dimensional beam is defined as

$$\{u^T\} = \{u_a \ v_a \ w_a \ \theta_{xa} \ \theta_{ya} \ \theta_{za} \ u_b \ v_b \ w_b \ \theta_{xb} \ \theta_{yb} \ \theta_{zb}\} \quad (5)$$

In a displacement-based finite element should be related to those at the element nodes by interpolation functions including the axial displacement u and the angle of twist θ are interpolated by linear functions and the transverse displacements v and w by cubic functions, both of them remain an exact solution to the linear differential equations of three-dimensional solid beam free of any distributed loads.

The elastic stiffness matrix $[k_e]$ for 3D frame element can be derived from strain energy (δU) of the element (Yang & Kuo, 1994), with a matrix dimension of 12x12 as follows:

$$[k_e] = \begin{bmatrix} [k_1] & [k_2] \\ [k_2]^T & [k_3] \end{bmatrix} \quad (6)$$

Where:

$$[k_1] = \begin{bmatrix} \frac{EA}{L} & 0 & 0 & 0 & 0 & 0 \\ 0 & \frac{12EI_z}{L^3} & 0 & 0 & 0 & \frac{6EI_z}{L^2} \\ 0 & 0 & \frac{12EI_y}{L^3} & 0 & \frac{-6EI_y}{L^2} & 0 \\ 0 & 0 & 0 & \frac{GJ}{L} & 0 & 0 \\ 0 & 0 & \frac{-6EI_y}{L^2} & 0 & \frac{4EI_y}{L} & 0 \\ 0 & \frac{6EI_z}{L^2} & 0 & 0 & 0 & \frac{4EI_z}{L} \end{bmatrix}$$

$$[k_2] = \begin{bmatrix} -\frac{EA}{L} & 0 & 0 & 0 & 0 & 0 \\ 0 & \frac{-12EI_z}{L^3} & 0 & 0 & 0 & \frac{6EI_z}{L^2} \\ 0 & 0 & \frac{-12EI_y}{L^3} & 0 & \frac{-6EI_y}{L^2} & 0 \\ 0 & 0 & 0 & -\frac{GJ}{L} & 0 & 0 \\ 0 & 0 & \frac{6EI_y}{L^2} & 0 & \frac{2EI_y}{L} & 0 \\ 0 & \frac{-6EI_z}{L^2} & 0 & 0 & 0 & \frac{2EI_z}{L} \end{bmatrix}$$

$$[k_3] = \begin{bmatrix} \frac{EA}{L} & 0 & 0 & 0 & 0 & 0 \\ 0 & \frac{12EI_z}{L^3} & 0 & 0 & 0 & -\frac{6EI_z}{L^2} \\ 0 & 0 & \frac{12EI_y}{L^3} & 0 & \frac{6EI_y}{L^2} & 0 \\ 0 & 0 & 0 & \frac{GJ}{L} & 0 & 0 \\ 0 & 0 & \frac{6EI_y}{L^2} & 0 & \frac{4EI_y}{L} & 0 \\ 0 & \frac{-6EI_z}{L^2} & 0 & 0 & 0 & \frac{4EI_z}{L} \end{bmatrix}$$

In order to derive the geometric stiffness matrix $[k_g]$ for the space frame element, we shall relate all forces. Based on the conditions of equilibrium at the current configuration, such relations can be expressed as Figure 2.6.

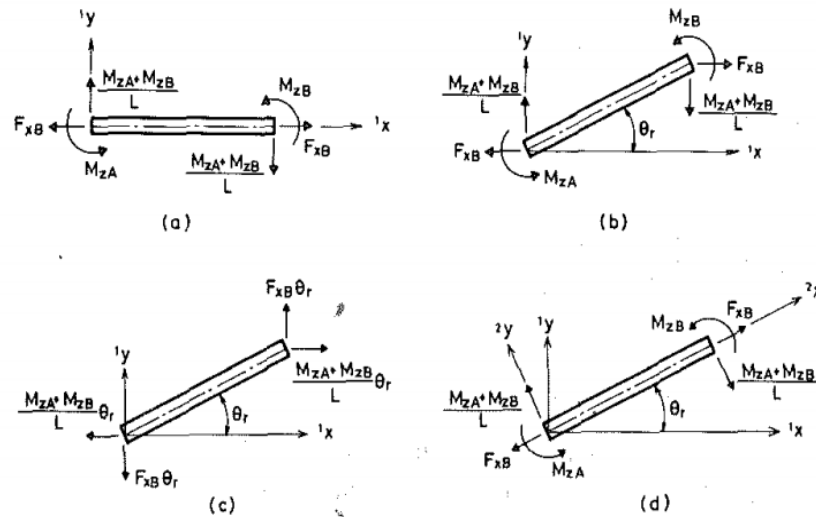


Fig . 2.6 Behavior of Beam with Rigid Body Motion (a) Initial Forces $\{^1f\}$ at C_1 , (b) Initial Forces $\{^1f\}$ at C_2 , (c) Forces Generated by $[k_g]$, (d) Final Forces $\{^2f\}$ at C_2 (Yang & Chiou, 1987)

The geometric stiffness matrix $[k_g]$ that is derived from the potential energy (δV).

$$[k_g] = \begin{bmatrix} 0 & a & c & 0 & 0 & 0 & 0 & -a & -c & 0 & 0 & 0 \\ a & b & d & g & -h & -a & -b & 0 & l & -g & -h & 0 \\ c & 0 & b & e & h & g & -c & 0 & -b & m & h & -g \\ 0 & d & e & f & i & k & 0 & -d & -e & -f & -i & -k \\ 0 & g & h & i & j & 0 & 0 & -g & -h & -i & n & -p \\ 0 & -h & g & k & 0 & j & 0 & h & -g & -k & p & n \\ 0 & -a & -c & 0 & 0 & 0 & 0 & a & c & 0 & 0 & 0 \\ -a & -b & 0 & -d & -g & h & a & b & 0 & -l & g & h \\ -c & 0 & -b & -e & -h & -g & c & 0 & b & -m & -h & g \\ 0 & l & m & -f & -i & -k & 0 & -l & -m & f & a & c \\ 0 & -g & h & -i & n & p & 0 & g & -h & a & j & 0 \\ 0 & -h & -g & -k & -p & n & 0 & h & g & c & 0 & j \end{bmatrix} \quad (7)$$

Where

$$\left\{ \begin{array}{l} a = \frac{{}^1M_{za} + {}^1M_{zb}}{L^2}, b = \frac{6{}^1F_{xb}}{5L}, c = -\frac{{}^1M_{ya} + {}^1M_{yb}}{L^2}, d = \frac{{}^1M_{ya}}{L}, e = \frac{{}^1M_{za}}{L}, f = \frac{{}^1F_{xb}J}{AL}, g = \frac{{}^1M_{xb}}{L} \\ h = \frac{{}^1F_{xb}}{10}, i = \frac{{}^1M_{za} + {}^1M_{zb}}{6}, j = \frac{2{}^1F_{xb}L}{15}, k = -\frac{{}^1M_{ya} + {}^1M_{yb}}{6}, l = \frac{{}^1M_{yb}}{L}, m = \frac{{}^1M_{zb}}{L}, n = \frac{-{}^1F_{xb}L}{30} \\ p = -\frac{{}^1M_{xb}}{2} \end{array} \right.$$

The stiffness equation can be rewritten for the three dimensional frames by combining Eqs. (4), (5), (6) and (7) as follows:

$$\begin{aligned} \delta U + \delta V &= \{\delta u\}^T \left(\{ {}^2 f \} - \{ {}^1 f \} \right) \\ [k_e] \{u\} + [k_g] \{u\} &= \{ {}^2 f \} - \{ {}^1 f \} \end{aligned} \quad (8)$$

2.3.3 Influences of Second-Order Geometry Effects

Linear structural analysis is not actual behavior of structures. When deformations are large and the structure behaves nonlinearly, the stiffness of structure changes even though the material has shown a linear elastic behavior. Therefore, the second-order nonlinear geometry effects should be considered as illustrated in Figure 2.7.

The nonlinear elastic analysis causes the deformation of the structure, resulting in additional moments while the material remains linear. Because the effects of loading are taken into account and the equilibrium is formulated on the deformed geometry, the load-deflection behavior becomes nonlinear (King, 1990). Namely, this type of analysis includes both P- Δ effect (chord rotation) for non-linear elastic analysis and P- δ effect (member curvature) for linear elastic analysis. The P- Δ effect reduces the element flexural stiffness against sidesway. While, the P- δ effect reduces the element flexural stiffness in both sidesway and non-sidesway modes of deformation.

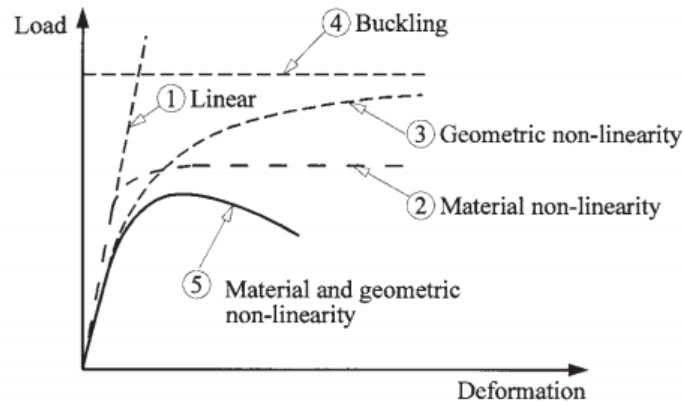


Fig . 2.7 Predictions of structural analyses (White & Hajjar, 1991).

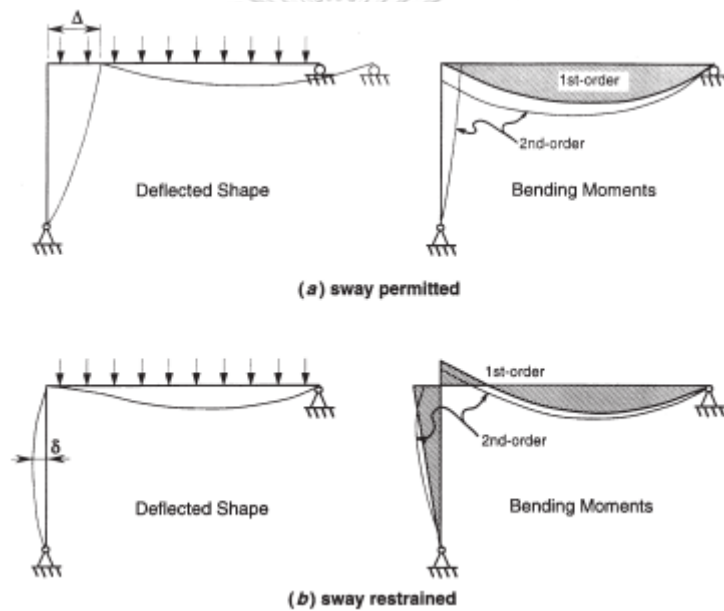


Fig . 2.8 Second-order $P-\delta$ and $P-\Delta$ moment (Ziemian, 2010).

As reported in the textbook written by Ziemian (2010), for the frame in Figure 2.8(a) with sidesways, the additional moments are due primarily to the $P-\Delta$ effect, where Δ is the lateral drift of the frame and P is the total vertical load that translates through Δ . For the frame in Figure 2.8(b) with preventing sidesways, the additional moment in the column is equal to the column load P times the deflection δ . There is a reduction in the negative moment at the end of the beam due to the loss in rotational restraint of the column caused by the $P-\delta$ effect.

2.4 Structural Optimization

2.4.1 Overview of Structural Optimization Problems

In the structural optimization problems, the aim is often to minimize some kinds of physical properties of the structures such as to minimize strain energy (equal to maximize global stiffness), minimize deflection of some chosen point and minimize the maximum stress. Other physical properties that can popularly use as optimization objectives are volume, weight and area. In addition, the constraints imposed by the design codes are satisfied under applied loads. A particular structural optimization problem is formulated depending on the objectives of the problem, the constraints and the nature of the design variables which can be mathematically stated as the following standard form.

$$\begin{aligned} &\text{Find} && \mathbf{X} = \{x_1, x_2, \dots, x_n\} \\ &\text{Optimize} && W(\mathbf{X}) \\ &\text{Subject to:} && \begin{cases} g_j(\mathbf{X}) \leq 0 & (j = 1, m) \\ x_i^L \leq x_i \leq x_i^U & (i = 1, n) \end{cases} \end{aligned}$$

Where: $W(\mathbf{X})$ is objective function, $g_j(\mathbf{X})$ is constraint function, x_i^L, x_i^U are lower and upper limits for design variables x_i .

The optimum design of skeletal structures can be divided into three main categories as sizing, shape, and topology optimization as shown in Figures 2.9.

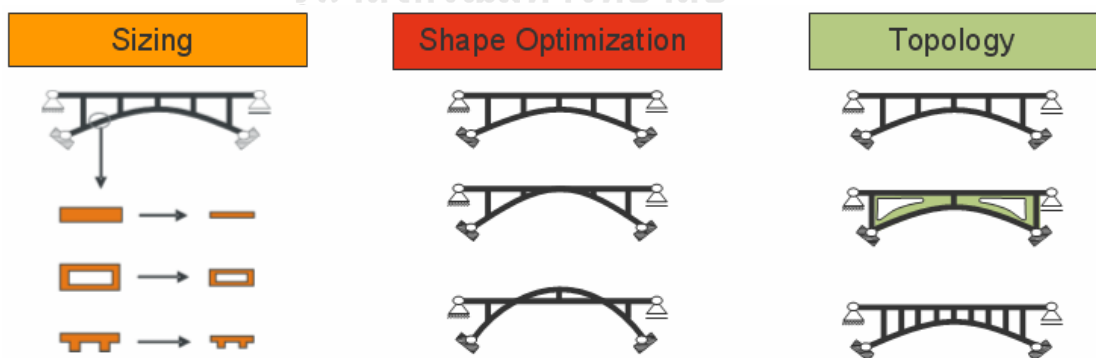


Fig . 2.9 Three main categories of structural optimization problems

In shape optimization, the target is to find the best shape of the structure. In topology optimization, the target is to find the optimum structure by changing the amount and the location of material or components in the structure. While, in sizing

optimization, the cross sectional areas of structural members are considered design variables what can be divided into two subcategories, such as continuous and discrete (O Hasançebi & Azad, 2012). For the continuous sizing optimization, it is usually not the case in practical applications, where structural members should be selected from a set of available sections from manufacturers. Whereas, the discrete optimization problems is the most common case in the practical design of structural optimization. However, the discrete variable space is hardly organized for algorithms to converge to good solutions of steel frame design optimization.

2.4.2 Structural Optimization Methods for Steel Frame Problems

In the optimum design of steel frames, the objective and constraint functions are non-smooth and non-convex optimization problems. Over the past years, many different algorithms for optimization have been developed. Most of these algorithms are based on numerical methods which can be typically classified into two groups including deterministic and stochastic techniques (Saka & Geem, 2013). Unfortunately, the best method has not been known yet, but rather problematic-dependent to specific applications concerned (Tangaramvong & Tin-Loi, 2015). Therefore, to make a decision which algorithm is a suitable solution, a few important criteria are given as displayed in Figure 2.11.



Fig . 2.10 A few important motivations for choosing a suitable algorithm

2.4.2.1 Deterministic Techniques for Steel Frame Optimization Problems

(1) Mathematical Programming Methods for Steel Frame Design Optimization

In the programming methods, the gradient information of the objective function and constraints relating to the design variables is required. In the case of minimization problems, to find the next point until there is no major discrepancy

between the design variable values within two consecutive iterations, they take a step in the negative direction of the gradient of the objective function. There are various mathematical programming methods for solving complicated optimization problems. Several techniques include sequential linear programs, penalty function methods and gradient method. However, when using these techniques to the design real-size practical steel frames, numerical difficulties were met (Saka & Geem, 2013).

(2) Optimality Criteria Methods for Steel Frame Design Optimization

The way solving the optimum design problem of optimality criteria methods is different from that of the mathematical programming methods. While mathematical programming techniques exert to minimize the objective function directly taking into account the constraint conditions, the optimality criteria methods derive a criterion based on intuitive such as fully stressed design or a mathematical statement such as Kuhn-Tucker conditions. The objective function of optimality criteria methods is formulated in form of a Lagrangian function instead of the original one. They then establish an iteration procedure to achieve this criterion. Although optimality criteria methods are not as general as the mathematical programming techniques, they are computationally more efficient. However, in certain cases, they may not converge to the optimum solution (Saka & Geem, 2013).

(3) Concluding Remarks

The deterministic techniques can offer efficient solutions in the optimum design of linear elastic, nonlinear elastic and elastic-plastic frame. Furthermore, they can even be used in the shape optimization and skeleton structures for the cases of the design variables continuous. However, variables in most of the steel frame design problems are to be selected from the list of steel sections which contains discrete values while these methods can only handle problems with continuous design variables. Altering optimality criteria algorithms and mathematical programming algorithms to deal with discrete variables makes the algorithms more complicated and inefficient in the optimum design of large-size steel frames.

2.4.2.2 Stochastic Search Methods

The stochastic search techniques are efficient for achieving the solution of both continuous and discrete optimization problems. The basic idea behind these techniques is to simulate the natural phenomena such as survival of the fittest, immune system, swarm intelligence, and cooling process. These methods are nontraditional stochastic search and they do not require the gradient information or the convexity of the objective function and constraints. In addition, they use probabilistic transition rules, not deterministic rules (Saka & Geem, 2013).

Numerous of researcher have paid much attention on the meta-heuristic search procedures. The meta-heuristic techniques are successfully used in the optimum design steel frames. Ali Kaveh and Ghazaan (2017) reported that some of the well-known methods being a genetic (GA) is inspired by Darwin's theory about biological evolution. Simulated annealing (SA) algorithm utilizes energy minimization that happens in the cooling process of molten metals. Harmony search (HS) algorithm was conceptualized using the musical process of searching for a perfect state of harmony. Charged system search (CSS) uses the electric laws of physics and the Newtonian laws of mechanics to guide the charged particles. Especially, Swarm intelligence (SI) based algorithm is one of the best choices to obtain the optimum solutions by using special strategies. The algorithm based on collective behaviors of animals such as birds, insects, or fishes. The most widely swarm intelligence algorithms are particle swarm optimization (PSO) simulating the social interaction behavior of the birds flocking and fish schooling. Ant colony optimization (ACO) imitates the manner that ant colonies find the shortest route between the food and their nest. Firefly algorithm (FA) is based on the flashing patterns and behaviors of fireflies. Table 2.1 given below is to illustrate the development of different algorithms with respect to their development years (Gandomi, Yang, & Alavi, 2013).

Table 2.1 Timeline of main meta-heuristic algorithms (Gandomi et al., 2013)

Meta-Heuristic Algorithms	2010 - Charge system, Bat Search Algorithm,
	2009 - Cuckoo Algorithm
	2007 - Firefly Algorithm, Improved Harmony Search
	2005 - Bee Colony Algorithm, Glowworm Swarm Optimization
	2001 - Harmony Search
	1995 - Particle Swarm Optimization
	1992 - Ant Colony Optimization
	1989 - Swarm Intelligence
	1986 - Tubu Search, Artificial Immune System
	1983 - Simulated Annealing
	1970 - Genetic Algorithm

According to Saka and Geem (2013), they also have some drawbacks as follows. The first one is that because they do not use mathematical derivations, it is not possible to demonstrate whether the optimum solution they attain is the global optimum or it is near optimum. The second is that they work with random numbers and they have several param needing to be given values by the user. The third drawback is that they need a large number of structural analysis which becomes computationally expensive for the large size steel frames. Therefore, it is difficult to conclude which one of these techniques will become the standard one for the design tools in the finite element packages.

2.4.3 Application of Optimum Steel Structures

Optimization of steel structures is one of the major concerns of structural engineers. The use of modern optimization methods becomes a great opportunity in the area of civil and structural engineering. As above mentioned, one of the judicious choices is meta-heuristic technique along with their various hybrid approaches, they are very suitable and efficient in finding the solution for the optimum design of steel frames.

2.4.3.1 Application of Meta-Heuristic Algorithms for Steel Frame Design

A huge number of studies have been performed by applying meta-heuristic methods to solve the optimum design of steel frames. An extensive review of meta-heuristic techniques employed in developing optimum design algorithms for steel frames in the literature until now.

C. Camp, Pezeshk, and Cao (1998) developed a method for the optimum of rigid plane skeleton structures subjected to multiple loading cases using the genetic algorithm. The design constraints were implemented according to Allowable Stress Design specifications of American Institutes of Steel Construction (AISC-ASD). Pezeshk et al. (2000) also presented a genetic algorithm based optimization procedure for the design of plane frames including geometric nonlinearity.

Degertekin (2008) developed for the optimum design of steel frames in which the objective of the design algorithm is to obtain minimum weight frames by selecting suitable sections from a standard set of steel sections. Oğuzhan Hasançebi, Erdal, and Saka (2009) proposed an adaptive harmony search algorithm for solving optimization problems. The efficiency of the proposed algorithm is numerically investigated using two large-scale steel frameworks that are designed for minimum weight according to the provisions of ASD-AISC specification. Degertekin (2012) developed HS algorithm to decrease the parameter-dependency character. Two improved harmony search algorithms called efficient harmony search algorithm (EHS) and self-adaptive harmony search algorithm (SAHS) are also proposed for sizing optimization of truss structures. Murren and Khandelwal (2014) carried out a design-driven harmony search (DDHS) algorithm for optimization of steel moment frames. Based on the harmony method, DDHS incorporates intelligence in the stochastic search.

C. V. Camp et al. (2005) the work is extended to rigid steel frames. The serviceability and strength constraints are imposed from LRFD-AISC code. A comparison is presented between ant colony optimization frame design and designs obtained using the genetic algorithm. A Kaveh and Shojaee (2007) also used the ant colony optimization algorithm to develop an approach for the discrete optimum

design of steel frames. The design constraints considered consist of combined bending and compression and deflection limitations which are specified according to ASD-AISC design code. A Kaveh and Talatahari (2010) presented an improved ant colony optimization algorithm for the design of steel frames.

A Kaveh and Bakhshpoori (2013) conducted the optimum design of two-dimensional steel frames for discrete variables based on the Cuckoo Search (CS) algorithm is developed. Strength constraints of AISC load and resistance factor design specification and displacement constraints are imposed on frames. A performance comparison is made between CS and other algorithms for some benchmark frames.

In the study by Carbas (2016), the firefly algorithm (FFA) belonging to the swarm intelligence group of meta-heuristics was shown. The optimum design problem of steel space frames is formulated according to LRFD-AISC specification. Two real-world-sized design examples are selected from the literature to examine and compare the numerical performance of the proposed FFA.

Carraro et al. (2017) presented a design procedure employing Search Group Algorithm (SGA) for discrete optimization of planar steel frames. The algorithm is used in a structural optimization problem to obtain minimum weight frames subjected to strength and displacement requirements imposed by AISC-LRFD. Three frame examples from the literature are examined to verify the effectiveness and robustness of the SGA.

In the work by Farshchin et al. (2018), a school-based optimization (SBO) algorithm is applied to the design of steel frames. The objective is to minimize total weight of steel frame subjected to both strength and displacement requirements specified by AISC-LRFD. To investigate the efficiency of SBO algorithm, several popular benchmark frame examples are optimized, and the design data are compared to other optimization methods.

2.4.3.2 Application of PSO Algorithms for Steel Frame Design

In recent years, many attempts have been performed to enhance the computational abilities of the PSO algorithm. Additionally, various hybrid methods are also combined with the primitive PSO algorithm to deal with many structural

optimization problems. The outstanding researches relating to the PSO algorithm in the optimization of structural design are presented in the following paragraphs.

Fourie and Groenwold (2002) applied particle swarm optimizer algorithm to optimal design of structure with sizing and shape variables. Standard size and shape design problems selected from the literature are used to evaluate the performance of the algorithm developed. The performance of the PSO algorithm is compared with that of three gradient based methods, as well as the genetic algorithm.

Schutte and Groenwold (2003) represented a simple approach to accommodate the stress and displacement constraints during initial iterations, when a large number of particles may be infeasible. The application of the PSOA to the optimal sizing design of truss structures is studied.

Venter and Sobieszczanski-Sobieski (2003) applied particle swarm optimization to structural design problems. This paper focused on enhancements to the basic PSO algorithm. These include the introduction of a convergence criterion and dealing with constrained and discrete problems. The basic algorithm is tested on mathematical example problem with both continuous and integer/discrete versions of the cantilevered beam problem.

In the study written by He, Prempan, and Wu (2004), particle swarm optimizer is improved by introducing a fly-back mechanism in order to maintain a feasible population. Furthermore, the proposed algorithm is extended to handle mixed variables using a simple scheme and used to determine the solution of five benchmark problems from the literature that are solved with different optimization techniques. It is reported that the proposed algorithm outperformed better than other techniques.

L. Li, Huang, Liu, and Wu (2007) presented a heuristic particle swarm optimizer for the optimum design of pin jointed steel frames. The algorithm is based on the particle swarm optimizer with passive congregation and harmony search scheme. The method is applied to optimum design of five-planar and spatial truss structures. The results show that proposed improvements accelerate the convergence rate and reach to optimum design quicker than other methods.

Perez and Behdinan (2007) presented particle swarm based optimum design algorithm for pin jointed steel frames. Effect of different setting param and further improvements are studied. Effectiveness of the approach is tested by considering three benchmark trusses from literature as used to evaluate the performance of the algorithm developed. It is reported that the proposed algorithm found better optimum solutions than other optimum design techniques considered in these design problems.

In the research of A Kaveh and Talatahari (2009), a particle swarm optimizer with passive congregation (PSOPC), ant colony optimization (ACO) and harmony search scheme (HS) are combined to reach to an efficient algorithm, called discrete heuristic particle swarm ant colony optimization (DHPSACO). This method is employed to optimize truss structures with discrete variables.

L. Li, Huang, and Liu (2009) applied a heuristic particle swarm optimizer (HPSO) algorithm for truss structures with discrete variables. The algorithm is presented based on the standard particle swarm optimizer (PSO) and the harmony search (HS) scheme. The HPSO is tested on several truss structures with discrete variables. The results show that the HPSO is able to accelerate the convergence rate effectively and has the fastest convergence rate. The research shows the proposed HPSO can be effectively used to solve optimization problems for steel structures with discrete variables.

Doğan and Saka (2012) represented particle swarm based optimum design algorithm for unbraced steel frames. The design constrains are imposed in accordance with LRFD-AISC specification. The design variables are selected from optimum W sections for beams and conlumns of unbraced steel frames such that the design constraints are satisfied.

CHAPTER 3

STATE FORMULATIONS AND OPTIMIZATION PROBLEMS

3.1 Finite Element Modelling

3.1.1 Finite Element Type and Discretization

In the approach, for three-dimensional spatial behavior, straight-beam finite elements that may be used to form chords of arcs of curved members have been formulated by (Bathe & Bolourchi, 1979; Kang & Yoo, 1994).

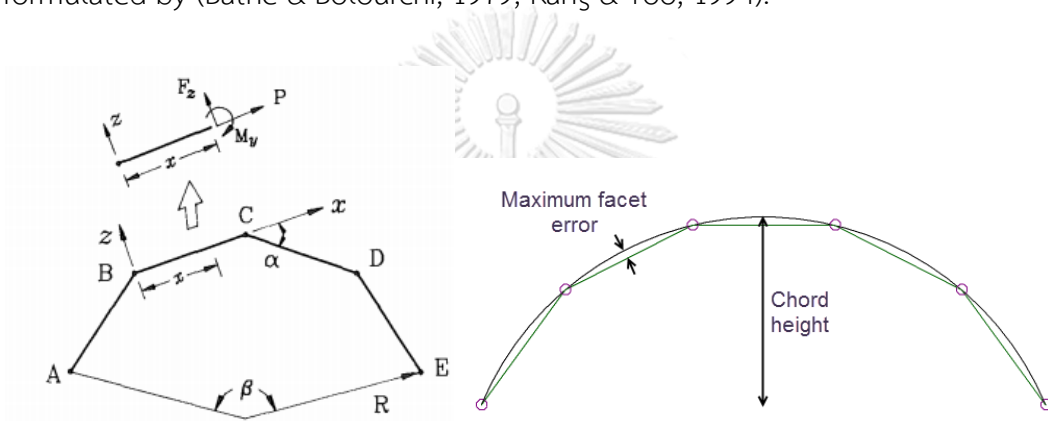


Fig . 3.1 Straighth-Beam Approximation (Yang, Kuo, & Yau, 1991)

In this thesis, the entire curvature of arches is broken down into number of straight-beam finite element or straight-line elements. The line element model is constructed of 2 noded linear elements in space. Specifying a smaller “maximum effect errors” results in a larger number of straight line elements being used. The meshed line element model is shown in Figures 3.1 and 3.2.

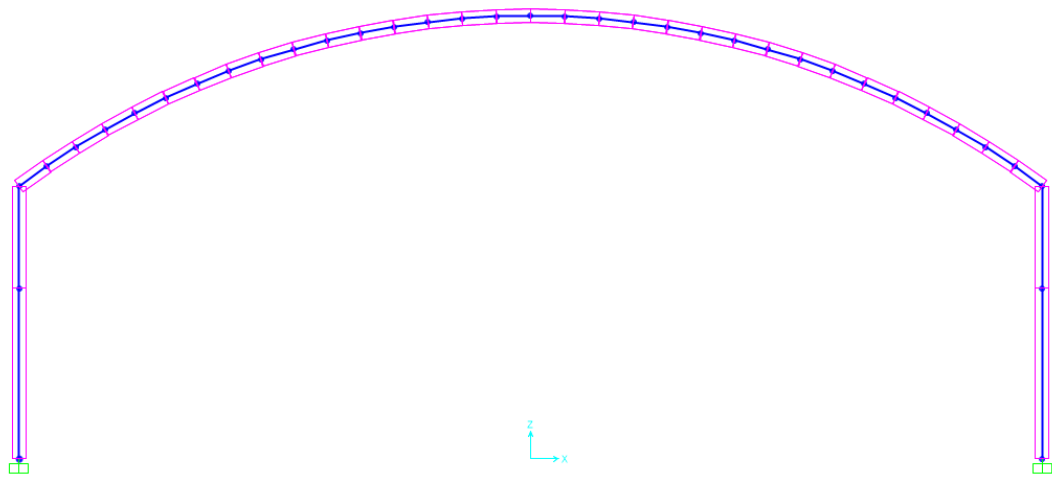


Fig . 3.2 The meshed line element model of arch structures

3.1.2 Boundary Conditions

The major arch frame is supported by fixed supports to reduce the overall bending moment on the main frame. In fact, warehouse building normally uses bridge cranes, therefore, to be safe during the operation under the horizontal movement of cranes and along with effecting the horizontal direction of wind load influencing on the main frame, the fixed support is suitable. Of course, the cost of foundations is more expensive than that of the pinned supports. For the longitudinal direction, this direction is supported by pinned supports, since the longitudinal direction of industrial buildings is rather long. Additionally, the stability of this direction is enhanced by using the system of column bracings. Consequently, aforementioned discussions are reasonable solutions in this study (Figures 3.3 and 3.4).

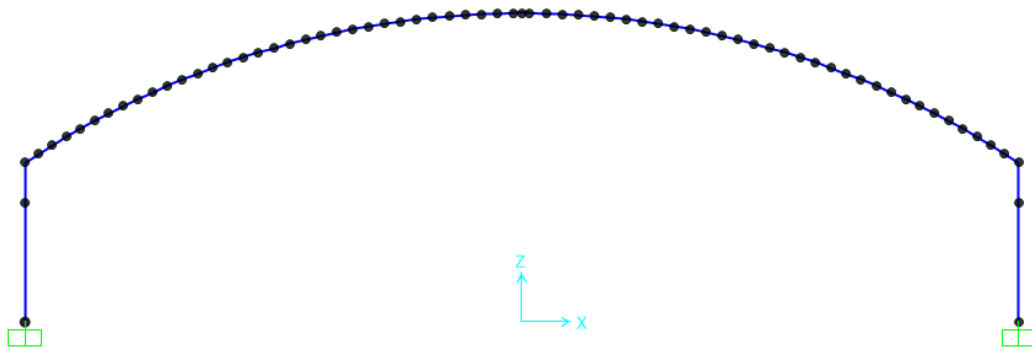


Fig . 3.3 The restraint conditions in the major direction of arch frame

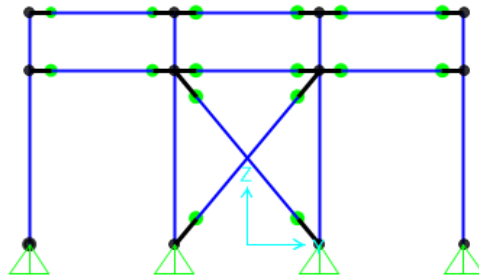


Fig . 3.4 The restraint conditions in the minor direction of arch frame

3.1.3 Dimensions and Configuration of Arch Warehouse Structures

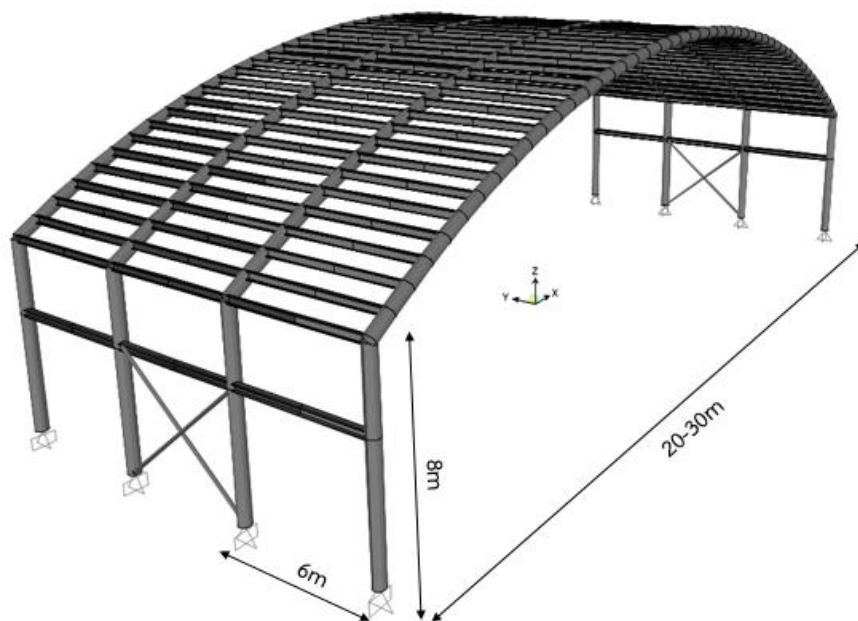


Fig . 3.5 The entire configuration of long-spanned arch warehouse.

In this thesis, arch warehouse structures are considered with roof spans ranging between 20 m and 30 m, bay length of 6 m, and eave height of 8 m. The span length will be varied during modeling and optimum design processes.

The basic geometry of arch warehouse structures will not be changed during the analysis and the optimum design, the eave height of columns and the bay length are also unchanged. Whole three-dimensional arch structure is shown in Figure 3.5. Because of varying span length, this leads to the change of chord-height. Therefore, chord-height will be estimated as discussed in section 2.2.3. The components of arch

steel warehouse structures include the main arch frames (arch roofs, columns) and secondary members (purlins, column bracings, roof beams).

3.1.4 Finite Element Analysis

The behavior of 3D arch warehouse structure is performed by using the SAP2000 commercial software. In SAP2000, linear static and nonlinear static frame analysis is used in this study to save computation time. Moreover, SAP2000 is easy to access and communicate with the model by coding within a computational language through a so-called Open Application Programming Interface (OAPI) function. This advantages can transfer of model and control all of the analysis and design from SAP2000.

3.1.5 Material Properties and Profiles

Table 3.1 represents the detailed material properties that will be used to calculate.

Table 3.1 Material properties

Description	Symbol	Value	Unit
Yield Strength of Cold-formed hollow Steel TIS107 (Gr.SS490)	F_y	315	MPa
Yield strength of Cold-formed C Purlins S450GD	F_y	315	MPa
Modulus of Elasticity	E	210000	MPa
Shear Modulus	G	81000	MPa
Density	ρ	7850	kg/m ³
Poisson's Ratio	ν	0.3	-

In this thesis, an available steel table of cold-formed steel hollow sections and C-sections from manufacturers is used for the optimum design, namely circular

hollow steel (CHS), rectangular hollow steel (RHS) and square hollow steel (SHS) with a set of 192 HS-sections and 13 C-sections.

3.1.6 Loading Conditions

The loads acting on the structure includes dead load, roof load, wind load, and crane load. The load calculation complies with ASCE 7-10, and MBMA-2012 specifications. Load combinations of all loading types are incorporated during the design.

3.1.6.1 Dead Load

The self-weight of the overall arch structure is calculated automatically by the commercial finite element software. In addition, the additional dead load on the roof of the structure are considered such as metal sheet roof has a self-weight of 0.05 (kN/m²) and the other loads have a self-weight of 0.1 (kN/m²).

3.1.6.2 Live Load.

According to ASCE 7-10 and MBMA-2012 specifications, the uniform roof live loads for curved roofs is taken 0.96 (kN/m²). However, the reduction in roof live loads is considered. For ordinary flat, pitched and curved roofs, they are permitted to be designed for a reduced roof live load. On such structures, the minimum roof live load shall be 0.58 (kN/m²).

3.1.6.3 Wind Load.

Wind effect on structures is calculated according to Metal Building Systems Manual (MBMA-2012) that based on Minimum Design Loads for Buildings and Other Structures ASCE 7-10 specification. Standards provided for the application of wind loads in a form more easily applied to a wider variety of building and roof types as appropriate for metal building systems.

The low-rise analytical procedure complied with ASCE 7-10 Chapter 28, part 1 for the main wind force resisting system (MWFERS) on enclosed or partially enclosed building. The roof height is assumed not to exceed 60 feet (18 m) by using the Directional Procedure which is presented the following parameters in Table 3.2.

Table 3.2 Parameters of velocity pressure

Param	Discussion
Building classification	The building function is commercial industrial. It is not considered an essential facility or likely to be occupied by 300 persons at one time. Risk Category II is consistent (Table 1.5-1 ASCE 7-10)
Basic wind speed	In this thesis, the basic wind speed is taken as $V=25$ (m/s) in Thailand
Surface roughness categories	The building is assumed the location on urban and suburban areas. Therefore, exposure B is used
The wind directinal factor K_d	For arched roofs, the K_d is taken as 0.85 (Table 26.6-1 ASCE 7-10)
The velocity pressure exposure coefficient K_z	The velocity pressure exposure coefficient is calculated, depending on height above ground level and surface roughness categories. See table 6-3 (ASCE 7-10)
The topographic factor K_{zt}	For a site located in a transition zone between exposure categories that is near to a change in ground surface roughness, $K_{zt}=1$ for site conditions and locations of structures do not meet all the conditions specified in Figure 26.8-1 (ASCE 7-10)
Windward coefficient	$C_p=0.8$
Leeward coefficient	$C_p=-0.5$
the internal pressure coefficient C_{pi}	C_{pi} is provided in Figure 27.4-3 (ASCE 7-10). However, the internal coefficient are not taken in this work.
Arched roof coefficient	Arched roof coefficient is divided into three zones, including windward quarter, center half and leeward quarter. The distribution of the external pressure is non-uniform. Hence, the roof is subjected either to uplift or to pressure, depending on the rise-to-span ratio r as illustrated in Figure 27.4-3 (ASCE 7-10).

	Conditions	Rise-to-span ratio, r	C_p		
			Windward quarter	Center half	Leeward quarter
	Roof on elevated structure	$0 < r < 0.2$	-0.9	$-0.7 - r$	-0.5
		$0.2 \leq r < 0.3^*$	$1.5r - 0.3$	$-0.7 - r$	-0.5
		$0.3 \leq r \leq 0.6$	$2.75r - 0.7$	$-0.7 - r$	-0.5
	Roof springing from ground level	$0 < r \leq 0.6$	$1.4r$	$-0.7 - r$	-0.5
Gust effect factor G	For low-rise building are permitted to be considered rigid with fundamental frequency is greater than or equal to 1Hz and the gust-effect factor for a rigid building is permitted to be taken as 0.85				

The velocity pressure:

$$q_z = 0.00256K_zK_{zt}K_dV^2 (\text{lb} / \text{ft}^2) = 0.613K_zK_{zt}K_dV^2 (\text{N} / \text{m}^2) \quad (9)$$

$$\Rightarrow q_z = 0.613 \times 0.7 \times 1 \times 0.85 \times 25^2 / 1000 = 0.228 (\text{kN} / \text{m}^2)$$

The wind pressure on each surface for arch warehouse structure:

$$\begin{cases} \text{windward} = q_z(GC_p)s = 0.228 \times (0.85 \times 0.8) \times 6 = 0.93 (\text{kN} / \text{m}) \\ \text{Leeward} = q_z(GC_p)s = 0.228 \times (0.85 \times (-0.5)) \times 6 = -0.58 (\text{kN} / \text{m}) \end{cases} \quad (10)$$

3.1.6.4 Crane Load

Table 3.3 Parameters of crane bridge (16Tons)

Load capacity (T)	Span length (m)	Span length of crane bridge (m)	Total Weight (T)		Max wheel load (T)		Min wheel load (T)		Basic size (mm)						
									H3	B	W	C2	C1	H2	H1
16	30	29	11,2	10,7	11,6	11,2	2,89	2,74	1550	4500	4000	1230	1830	2000	1200

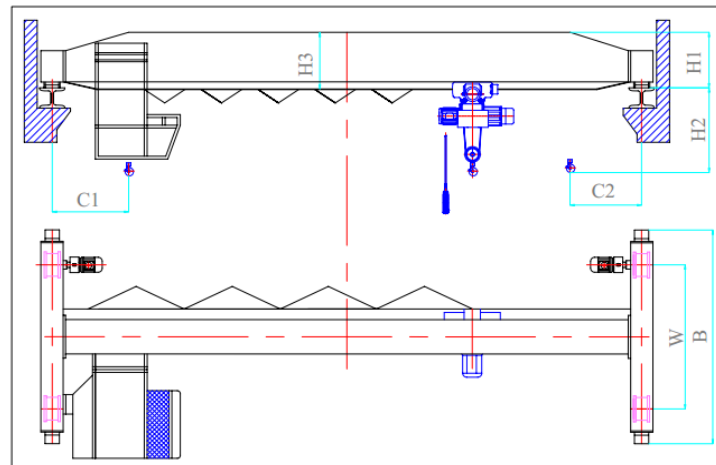


Fig . 3.6 The typical dimensions of a crane bridge

The crane load is determined according to MBMA-2012 and MacCrimmon (2005), Crane buildings must be designed for forces induced by the operation or movement of the bridge. The following main loads are needed to determine:

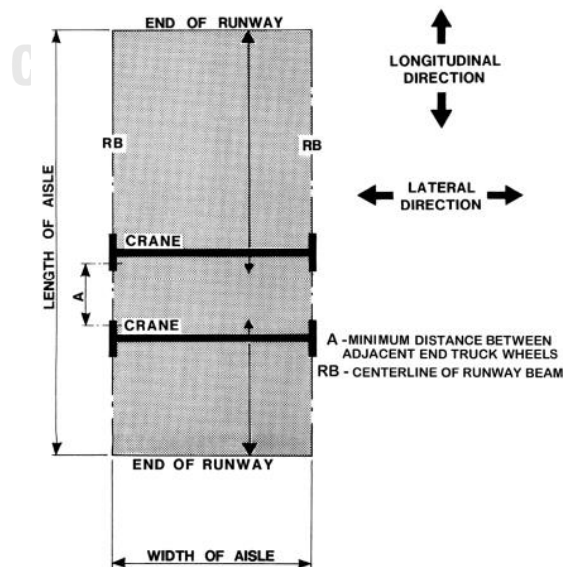


Fig . 3.7 Plane view of a crane aisle (MBMA 2012)

(1) The crane vertical loads on building columns

Crane manufacturers provide information on maximum wheel loads as shown in Table 3.3. These loads may differ from wheel to wheel, depending on the relative positions of the crane components and the lifted load.

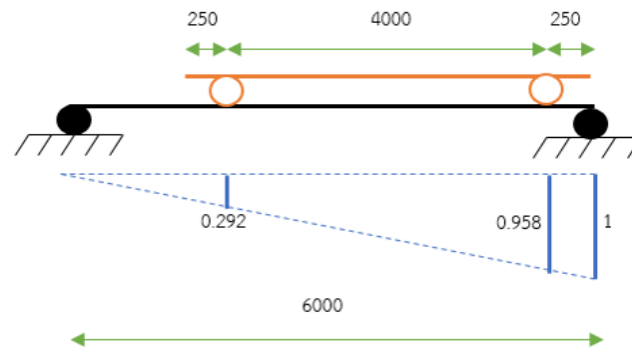


Fig . 3.8 The influence line due to the movement of crane on runway beam

Estimate of runway beam weight is 8.64 (kN) with 6 m by bay length. Based on the influence line in Figure 3.8, vertical load is calculated as follows

$$P_{v1} = 11.57 \times 0.958 \times 10 + 11.22 \times 0.292 \times 10 + 8.64 = 152.2 \text{ (kN)} \quad (11)$$

$$P_{v2} = 2.89 \times 0.958 \times 10 + 2.74 \times 0.292 \times 10 + 8.64 = 44.327 \text{ (kN)}$$

Determine bending moments on columns due to the eccentricity of vertical loads

$$M_{v1} = 152.2 \times 0.5 = 76.1 \text{ (kN / m)} \quad (12)$$

$$M_{v2} = 44.327 \times 0.5 = 22.163 \text{ (kN / m)}$$

(2) The crane lateral loads on building columns

The lateral force on bridge crane runway beams with electrically powered trolleys shall be calculated as 20 percent of the sum of the rated capacity of the crane and the weight of the hoist and trolley.

$$\text{Lateral force} = 20\% \frac{(16 + (11.17 - 10.66)) \times 10}{4} = 8.255 \text{ (kN)} \quad (13)$$

(3) The crane longitudinal loads.

Runway beams, including monorails, their connections and the longitudinal bracing system shall be designed to support horizontal forces calculated as 10 percent of the maximum wheel loads excluding vertical impact. Longitudinal forces

shall be assumed to act horizontally at the top of the rails and in each direction parallel to each runway beam (MBMA-2012).

$$\text{Longitudinal force} = 10\% \times 11.57 \times 10 = 11.57 \text{ (kN)} \quad (14)$$

(4) Crane load combinations

For crane load combinations, the location and lateral movement of the trolley shall be considered in the design of crane buildings as shown in the bellow Figure 3.9

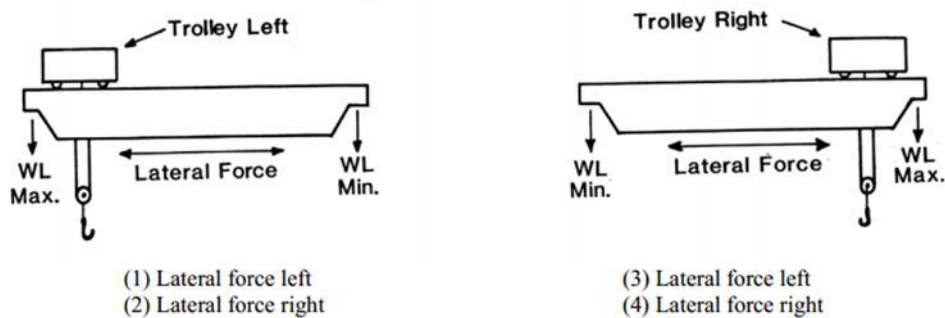


Fig . 3.9 The crane loading conditions (MBMA-2012)

The following four crane loading conditions according to MBMA-2012 specification:

- The maximum wheel load at the left end truck and the minimum wheel load at the right end truck, acting simultaneously with the lateral force acting to the left.
- The maximum wheel load at the left end truck and the minimum wheel load at the right end truck, acting simultaneously with the lateral force acting to the right.
- The maximum wheel load at the right end truck and the minimum wheel load at the left end truck, acting simultaneously with the lateral force acting to the left.
- The maximum wheel load at the right end truck and the minimum wheel load at the left end truck, acting simultaneously with the lateral force acting to the right.

3.1.6.5 Combination Loads.

(1) For strength conditions

In any combination, the dead load and the first transient load are the principal loads and the second transient load is the companion load. The most unfavorable combination governs is proposed followed Table 3.4 according to CISC-2005 Guide for the Design of Crane Supporting Steel Structures (MacCrimmon, 2005) and Thompson (2007).

Table 3.4 Load combinations for strength conditions (Thompson, 2007).

Case	Principle Loads	Companion Loads
1	1.4D	
2	1.25D+1.5C+1.0L _r	0.4W
3	1.25D+1.5L _r +1.0C	0.4W
4	1.25D	1.0C+0.5L _r
5	1.25D+1.4W	1.0C+0.5L _r

D=Dead load, L_r=Roof load, W=Wind load, C=Crane load

Note that: For single crane in a single aisle

C = 1.0 Vertical loads+1.0 Lateral loads+1.0 Logitudinal loads

(2) For serviceability conditions

According to MBMA-2012, ASCE 7-05, ASCE 7-10, AISC-Steel Design Guide 3 (Serviceability Design Considerations for Steel Buildings-2nd), and AISC-Steel Design Guide 7 (Industrial Buildings-2nd). For the serviceability limit states “involving long-term effects and short-term effects are checked as the following load combinations in Table 3.5.

Table 3.5 Load combinations for serviceability conditions

Case	Principle Loads	Companion Loads
1	1.0D+0.5L _r	
2	1.0D+0.5L _r	0.7W

The AISC specifications prescribe the evaluation of total frame drift ratio Δ/H and inter-storey drift ratio δ/h under service loads in order to guarantee the serviceability of the structure as illustrated in Figure 3.10.

Every type of framed system	Recommended limiting values for horizontal deflections	
	δ/h	Δ/H
Range of common values	1/200	1/100
Most widely used values	1/600	1/600
	1/400	1/400
	1/500	1/500

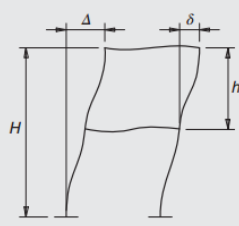


Fig . 3.10 Deflection limit ratios for structures under horizontal load according to AISC

For metal sheet wall, the frame deflection perpendicular to the wall surface of frame: $H/60$ or $H/100$. In this case, the main frame carrying crane load. Therefore, the horizontal deflection limit is $H/100$ (H is the overall height of frame). And the vertical deflection limit is $L/240$ (L is the span length).

3.2 Advanced Analysis of 3D Steel Arch Structures

According to (SAP) (CSI analysis reference manual), the FE software SAP2000 is capable of considering geometric nonlinearity in the form of either P-Delta effects or large displacement/rotation effects. The program tracks the position of the element using an updated Lagrangian formulation. All equilibrium equations are written in the deformed configuration of the structure. The nonlinear equations are solved iteratively in each load steps. This may require a large amount of iteration due to re-forming and re-solving the stiffness matrix until the solution converges, Newton-Raphson iterations are usually most effective. Although large displacement and large rotation effects are modeled, all strains are assumed to be small. P-Delta effects are also included.

The nonlinear static analysis is used for performing P-Delta or large displacement analysis to get the stiffness. When using iteration, the relative convergence tolerance used to compare the magnitude of force error with the magnitude of the force acting

on the structure. The use of significantly smaller values of convergence tolerance to get good results for large displacement problems than for other types of nonlinearity.

Try decreasing this value until getting consistent results. For each step, constant-stiffness iteration is tried first. If convergence is not achieved, Newton-Raphson iteration is tried next. If both fail, the step size is reduced, and the process is repeated. Although constant-stiffness iterations are faster than Newton-Raphson iterations, but the latter is usually more effective, especially for geometric nonlinearity as illustrated in CSI analysis reference manual (SAP).

3.3 Formulation of the Optimum Design Problem

3.3.1 Design Variables

The design variables are mostly chosen from a list of standard sections available on the construction market. Therefore, the cross-sections of structural steel members are discrete sizing design variables and the optimization process is called as the discrete structural optimization.

During modeling of the structural optimization process, members are grouped to reduce the population size and computational time. Mathematically, design variables can be formulated as follows:

$$\begin{aligned} \text{Find } \mathbf{X} \in \mathcal{R}^{ng} &= [A_1, A_2, A_3, \dots, A_i] \\ A_i &= [x_1, x_2, x_3, \dots, x_{nd}], \quad i = 1, \dots, nd \end{aligned} \quad (15)$$

Where $1 \leq A_i \leq ms$ (ms shows the total number of cross sections considered in the design for group i); \mathbf{X} is a vector of cross-sectional areas for each member group.

3.3.2 Objective Function

In this thesis, the discrete variable optimization of steel structures, where minimum weight is considered, as an objective function can be stated as follows:

$$\text{Minimize } W(\mathbf{X}) = \sum_{i=1}^{ng} A_i \sum_{j=1}^{mk} \rho_j L_j \quad (16)$$

Where $W(\mathbf{X})$ is the total weight of steel frame; ng is the total numbers of groups as unknown discrete cross-sectional areas in the frame; mk is the total number ber of

members in group i ; A_i is the cross-sectional area of member group i ; L_i and γ_i are the length of the j th member in the i th member group and the density of steel, respectively.

3.3.3 Constraints

To minimize the weight of structure subject to serviceability constraints and strength constraints are utilized in the design process.

$$\text{Subject to } g_t(x) = \begin{cases} \lambda_j^\sigma \leq 0 & j = 1, \dots, nc \\ \lambda_r^d \leq 0 & r = 1, \dots, ns \end{cases} \quad (17)$$

Where nc is the number of beam-columns of group i ; ns is the total number of stories.

3.3.3.1 Strength Constraints

The strength constraints taken from interaction formula of the AISC-LRFD (ANSI/AISC 360-16) and AISI-LRFD (AISI S100-16) specifications are expected in the following. For member subjects to bending moment and axial force.

$$\lambda_j^\sigma = \frac{|\sigma_j|}{\sigma_j^a} - 1 \leq 0, \left(S_s = \frac{|\sigma_j|}{\sigma_j^a} \right) \quad (18)$$

Where σ_j are stresses in the j th element of member group i .

$$\sigma_j = \begin{cases} \left(\frac{P_u}{\phi P_n} \right) + \frac{8}{9} \left(\frac{M_{ux}}{\phi_b M_{nx}} + \frac{M_{uy}}{\phi_b M_{ny}} \right) & \text{if } \frac{P_u}{\phi P_n} \geq 0.2 \\ \left(\frac{P_u}{2\phi P_n} \right) + \left(\frac{M_{ux}}{\phi_b M_{nx}} + \frac{M_{uy}}{\phi_b M_{ny}} \right) & \text{if } \frac{P_u}{\phi P_n} < 0.2 \end{cases} \quad (19)$$

Where P_u is the required axial strength; P_n is the nominal axial strength; M_{ux} and M_{uy} are the required flexural strengths about the major and the minor axes, respectively; M_{nx} is the nominal flexural strength about the major axis; M_{ny} is the nominal flexural strength about the minor axis; ϕ is the resistance factor shown as $\phi = \phi_c = \phi_t$ for compression (equal to 0.9) and tension (equal to 0.9), respectively; ϕ_b is the flexural resistance factor, which is equal to 0.9.

3.3.3.2 Serviceability Constraints

The displacement constraints, representing the evaluation of total frame drift ratio Δ/H and inter-storey drift ratio d/h under service loads in order to guarantee the serviceability of the structure.

$$\begin{cases} \lambda_r^d = \frac{|\Delta^*|}{\Delta_{ru}} - 1 \leq 0, \left(S_d = \frac{|\Delta^*|}{\Delta_{ru}} \right) \text{ and } |\Delta^*| < \Delta_{ru} \\ \lambda_r^d = \frac{|d^*|}{d_{ru}} - 1 \leq 0, \left(S_d = \frac{|d^*|}{d_{ru}} \right) \text{ and } |d^*| < d_{ru} \end{cases} \quad (20)$$

For a typical column, Δ^* and d^* are the total frame drift ratio and the maximum inter-storey displacement in storey r ; Δ_{ru} and d_{ru} are the allowable horizontal displacement (equal to $H/100$, where H is the overall height of frame) and the allowable inter-storey displacement (equal to $h_r/400$, where h_r is the storey height), S_d is the horizontal displacement uniform scaling factor.

For a typical beam, $d^* = d_j$ are the maximum vertical displacement of j th element of group i , d_{ru} is the allowable vertical displacement (equal to $L/240$, where L is a span length), S_d is the vertical displacement uniform scaling.

CHAPTER 4 SOLUTION ALGORITHM

4.1 Evolutionary Structural Optimization (ESO)

4.1.1 Algorithm Overview

Yi M Xie and Steven (1993) discovered an efficient technique applied to structural design, which was later termed as an evolutionary structural optimization (ESO). An ESO gained quickly the popularity among both research and professional communities due to its easy and understandable implementation without complicated mathematics. The method is based on the simple idea that the optimal structure (maximum stiffness, minimum weight) can be produced by slowly removing (resizing) any inefficient material (discrete) design variables through the iterative process. Compared to other structural optimization methods, the ESO method is more attractive than traditional optimization techniques due to simplicity and effectiveness (Tanskanen, 2006). One of the most famous architectural innovations using ESO algorithm is the Qatar National Convention Centre designed by the eminent Japanese architect Mutsuro Sasaki and his co-workers (Figure 4.1).



Fig . 4.1 The Qatar National Convention Centre (<http://www.amlak.com.qa>).

The ESO method has well proven for its fruitful implementation to provide the approximate answers to many design problems, e.g. sizing, shape and/or topology optimum design under multiple load cases for static and dynamic problems. For sizing optimization, this method can directly apply to other types of structures such

as trusses and frames. For beam elements, one can choose a range of sections commercially available from manufacturers as a given set of discrete sections for sizing. Additionally, the ESO method is simple to program via the interaction between computational languages and finite element analysis (FEA) packages. They require a relatively small amount of analysis time. Various applications have been implemented to demonstrate effectiveness and simplicity of the ESO methods (Li, Qing Steven, & Grant P Xie, 2000; Manickarajah, Xie, & Steven, 2000; Nha, Xie, & Steven, 1998; Steven, Querin, & Xie, 2000),

4.1.2 Basic of Evolutionary Optimization Algorithm

Evolutionary structural optimization involves two main steps, namely one called “*uniform scaling*” with “*critical scaling factors*” and the other named “*element sensitivity number*”. For sizing optimization, the design variables such as thickness and cross-section properties are discrete and taken from a range of available section provided by manufacturers. Material Removal Ratio (MRR) is an crucial parameter defined by the percentage of removed material (area or volume) around 5-10% between two consecutive designs (Chu, Xie, Hira, & Steven, 1996).

4.1.2.1 Uniform Scaling and Critical Scale Factor

During the optimization process, it is convenient to obtain a feasible design after each iteration by scaling the design uniformly in order to satisfy the most critical constraint. This helps “*to keep track of the reduction*” in the weight of the structure after each iteration and also helps “*to pick up the most active constraints*”. Uniform scaling factors of constraints are explicitly given in section 3.3.3, including stress scaling factor S_s and displacement scaling factor S_d . The scaling design should be critical to the most active constraint. Hence critical scale factors (S_{crit}) is determined from the maximum of uniform scaling factors among S_s, S_d (Manickarajah et al., 2000).

4.1.2.2 Element Sensitivity Number for Resizing

According to Manickarajah et al., (2000), sensitivity analysis plays a central role in the structural optimization since virtually all the optimization methods require the

computation of the derivatives of structural responses quantities with respect to design variables. According to Nha et al. (1998), sensitivity numbers can be formulated using optimality criteria methods. A sensitivity number is calculated for each element depending on its influence on the strength, displacement and buckling load of the structure. For cross-sectional optimization, the effects of element sensitivity on the structural behaviors due to local modification of each element need to be estimated. The local modification of an element may be the change in plate thickness or the change in cross-sectional dimensions of beam or bar element etc. The indication of an element with respect to the required structural response is referred to the sensitivity number of that particular element and is denoted by α_j for j^{th} element of group i .

(1) *Optimization with stress constraint*

The calculation of the approximate stress from the approximate element forces is inexpensive using an explicit relationship such as in Eq. (21) (Manickarajah et al., 2000). The following element sensitivity numbers are defined for stress constraint:

$$\alpha_{js}^+ = \frac{\sigma_j^+}{l_j} = \sigma_j^+ \frac{(A + \Delta A)}{l_j} \quad (21)$$

$$\alpha_{js}^- = -\frac{\sigma_j^-}{l_j} = -\sigma_j^- \frac{(A - \Delta A)}{l_j} \quad (22)$$

Where $\alpha_{js}^+, \alpha_{js}^-$ are the sensitivity number for stress constraints; A is cross-sectional area; σ_j^+ is the maximum stress of an element j^{th} , when the area is increased by ΔA ; and vice versa for the minimum stress σ_j^- ; l_j is the length of an element j .

(2) *Optimization with displacement constraint*

The static behavior of a structure is represented by Eq. (23).

$$[K]\{d\} = \{P\} \quad (23)$$

The change in displacement can be determined by considering equilibrium conditions before and after change (Nha et al., 1998; Yi Min Xie & Steven, 1997). This gives by Eq. (24).

$$[K + \Delta K]\{d + \Delta d\} = P \quad (24)$$

Where $[K]$ is the global stiffness matrix; $\{d\}$ is the global nodal displacement vector. By subtracting Eq. (23) from Eq. (24) and ignoring the higher order term, the change in displacement vector, according to Li et al. (2000), Δd is approximated to

$$\Delta d = -[K]^{-1}[\Delta K]\{d\} \quad (25)$$

To determine the change in the k^{th} degrees of freedom displacement, Δd_k , a unit virtual load vector $\{F_k\}$ (Nha et al., 1998). Multiplying Eq. (25) by $\{F_k\}^T$ leads

$$\begin{aligned} \Delta d_k &= \{F_k\}^T \{ \Delta d \} = - \underbrace{\{F_k\}^T [K]^{-1} [\Delta K]}_{\{d_k\}^T} \{d\} \\ &= -\{d_k\}^T [\Delta K] \{d\} = -\{d_{jk}\}^T [\Delta K_j] \{d_j\} \end{aligned} \quad (26)$$

Where $[\Delta K_j] = [K_j]^{new} - [K_j]^{old}$ is the change in global stiffness matrix for the j^{th} element; $\{d_k\}$ is the displacement vector due to the unit virtual load vector $\{F_k\}$, and $\{d_{jk}\}$ are the j^{th} element displacement vectors associated with d and $\{d_k\}$. It should be noted that the displacement Δd_k may take a positive or a negative value, which implies that d_k may increase or decrease.

The virtual energy of the j^{th} element

$$\alpha_{jk} = \{d_{jk}\}^T [K_j] \{d_j\} \quad (27)$$

According to Nha et al. (1998), the change in the element virtual energy due to only sizing as:

$$\begin{aligned} \Delta \alpha_{jk} &= \alpha_{jk}^{new} - \alpha_{jk}^{old} = \{d_{jk}\}^T [K_j]^{new} \{d_j\} - \{d_{jk}\}^T [K_j]^{old} \{d_j\} \\ \Leftrightarrow \Delta \alpha_{jk} &= \{d_{jk}\}^T [\Delta K_j] \{d_j\} \quad (j = 1, \dots, n) \end{aligned} \quad (28)$$

From Eq. (26) and Eq. (28), Eq. (29) can be drawn.

$$\Delta d_k = -\{d_{jk}\}^T [\Delta K_j] \{d_j\} = -\Delta \alpha_{jk} \quad (j = 1, \dots, n) \quad (29)$$

Which means that, in absolute values, the change in the specified displacement is equal to the change in the virtual energy within an element due to changing its sizes by taking sum of α_{jk} in Eq. (27)

$$d_j = \sum_{j=1}^n \alpha_{jk} \quad (30)$$

Where α_{jk} is also referred to as the element contribution.

By using Eq. (29), when $\Delta\alpha_{jk}$ is close to zero or $|\Delta\alpha_{jk}|$ is the lowest, the result in the minimum change in the displacement will be induced. The reduction of the element with the lowest $|\Delta\alpha_{jk}|$ is always the best choice.

As already mentioned, sensitivity numbers for the j^{th} element are derived using optimality criteria methods. The effect of element size reduction on a specified displacement can be evaluated using information available from a finite element analysis and then sensitivity numbers for element can be derived from optimality criteria for the general weight minimization problems (Nha et al., 1998). The objective is to minimize the weight of a structure.

$$W = \sum_{i=1}^n w_i = \sum_{i=1}^n A_i \sum_{j=1}^m \rho l_j \quad (31)$$

Consider a problem with multiple displacement constraints given as

$$|d_j| - d_j^* \leq 0 \quad (j = 1, m) \quad (32)$$

Where m is the number of constraints; d_j^* is the given limit for $|d_j|$.

The Lagrange multipliers plays an important role in any optimization procedure using an optimality criterion approach. The following using Lagrange multiplier approach for multiple constraints is

$$L = W - \sum_{j=1}^m \lambda_j (|d_j| - d_j^*) \quad (33)$$

Where λ_j are m Lagrange multipliers. The optimality conditions are

$$\frac{\partial L}{\partial w_i} = \frac{\partial W}{\partial w_i} - \sum_{j=1}^m \lambda_j \left| \frac{\partial d_j}{\partial w_i} \right| = 1 - \sum_{j=1}^m \lambda_j \left| \frac{\partial d_j}{\partial w_i} \right| = 0 \quad (j = 1, m), (i = 1, n) \quad (34)$$

Where $\lambda_j > 0$ for the active constraints $|d_j| - d_j^* = 0$, and $\lambda_j = 0$ for the passive constraints $|d_j| - d_j^* < 0$. The optimality conditions Eq. (34) can be approximated (Nha et al., 1998) by Eq. (35).

$$1 - \sum_{j=1}^m \lambda_j \left| \frac{\Delta d_j}{\Delta w_i} \right| = 0 \quad (i = 1, n) \quad (35)$$

Using Eq. (29), the optimality condition Eq. (35) becomes

$$1 - \sum_{j=1}^m \lambda_j \left| \frac{\Delta\alpha_{jk}}{\Delta w_i} \right| = 0 \quad (i = 1, n) \quad \text{or} \quad \sum_{j=1}^m \lambda_j \left| \frac{\Delta\alpha_{jk}}{\Delta w_i} \right| = 1 \quad (i = 1, n) \quad (36)$$

Where λ_j is a simple Lagrange multipliers given in the form as

$$\lambda_j = \frac{|d_j|}{d_j^*} \quad (j=1,m) \quad (37)$$

Equation (36) represents an optimality criterion for multiple constraints as a measure of the efficiency of the change of an element in the case of multiple constraints. From Eq. (29), (36) and (37), the following sensitivity numbers are defined for the j^{th} displacement constraint which are represented by Eqs. (38) and (39) (Manickarajah et al., 2000).

$$\alpha_{jd}^+ = \frac{|d_j| \{d_{jk}\}^T [\Delta K_j]^+ \{d_j\}}{d_j^* l_j} = \frac{|d_j| \{d_{jk}\}^T [K_j(t+\Delta t) - K_j(t)] \{d_j\}}{d_j^* l_j} \quad (38)$$

$$\Leftrightarrow \alpha_{jd}^+ = \frac{|d_j| \Delta \alpha_{jd}^+}{d_j^* l_j} = \frac{|d_j| - \Delta d_j^+}{d_j^* l_j} = -\lambda_j \frac{\Delta d_j^+}{l_j}$$

$$\alpha_{jd}^- = \frac{|d_j| - \{d_{jk}\}^T [\Delta K_j]^- \{d_j\}}{d_j^* l_j} = \frac{|d_j| - \{d_{jk}\}^T [K_j(t-\Delta t) - K_j(t)] \{d_j\}}{d_j^* l_j} \quad (39)$$

$$\Leftrightarrow \alpha_{jd}^- = \frac{|d_j| \Delta \alpha_{jd}^-}{d_j^* l_j} = \frac{|d_j| - \Delta d_j^-}{d_j^* l_j} = -\lambda_j \frac{\Delta d_j^-}{l_j}$$

(3) Optimization with all constraints considered simultaneously

To measure the influence of each constraint, we use the critical scaling factors defined in Section 3.3.3. It's worth noting that the critical scaled factors are determined by taking the maximum value of each uniform scaling factor of the j^{th} element of group i . Taking all constraints into account, finally for each element the following two new sensitivity numbers are defined (Manickarajah et al., 2000):

$$\alpha_j^+ = \sum_{p=1}^n S_{sp} \frac{\alpha_{jsp}^+}{\alpha_{sp,av}^+} + S_{dp} \frac{\alpha_{jdp}^+}{\alpha_{dp,av}^+} \quad (40)$$

$$\alpha_j^- = \sum_{p=1}^n S_{sp} \frac{\alpha_{jsp}^-}{\alpha_{sp,av}^-} + S_{dp} \frac{\alpha_{jdp}^-}{\alpha_{dp,av}^-} \quad (41)$$

Where $\alpha_{sp,av}^+$ is the average of the α_{jsp}^+ values of all elements and other average values are similarly defined. The design variables are allowed to vary in small steps in a prescribed manner. Hence the change in the element displacement Δd_k can be easily calculated. All the other information required for the calculation of sensitivity numbers is readily available from the finite element solution.

4.1.2.3 Termination Criteria

In the present work, the ESO algorithm is terminated until the constraints reach the prescribed limits. Namely, a proposed tolerance δ corresponding to the most active constraint has the largest value which lies in a predefined allowable zone. The activeness of each constraint in section 3.3.3, are characterised by the value $\phi_j = \left(\frac{|\sigma_j|}{\sigma_j^a} \right)$, $\phi_r = \left(\frac{|\Delta^*|}{\Delta_{ru}} \right)$ ($j=1,nc; r=1,ns$). If the value of $\phi_j; \phi_r$ are close to unity as well as satisfying the predefined tolerance, then the ESO process terminates. The scaling factors for the termination are determined as Eq. (42).

$$\begin{aligned}
 \phi &= \max_{j=1,nc} \phi_j = \max_{j=1,nc} \left(\frac{|\sigma_j|}{\sigma_j^a} \right) \\
 \phi &= \max_{r=1,ns} \phi_r = \max_{r=1,ns} \left(\frac{|\Delta^*|}{\Delta_{ru}} \right) \left. \vphantom{\begin{aligned} \phi &= \max_{j=1,nc} \phi_j \\ \phi &= \max_{r=1,ns} \phi_r \end{aligned}} \right\} \Rightarrow |1 - \phi| \leq \delta_{\max} \\
 \phi &= \min_{j=1,nc} \phi_j = \min_{j=1,nc} \left(\frac{|\sigma_j|}{\sigma_j^a} \right) \\
 \phi &= \min_{r=1,ns} \phi_r = \min_{r=1,ns} \left(\frac{|\Delta^*|}{\Delta_{ru}} \right) \left. \vphantom{\begin{aligned} \phi &= \min_{j=1,nc} \phi_j \\ \phi &= \min_{r=1,ns} \phi_r \end{aligned}} \right\} \Rightarrow |1 - \phi| \leq \delta_{\min}
 \end{aligned} \tag{42}$$

4.1.3 Procedure of ESO algorithm

For discrete optimization, the ESO algorithm is called as “Elimination Process”. Based on the basic concept of ESO method, an iterative procedure needs to be set up. The procedure of an optimum design algorithm for steel frames using an ESO algorithm consists of:

Step 1. Initially, create group frame elements, then all elements are assigned to arbitrary cross-sectional areas which are normally the maximum area values. The material removal ratio (MRR) is proposed around 4-10% between two consecutive designs. This parameter is dynamically applied during the ESO process.

Step 2. Simulate the structural model and set up preliminary param.

Step 3. Perform finite element analysis and design structure.

Step 4. Calculate a stress uniform scaling factor S_s and displacement uniform scaling factor S_d for j^{th} element of group i to gain the maximum stress and displacement ratios, along with the determination of critical scaling factors S_{crit} which is the maximum uniform scaling among S_s and S_d for each group.

Step 5. Calculate the sensitivity number with all the constraints considered simultaneously, where α_j^+ and α_j^- are introduced at j^{th} element within a group i .

Step 6. Check termination conditions. The algorithm terminates until the constraints reach the prescribed limits $\delta_{max}, \delta_{min}$ as shown in Eq. (42)

Step 7. Increase the cross-sectional area of elements for the highest α_j^+ and decrease the cross-sectional area for the lowest α_j^- .

Step 8. For the sizing selection, update the areas of group i at each iteration by multiplying MRR to the areas of the previous iteration $A^{new} = A^{old} \pm MRR(\%) \cdot A^{old}$. Then $A^{new} = A^{new} \pm \Delta A$, where ΔA is used to explore all neighborhoods (cross-sections) are close to the current areas of each group.

Step 9. A set of sections of group i is defined at each iteration. Based on the slenderness ratios, cross-section for each group with having largest slenderness ratios close to the allowable slenderness limitations is selected.

Step 10. Assign new sections for group frame elements. Repeat the Steps 3 to 9 until the constraints achieve the prescribed limits. The search space is gradually narrowed down to a relatively small search space. Finally, the feasible search space for each group is found.

Step 11. Before completely stopping the main ESO procedure, a tactical exploration as an improvement of the primitive ESO algorithm is applied for solving the discrete search space. All possible trials are scaled by using the critical scaling factors S_{crit} for each group. The design variables are only navigated either to reduce or increase over the feasible search space of group

i. Then, enumerative search of selected section is applied to match the feasible candidates of the defined groups.

Step 12. Select the steel sections resulted in the minimum weight for each design group. All constraints of the best solution satisfy the upper limit.

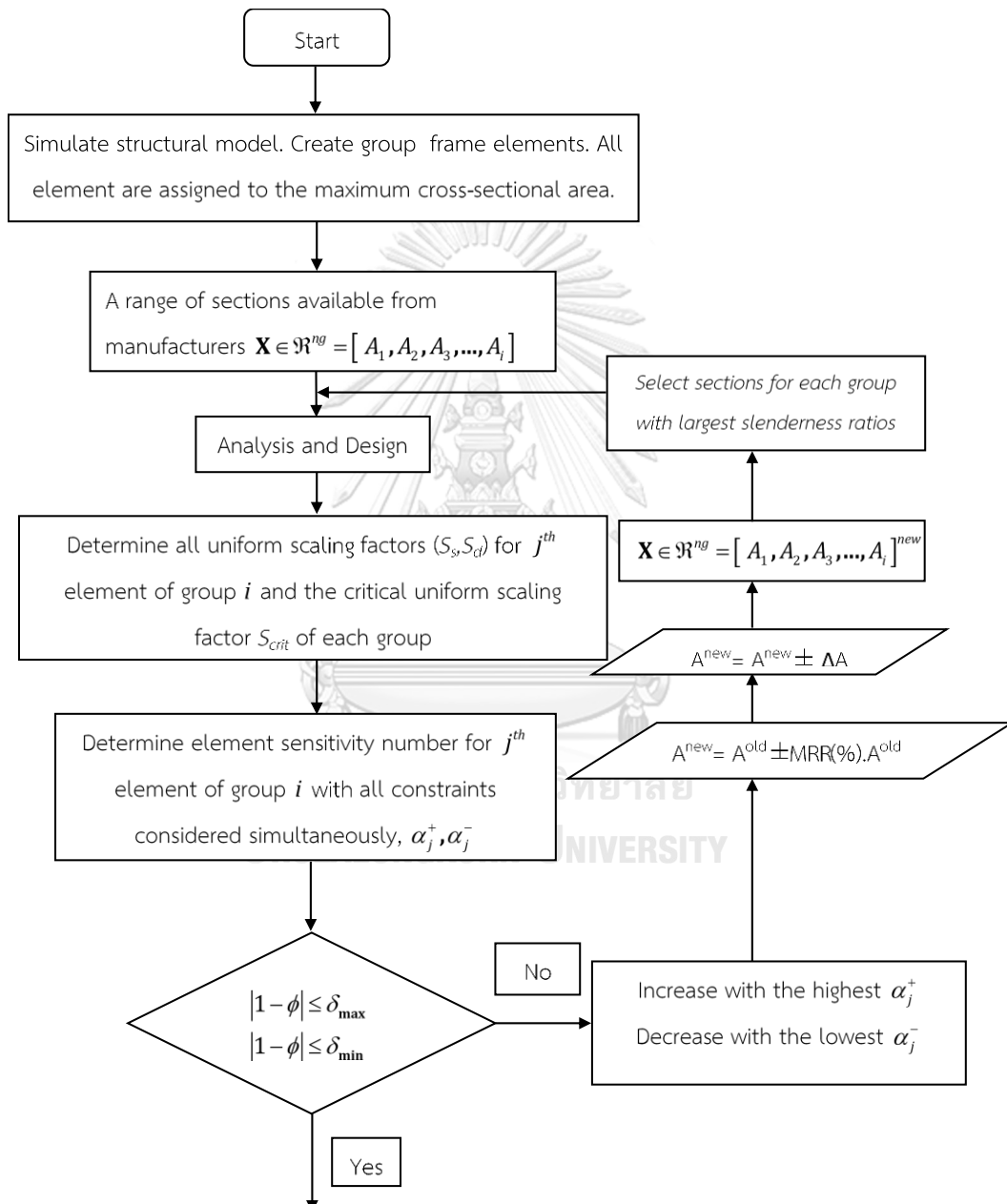


Fig . 4.2 Flowchart of the ESO algorithm

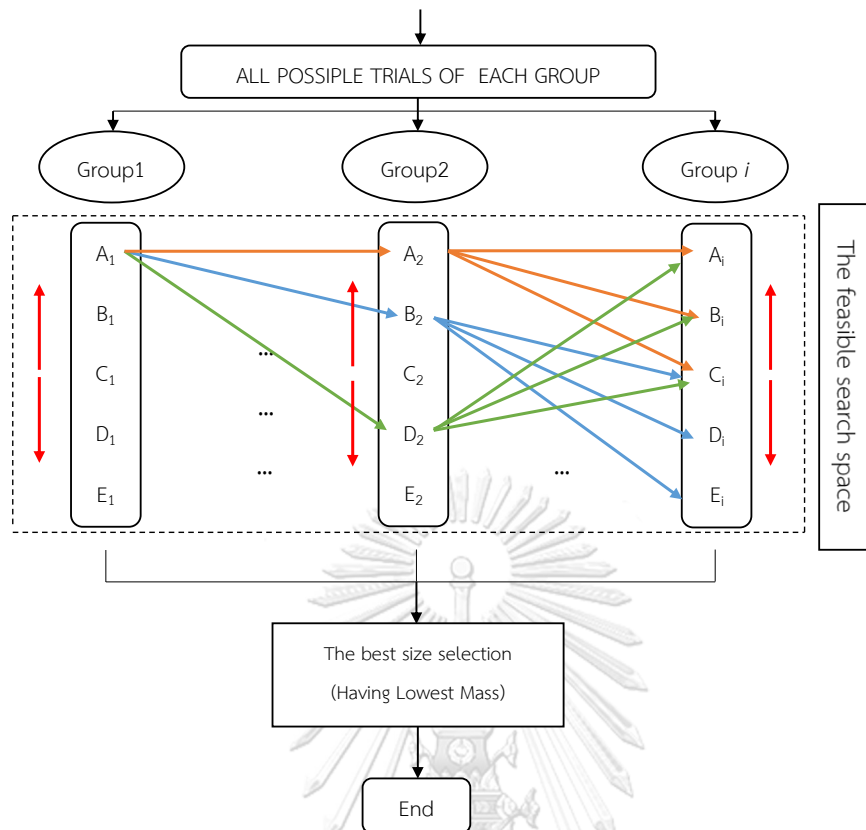


Fig . 4.2 Flowchart of the ESO algorithm (continued)

4.1.4 Test on BenchMark Steel Frame

In the optimization formulation, the objective function minimizes the total weight of planar steel frame, whilst the constraint functions describe an elastic stiffness method with an AISC-LRFD specification (AISC, 2001). The procedure is performed as an iterative process by encoding the ESO algorithm run between the two computer programming environments, namely a commercial structural analysis software SAP2000 and a post-processing Visual Basic Application (VBA) through a so-called Open Application Programming Interface (OAPI) function. This interaction can help to transfer of model and control all of the analysis and design from SAP2000 software.

4.1.4.1 Optimization of two-bay, three storey Steel Framed Structure

The two-bay, three-storey steel frame under a single-load case shown in Figure 4.3 was considered. This problem is set as a benchmark in many structural optimization literatures. The optimum design process complying with an AISC-LRFD specification. The elastic modulus (E) and yield stress (F_y) values were 29000 ksi and 36 ksi, respectively. The material density was 2.84×10^{-4} kip/in³.

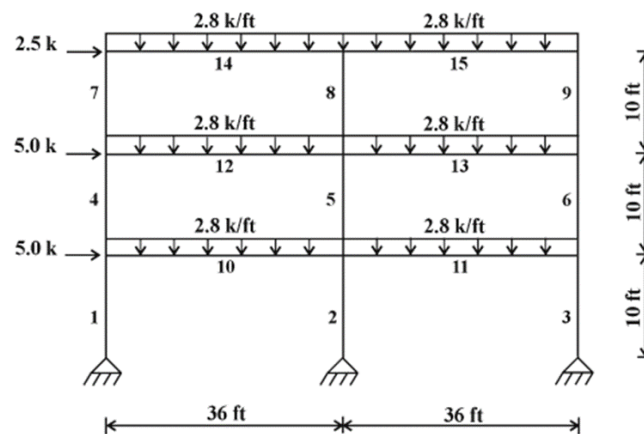


Fig . 4.3 Two-bay, three storey planar steel frame (Degertekin, 2008)

In this example, three cases are considered. In cases 1 and 2, members of the steel frame are divided into two groups, and three groups in Case 3. The imposed fabrication conditions require that all six beams be of the same group with a set of the entire 274 W-sections from AISC standard list. The column group section of Case 1 is limited to W10 sections (18 W-sections). The size of the resulting search space is approximately 4,932 designs. However, the column group sections in Case 2 and Case 3 are chosen from all 274 W-sections. The resulting search space has a size of 75,076 designs, and $2,057 \times 10^7$ design respectively.

Table 4.1 Optimization results obtained for the two-bay, three storey steel frame

Group no	GA	ACO (C.	DDHS	SGA	ESO Algorithm		
	(Pezeshk et al., 2000)	V. Camp et al., 2005)	(Murren & Khandelwal, 2014)	(Carraro et al., 2017)	Case 1	Case 2	Case 3
1 (Beams)	W24X62	W24X62	W24X62	W24X62	W24X62	W24X62	W24X62
2 (Inner columns)							W12X53
3 (Outer columns)	W10X60	W10X60	W10X60	W10X60	W10X60	W12X58	W14X53
Number of analyses	1,800	3,000	200	100	16	41	84
Weight (lb)	18,792	18,792	18,792	18,792	18,792	18,624	18,192

Table 4.1 and Figure 4.4 summarize the optimization results developed and compared with applying different algorithms for the two-bay, three-storey steel frame problem. In this example, the optimum weight of Case 1 has the same optimization results with the other algorithms. The ESO algorithm only obtained within the modest 16 analyses, which is significantly less than 1800 structural analyses for the genetic algorithm (GA), 3000 structural analyses for the ant colony optimization (ACO), 200 structural analyses for the design-driven harmony search (DDHS), and 100 structural analyses for the search group algorithm (SGA). However, for Case 2 and 3 the number of analyses are higher than Case 1. Because the number of sections and groups are increased to improve the lowest weight of the entire steel frame, the total weight in Case 2 yielding approximately 0.9% lighter weight than Case 1 and all other reported results. With three groups in Case 3, the total weight yielded 18,192 lb within 84 analyses which is approximately 3.3% lower than the total weight of the other reported results.

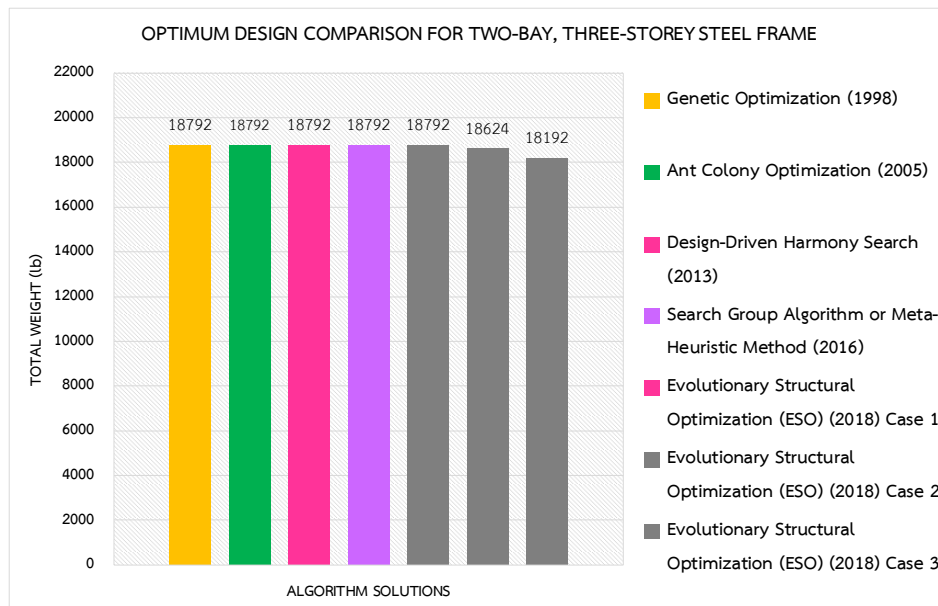


Fig . 4.4 Optimum design coMParison for two-bay, three storey steel frame

The convergence history and the critical scaling factor ratios obtained by the ESO algorithm are shown in Figures 4.5-4.10. The algorithm took only couple of minutes to converge the optimum solutions. All the critical scaling ratios of the maximum stress in three cases were under the upper limit. For all cases, the critical scaling ratio of maximum stress ratio within 100% at the best solution. This indicate that the optimum solution satisfied its given constraints.

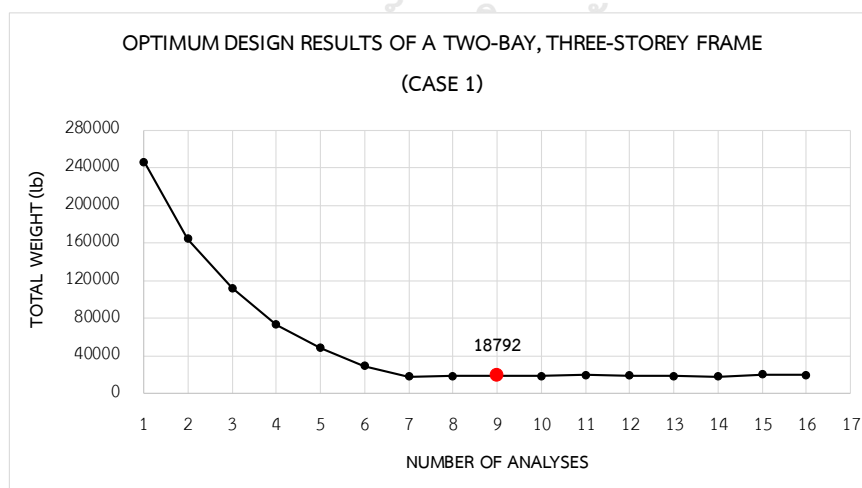


Fig . 4.5 Convergence history of two-bay three-storey frame design (Case 1)

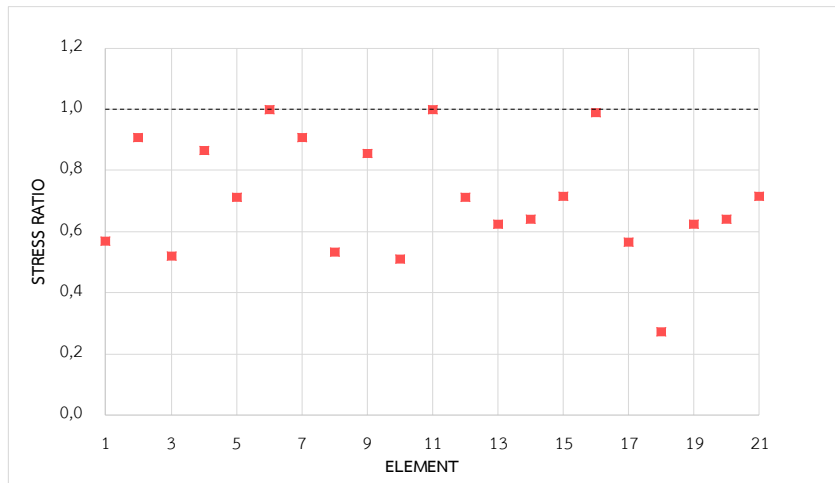


Fig . 4.6 Stress ratio for members of two-bay three storey frame (Case 1)

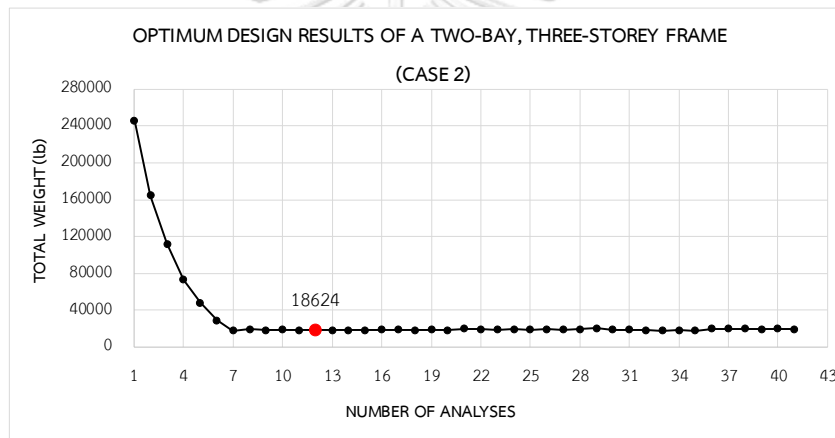


Fig . 4.7 Convergence history of two-bay three-storey frame design (Case 2)

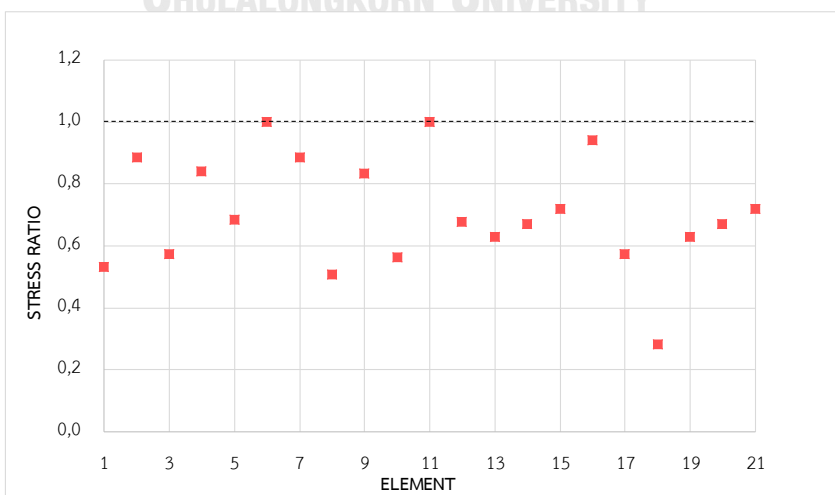


Fig . 4.8 Stress ratio for members of two-bay three storey frame (Case 2)

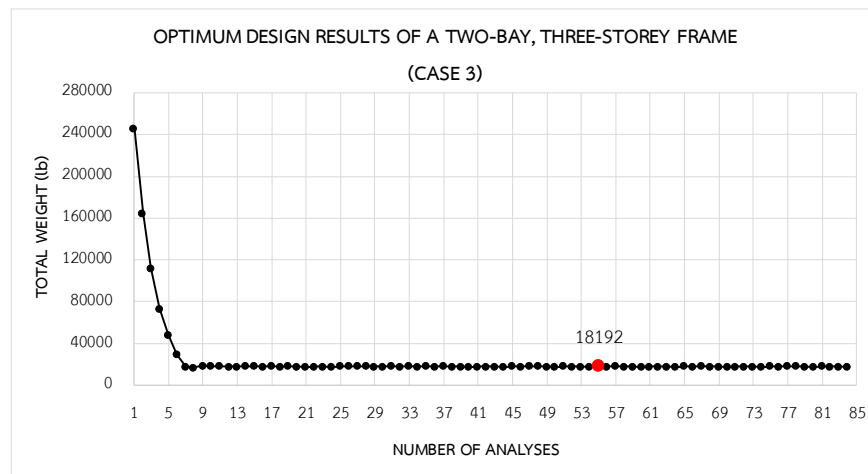


Fig . 4.9 Convergence history of two-bay three-storey frame design (Case 3)

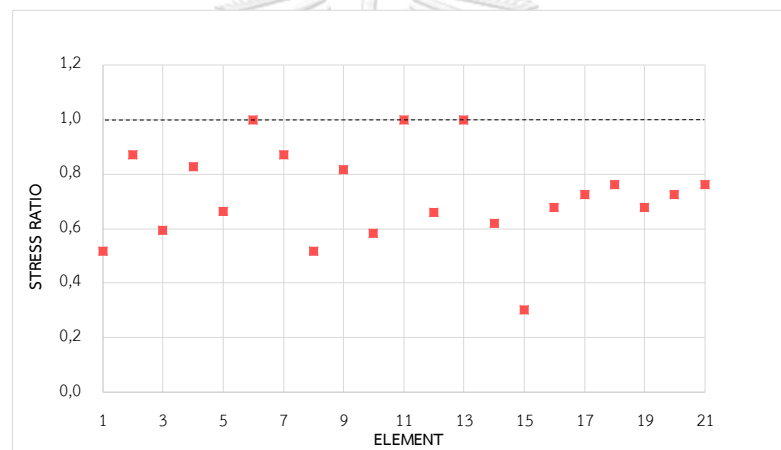


Fig . 4.10 Stress ratio for members of two-bay three storey frame (Case 3)

4.1.4.2 Optimization of one-bay, ten-storey steel frame

Figure 4.11 shows the layout of a one-bay, ten-storey frame. The frame consists of 30 members and the frame is divided into 9 groups due to fabrication conditions. The corresponding member groups, the dimension of the frame and the loading are shown in the figure. The material has a modulus of elasticity $E=29,000$ ksi and a yield stress of $f_y=36$ ksi. All of strength conditions and serviceability conditions are simultaneously considered complying with AISC-LRFD specification. Where the displacement constraints considered as inter-storey drift < storey height/300. The effective length factors of the members are calculated as $K_x \geq 1.0$ for a sway permitted frame using a simplified form of the transcendental equations from

Dumonteil (Dumonteil, 1992). The out-of-plane effective length factor is specified as $K_y = 1.0$. Each column is considered unbraced along its length, and the unbraced length for each beam member is specified as 1/5 of the span length. Beam element groups were chosen from available steel sections (AISC database) with a set of 279 W-sections, while the column element groups were chosen from W14 and W12 sections (65 W-shapes). The size of the resulting search space is approximately $7.03(10^{18})$ designs.

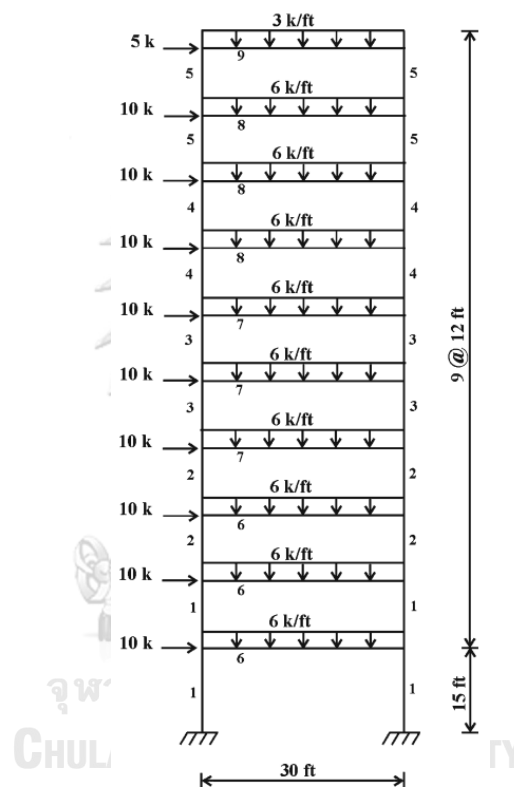


Fig . 4.11 One-bay ten-storey frame (Degertekin, 2008)

This frame was optimized by (Pezeshk et al., 2000) using a standard genetic algorithm (GA), (C. V. Camp et al., 2005) using an ant colony optimization (ACO), (Degertekin, 2008) using a harmony search (HS), (Toğan, 2012) using a teaching-learning based optimization (TLBO), (Doğan & Saka, 2012) using a particle swarm optimization (PSO), (A Kaveh & Talatahari, 2010) using an improved ant colony optimization (IACO), (Carraro et al., 2017) using a search group algorithm (SGA), (Farshchin et al., 2018) using a school-based optimization algorithm (SBO). The best design found by ESO algorithm is then compared with the above algorithms

Table 4.2 Optimization results obtained for the one-bay, ten-storey steel frame

Algorithm	Group no	Sections	Number of analyses	Weight (lb)
GA (Pezeshk et al., 2000)	1	W14X233	3000	65136
	2	W14X176		
	3	W14X159		
	4	W14X99		
	5	W12X79		
	6	W33X118		
	7	W30X90		
	8	W27X84		
	9	W24X55		
ACO (C. V. Camp et al., 2005)	1	W14X233	8300	62562
	2	W14X176		
	3	W14X145		
	4	W14X99		
	5	W12X65		
	6	W30X108		
	7	W30X90		
	8	W27X84		
	9	W21X44		
HS (Degertekin, 2008)	1	W14X211	3690	61864
	2	W14X176		
	3	W14X145		
	4	W14X90		
	5	W14X61		
	6	W33X118		
	7	W30X99		
	8	W24X76		
	9	W18X46		
TLBO (Toğan, 2012)	1	W14X233	4000	62562
	2	W14X176		
	3	W14X145		
	4	W14X99		
	5	W12X65		

	6	W30X108		
	7	W30X90		
	8	W27X84		
	9	W21X44		
PSO (Doğan & Saka, 2012)	1	W33X141		
	2	W14X159		
	3	W14X132		
	4	W14X99		
	5	W14X99	7500	64948
	6	W30X116		
	7	W21X68		
	8	W14X61		
	9	W40X183		
IACO (A Kaveh & Talatahari, 2010)	1	W14X233		
	2	W14X176		
	3	W14X145		
	4	W14X90		
	5	W12X65	2440	61820
	6	W33X118		
	7	W30X90		
	8	W24X76		
	9	W14X30		
SGA (Carraro et al., 2017)	1	W14X233		
	2	W14X176		
	3	W14X132		
	4	W14X99		
	5	W14X68	7980	62262
	6	W30X108		
	7	W30X90		
	8	W27X84		
	9	W21X50		
SBO (Farshchin et al., 2018)	1	W14X233		
	2	W14X176	11677	62430
	3	W14X145		

	4	W14X99		
	5	W14X61		
	6	W30X108		
	7	W30X90		
	8	W27X84		
	9	W18X46		
The present algorithm (ESO)	1	W14X257	4326	60974
	2	W14X211		
	3	W14X109		
	4	W14X82		
	5	W14X61		
	6	W30X99		
	7	W30X99		
	8	W24X62		
	9	W24X62		

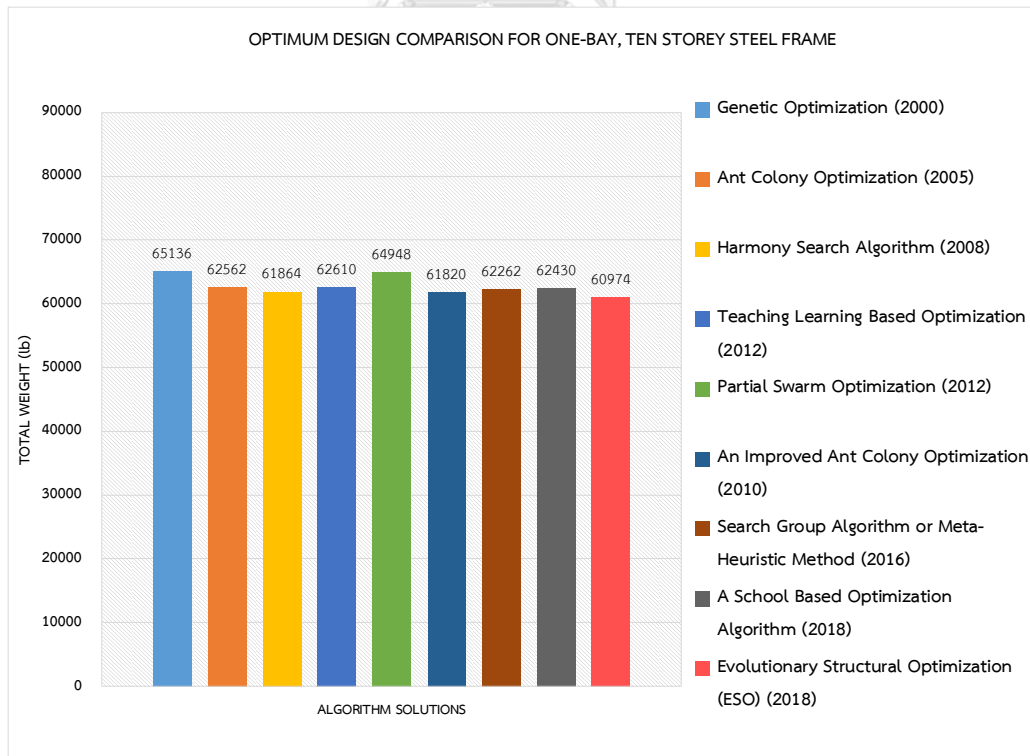


Fig . 4.12 Optimum design coMParison for one bay, ten-storey steel frame

The best solution obtained by the ESO algorithm are given in Table 4.2 and Figure 4.12. The optimum design is obtained after 4326 structural analyses with the minimum weight of 60974 lb, which is 6.4% lighter than the design of GA, 2.4% lighter than the design of ACO, 1.4% lighter than the design of HS, 2.6% lighter than the design of TLBO, 6.1% lighter than the design of PSO, 1.4% lighter than the design of IACO, 2.1% lighter than the design of SGA, 2.3% lighter than the design of SBO. The number of structural analyses required 4326, which is significantly less than 8300 frame analyses for the ACO, 7500 frame analyses for the PSO, 7980 frame analyses for the SGA, and 11677 frame analyses for the SBO. However, it was more than 3000, 3690, 4000, 2440 analyses required by GA, HS, TLBO and IACO, respectively.

The convergence history, the maximum stress ratio and the maximum inter-storey drift obtained by the ESO algorithm are presented in Figures 4.13-4.15. All the maximum stress ratios were under the upper limit. The critical scaling ratio of maximum stress ratio and the maximum inter-storey drift within 100% at the best solution. This indicate that the optimum solution satisfied its given constraints.

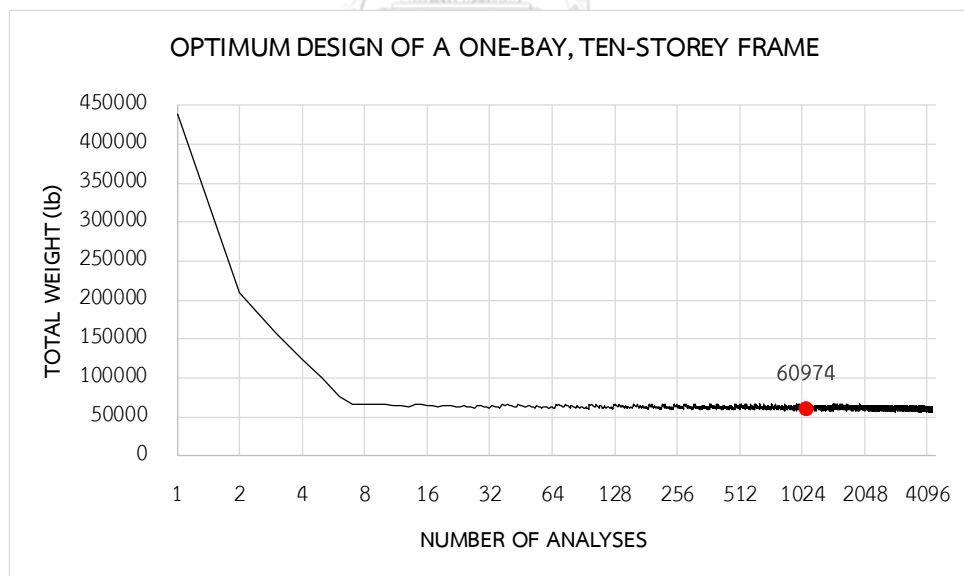


Fig . 4.13 Convergence history of one-bay ten-storey frame design

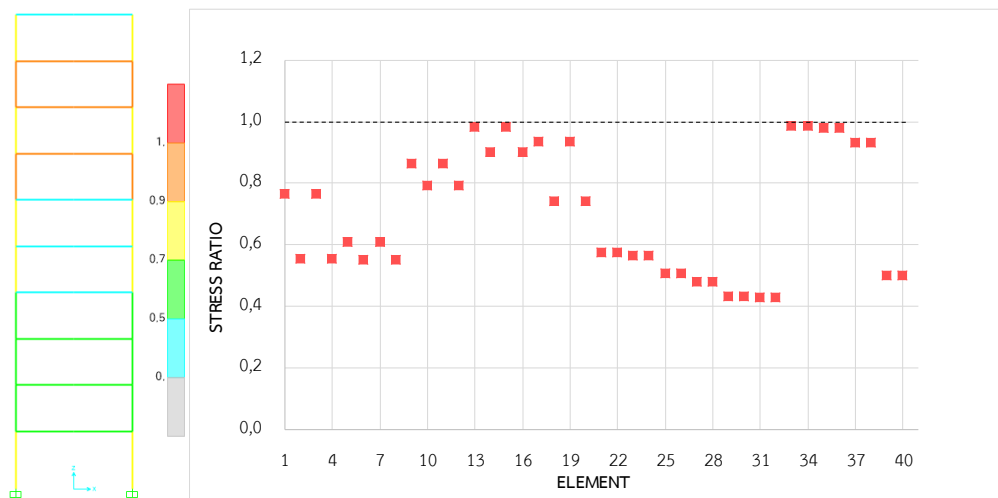


Fig . 4.14 stress ratio for members of one-bay ten storey frame

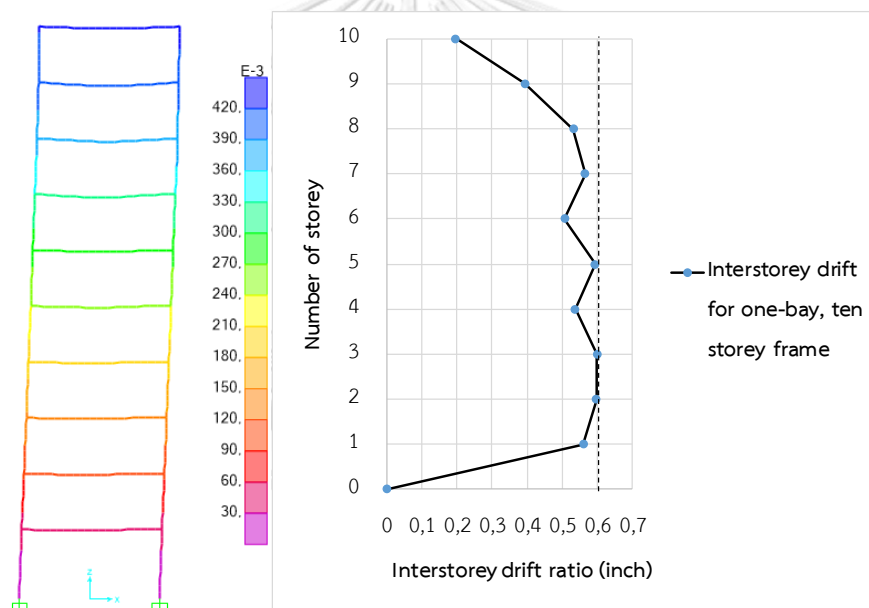


Fig . 4.15 Interstorey drift for one-bay ten-storey frame

4.1.5 Concluding Remarks

The ESO method is efficiently applied for discrete sizing optimization problems with strength and serviceability conditions complying with AISC-LRFD under applied forces. The optimum design of the structure is obtained by simply repeating the cycle of finite element analysis and resizing elements as an “*Elimination Process*” until one of the constraints reaches its given limit. Unlike other optimization methods, the number of design variable is not a restriction in the ESO. Hence this

method is suitable for designing practical structures with a large number of sections and it can be easily implemented any of the existing finite element codes.

The practical applications and simplicity of the ESO are demonstrated by testing on a benchmark steel frame, the optimum results are then compared with a number of successfully solved the same benchmark steel frame in the literature. Since the value of MRR is flexibly changed during the ESO process, it is also a drawback of the ESO algorithm. After terminating the main ESO procedure, the final area of each group is multiplied by the MRR to search all neighborhoods (cross-sectional areas) closed to the current cross-sectional areas. If the value of MRR is taken too large, resulting in a numerous number of sections are found in each group. Consequently, all possible trials of each group will perform the explosive search surrounding these area values over a large search space. This is not efficient in terms of computational time. Therefore, a PSO algorithm will be proposed to deal with this difficulty in the next section.

4.2 Particle Swarm Optimization (PSO)

4.2.1 Algorithm Overview

The development of meta-heuristic algorithm in stochastic search techniques of numerical optimization have provided efficient optimum design tools for the structural design. One of the attractive algorithms is particle swarm optimization (PSO). The first was developed by Eberhart and Kennedy (1995). The PSO algorithm is a population-based stochastic optimization technique, which belongs to the family of the algorithm based on the concept of swarm intelligence. The algorithm was inspired by the information circulation and the collective behavior was observed in bird flocks and fish schools. They will adjust their physical movement to avoid predators, seek food and mates. The behavior concerned with grouping by social force that depends on both the “memory” of each individual (particle) as well as the knowledge gained by the entire swarm (Doğan & Saka, 2012). The implementation of the algorithm can be summarized in terms of three main principles “*evaluating, comparing, and imitating*”.

4.2.2 Basic of Particle Swarm Optimization

4.2.2.1 Mathematical Formulation of PSO Algorithm

The PSO algorithm has been used to obtain the optimum solution by applying special strategies, which are derived from the kinematic equation in physics. The PSO make use of a velocity vector to update the current position of each particle in the swarm. The updated velocity and position equations are illustrated in the two simple mathematical equations (Perez & Behdinan, 2007; Venter & Sobieszczanski-Sobieski, 2003).

$$v_{k+1}^i = wv_k^i + c_1r_1 \frac{(p_k^i - x_k^i)}{\Delta t} + c_2r_2 \frac{(p_k^g - x_k^i)}{\Delta t} \quad (43)$$

$$x_{k+1}^i = x_k^i + v_{k+1}^i \Delta t \quad (44)$$

Where v_{k+1}^i is the corresponding updated velocity vector, and Δt is the time step value (Y. Shi & R. Eberhart, 1998). Throughout the present work a unit time step is used. The velocity vector of each particle is calculated as shown in Eq. (43) and illustrated in Figure 4.16.; v_k^i is the velocity vector at iteration k ; p_k^i represents the personal best position of particle i , and p_k^g corresponds to the global best position in the entire swarm up to iteration k ; w is the inertial weight; x_k^i is the position of particle i at iteration k ; x_{k+1}^i is the position of particles at iteration $k+1$ is numerically updated.

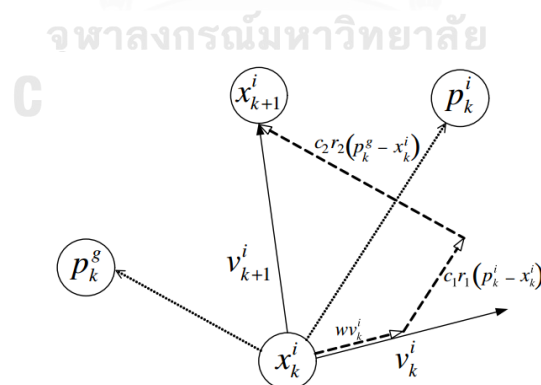


Fig . 4.16 PSO position and velocity update (Perez & Behdinan, 2007)

4.2.2.2 Initial Swarm

In this thesis, all initial swarms were randomly distributed throughout the design space. The design search space is controlled between the lower bound and the

upper bound. The number of particles (N) may be taken sufficient to get acceptable results. Each particle in the swarm maintains a velocity vector (both direction and speed) and a position vector to move around search space. The following equations are used to obtain the random initial position and velocity vectors (Venter & Sobieszczanski-Sobieski, 2003).

$$\begin{aligned} x_0^i &= x_{\min} + r_3(x_{\max} - x_{\min}) \\ v_0^i &= \frac{x_{\min} + r_4(x_{\max} - x_{\min})}{\Delta t} \end{aligned} \quad (45)$$

Where x_{\min} and x_{\max} represent the lower and upper design variables bounds respectively. Note that both magnitudes of the position and velocity values will be bounded, as large initial values will lead to large initial momentum and positional updates. This large momentum causes divergence of the global best solution.

4.2.2.3 Inertial Weight Update

The inertial weight plays an important role in the PSO convergence behavior. Since this is the consequence of excessive momentum in the particles, which results in large step sizes that exceed the best design areas. During the initial optimization stages, a large initial weight is needed in order to the design space to be searched thoroughly. Once the most promising areas of the design space have been discovered and the convergence rate starts to slow down, the inertia weight should be reduced so that the particles' momentum decreased, allowing them to concentrate in the best design areas. To accomplish the above strategy, Y. Shi and R. C. Eberhart (1998) proposed a dynamic variation of the inertia weight. Additionally, the authors suggested using $0.4 < w < 0.9$ to achieve the best performances, starting with larger w values (a more global search behavior) that is dynamically reduced (a more local search behavior) during the optimization. A commonly used inertia update rule is the linearly decreasing inertia weight (Marini & Walczak, 2015) what is calculated by the following formula in Eq. (46).

$$w_{k+1} = w_{\max} - \frac{w_{\max} - w_{\min}}{iter_{\max}} iter_{current}, \begin{cases} w_{\max} = 0.9 \\ w_{\min} = 0.4 \end{cases} \quad (46)$$

4.2.2.4 Design Variable Bounds Handling

We can easily determine x_{min} and x_{max} of design variables for each group (Plevris & Papadrakakis, 2011)

$$x_k \in U(x_k^{\min(lowerbound)}, x_k^{\max(upperbound)}), (k = 1, nd) \quad (47)$$

When the updated velocity vector and the updated position vector of Eq. (43) and Eq. (44) forced a particle to move outside the bounds, the design variable x_k is reset to the closest bound ($x_k = x_k^{lowerbound}$ or $x_k = x_k^{upperbound}$).

4.2.2.5 Main PSO Parameters

The basic PSO has only few parameters to adjust. Table 4.3 shows a list of the main parameters (Plevris & Papadrakakis, 2011).

Table 4.3 Main PSO parameters

Symbol	Description	Details
N	Number of particles	A typical range is 10-40. For most problems, 10 particles is sufficient enough to get acceptable results. For some difficult or special problems, the number can be increased up to 50-100.
w	Inertial weight	Usually is set to a value less than 1. It can also be updated during iterations. A linear, decreasing variation is common.
x^L, x^U	Vectors containing the lower and upper bounds of the n design variables, respectively.	They are determined by the problem to be optimized. Different ranges for different dimensions of particles can be applied in general.
c_1, c_2	Cognitive and social param	They represent "trust" param indicating how much confidence the current particle has in itself and in the swarm. Usually $c_1=c_2=2$.
r_1, r_2, r_3, r_4	Random numbers	They are independent random numbers with uniform distribution in the interval $r \in [0,1]$
$iter_{max}$	Maximum number of iterations for the termination criterion	Determined by the complexity of the problem to be optim

4.2.2.6 Constraint Handling Techniques

Various methods have been proposed for handling constraints for the PSO in general. One of which is based on penalty functions. The penalty function is an effective auxiliary tool to deal with constrained problems in general and has been a popular approach because of its simplicity and ease of implementation. This study considers a structural optimization problem where displacement and stress constraints are imposed. The objective function value is computed and a finite element analysis is performed for the constraints check where each structural element is checked for stress violation, and each model node is checked for displacement violation. If no violation is detected, then no penalty is imposed on the objective function $W(\mathbf{X})$. If any constraints are violated, a penalty is applied to the objective function (Fourie & Groenwold, 2002; Perez & Behdinan, 2007; Plevris & Papadrakakis, 2011).

$$W_{new} = W(\mathbf{X}) + \alpha \sum_{t=1}^T \theta_t (g_t) [g_t(x)]^2$$

with (48)

$$\theta_t (g_t) = \begin{cases} 1 & g_t(x) > 0 \\ 0 & g_t(x) \leq 0 \end{cases}$$

Where α is the penalty coefficient; θ_t is the weight coefficient for t^{th} constraint condition and $g_t(x)$ is the set of constraints.

However, some experimental results indicate that such a technique will reduce the efficiency of the PSO, because it resets the infeasible particles to their previous best position, which sometimes prevents the search from reaching a global minimum and some complex optimization problems in which require a careful fine-tuning of the penalty factors that estimate the degree of penalization to be applied in order to balance the objective and penalty functions (Coello, 2002; L. Li et al., 2007).

4.2.2.7 Termination Criteria

The convergence criteria have to be applied for the termination of the optimization procedure. Two convergence criteria were adopted for the PSO algorithm. The first one is the maximum number of iterations and the second

criterion terminates the process when an acceptable solution is achieved in some number of iterations. In this thesis, a predetermined maximum iteration number is used to terminate the PSO algorithm.

4.2.3 Strategy in PSO for Tackling Discrete Structural Optimization Problems

Originally PSO algorithm is developed for continuous design variables. However, the PSO algorithm is also well-suited to handle non-smooth and non-convex design space with discontinuities. In fact, the design variables are selected from standard sections or commercially available from manufacturers. Therefore, the presence of nonlinear design criteria and the requirement for discrete steel sections unfortunately makes the generic problem falling within a challenging class of non-convex and non-smooth optimization problems, called mixed integer nonlinear programming (MINLP) problem (Tangaramvong & Tin-Loi, 2013). In this thesis, a modified version of the PSO algorithm is presented in order to solve discrete optimization problems for steel structures.

First, a mapping is performed; every member of a predefined set for the design variables is mapped to an integer number which is called “*Integer Codification*”, starting from 1 to ms (L. Li et al., 2007; Plevris, Batavanis, & Papadrakakis, 2011). By this way, the discrete optimization problems transformed into an integer optimization problem. The integer design space represents the detailed position of each particle in a swarm, as well as the position of cross-sections are listed in each group. Based on the concept of the PSO algorithm a particle or a cross-section from vector I_i is assigned randomly to each member group in every iteration step.

$$\begin{cases} \mathbf{X} \in \mathfrak{R}^{ng} = [A_1, A_2, A_3, \dots, A_i] \\ A_i = [x_1, x_2, x_3, \dots, x_{nd}], i = 1, \dots, nd \end{cases} \Rightarrow \begin{cases} A_i \in \mathbb{Z}^n, 1 \leq A_i \leq ms \\ I_i = A_i(x_1 = 1) \in \{1, 2, 3, \dots, ms\} \end{cases} \quad (49)$$

Where ng is the total number of groups, ms is the total number of sections considered in the design for group i ; \mathbb{Z}^n is the set of integer numbers, A_i is now a vector of integer values, representing the sequence numbers of standard steel sections.

Second, the integer space is treated the same as the continuous one with the modification that Eq. (43) for the particle’s velocity is rounded to the nearest integer

value. A round-off function is used to round a number to its nearest integer. The equation for velocity takes the following format:

$$v_{k+1}^i = \text{round} \left[wv_k^i + c_1 r_1 \frac{(p_k^i - x_k^i)}{\Delta t} + c_2 r_2 \frac{(p_k^g - x_k^i)}{\Delta t} \right] \quad (50)$$

The main concern of the rounding-off approach is the selection of variables to be increased and the variables to be decreased. The strategy may no guarantee for (leaving alone the global one) optimum solution in view of the intrinsic non-convex and non-smooth optimization problems, especially in case of high nonlinearity and widely separated allowable discrete values (Arora, 2000).

4.2.4 Pseudo Code of PSO algorithm

The pseudo-code of PSO can be summarized as follows:

Step 1. Initialize Optimization

Step 1.1 Initialize algorithm constants, $N, iter_{\max}, c_1, c_2, x^L, x^U, I_i$

Step 1.2 Set $k=1$

Step 1.3 Initialize randomly all particles position $x_k^i \in A_i$ or $I_i, i=1, \dots, N$ in \mathbb{Z}^n and velocity v_k^i in Eq. (45).

Step 1.4 Evaluate objective function value as $W(x_k^i)$.

Step 1.5 Assign best position $p_k^i = x_k^i$ with

$$W(p_k^i) = W(x_k^i) = \min(W(x_k^1), W(x_k^2), W(x_k^3), \dots, W(x_k^i)), i = 1, \dots, N$$

Step 1.6 Assign $Pbest_k^i = W(p_k^i)$ and initialize $p_k^g = p_k^i$ and $Gbest_k = W(p_k^g)$

Step 2. Perform Optimization

While ($k \leq iter_{\max}$)

Step 2.1 Calculate inertial weight coefficient by Eq. (46).

Step 2.2 Update particle velocity v_k^i and position x_k^i , according to Eq. (43) and Eq. (44) of all N particles.

Step 2.3 Evaluate objective function value as $W(x_k^i)$ in Eq. (16) and Eq. (48).

Step 2.4 Update particle best position

$$p_{k+1}^i = \begin{cases} p_k^i & : W(x_{k+1}^i) \geq Pbest_k^i \\ x_{k+1}^i & : W(x_{k+1}^i) < Pbest_k^i \end{cases}, k \in [1, \dots, iter_{\max}]$$

Step 2.5 Find the personal best value, corresponding to the objective function value

$$Pbest_k = W(p_k^i)$$

and the global best value in the entire swarm up to the current iteration.

$$p_k^g \in \{p^1, p^2, p^3\} | W(p_k^g) \text{ with}$$

$$W(p_k^g) = \min(W(p^0), W(p^1), W(p^2), \dots, W(p^N))$$

$$\Rightarrow Gbest_k = W(p_k^g)$$

Step 2.6 Increment iteration count $k=k+1$

End while

Step 3. Report best solution p_k^g of the swarm with objective function value

$$Gbest = W(p_k^g), k = 1, \dots, iter_{max}$$

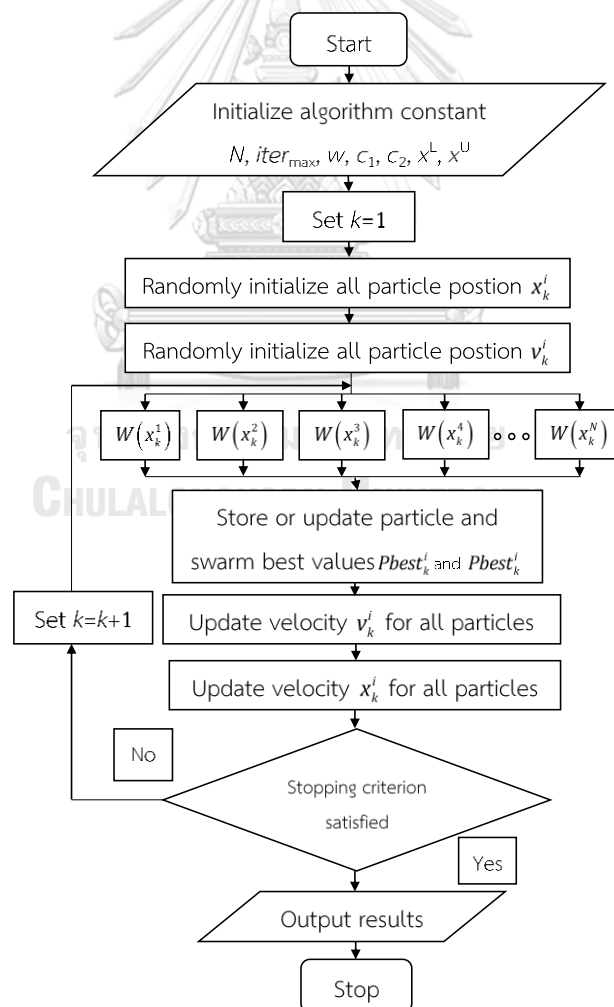


Fig . 4.17 Flowchart of PSO algorithm

4.2.5 BenchMark Test Function

Standard benchmark test function is used to test the accuracy, robustness and speed of coverage of the PSO algorithm. In this thesis, Rosenbrock's valley is known as a "banana function" as shown in Figure 4.18, which is applied to assess the quality of the PSO algorithm. Finding the valley is easy to find, but finding the global minimum is difficult because the global minimum lies in a narrow, parabolic valley. Many algorithms converge slowly because they must change their search direction repeatedly. This function is defined as:

$$f = \sum_{i=1}^{n-1} 100(x_{i+1} - x_i^2)^2 + (1 - x_i)^2; -2.048 \leq x_i \leq 2.048 \quad (51)$$

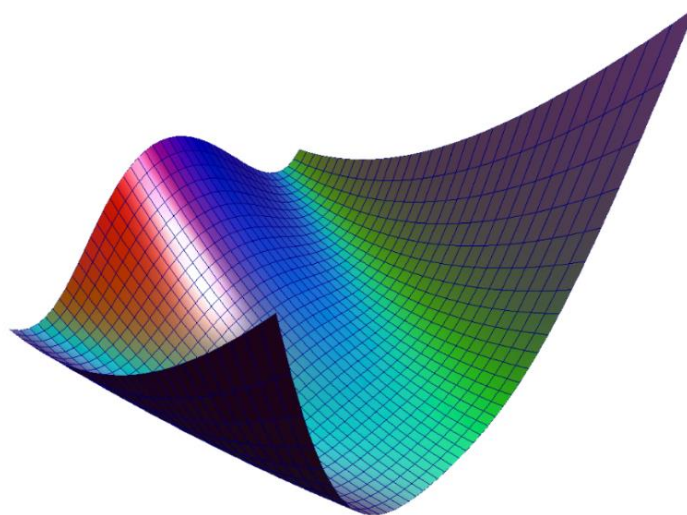


Fig . 4.18 Rosenbrock function (source on internet)

For this study, two design variables (x_1, x_2) were chosen. The global minimum value was known to be $f(x)=0.0$ with the corresponding design variable values $x=(1.0,1.0)$. To demonstrate the speed of convergence as well as the accuracy of the PSO algorithm, the function was tested on a set of the number of particles ($N=20, 40, 60, 80, 100$) with cognitive and social scaling parameters, $c_1=c_2=2.0$ with maximum and minimum values of inertial weights, $w_{\max}=0.9, w_{\min}=0.4$ with maximum number of iterations, $k_{\max}=100$. Details of the results are presented in Table 4.4 and Figure 4.19

Table 4.4 Results of the objective function value

N	$f(x_1, x_2)$	x_1	x_2
20	0.1084162	0.89186067	0.82651563
40	0.0456564	1.10881864	1.21108996
60	0.0039248	1.00857465	1.01101693
80	0.0011459	0.96821717	0.93627944
100	0.0007025	1.02600959	1.05218584

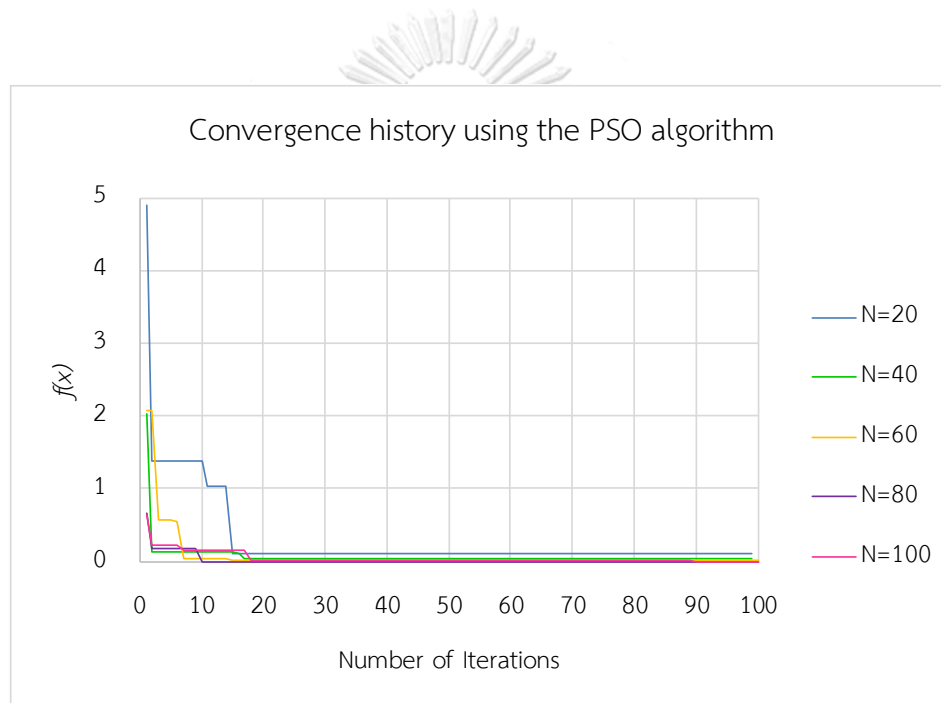


Fig . 4.19 Convergence history of Rosenbrock function using the PSO algorithm

Almost all the objective function values converge near the global minimum value $f(x) \approx 0$ and the algorithm can reach the optimum solution in relatively less number of iterations. The accuracy and the speed of convergence are improved when we use a large number of particles. It can be concluded that the PSO algorithm is rather efficient in terms of accuracy and computational time. However, the PSO algorithm is generally developed for continuous design variables. To be able to use method for solving discrete design variables, a discrete version of the PSO algorithm is proposed as illustrated in section 4.2.3.

4.3 A Mixed ESO-PSO Approach for Optimum Design

4.3.1 The procedure of the Mixed ESO-PSO Approach

This section presents an improvement in the ESO algorithm using the PSO algorithm, called a mixed ESO-PSO approach. The generic idea is based on the implementation of a well-known evolutionary structural optimization algorithm (ESO), and further integrates a mapping, underpinning particle swarm optimization (PSO). Their concept were explained in the previous sections. The flowchart of the mixed ESO-PSO approach is shown in Figure 4.20.

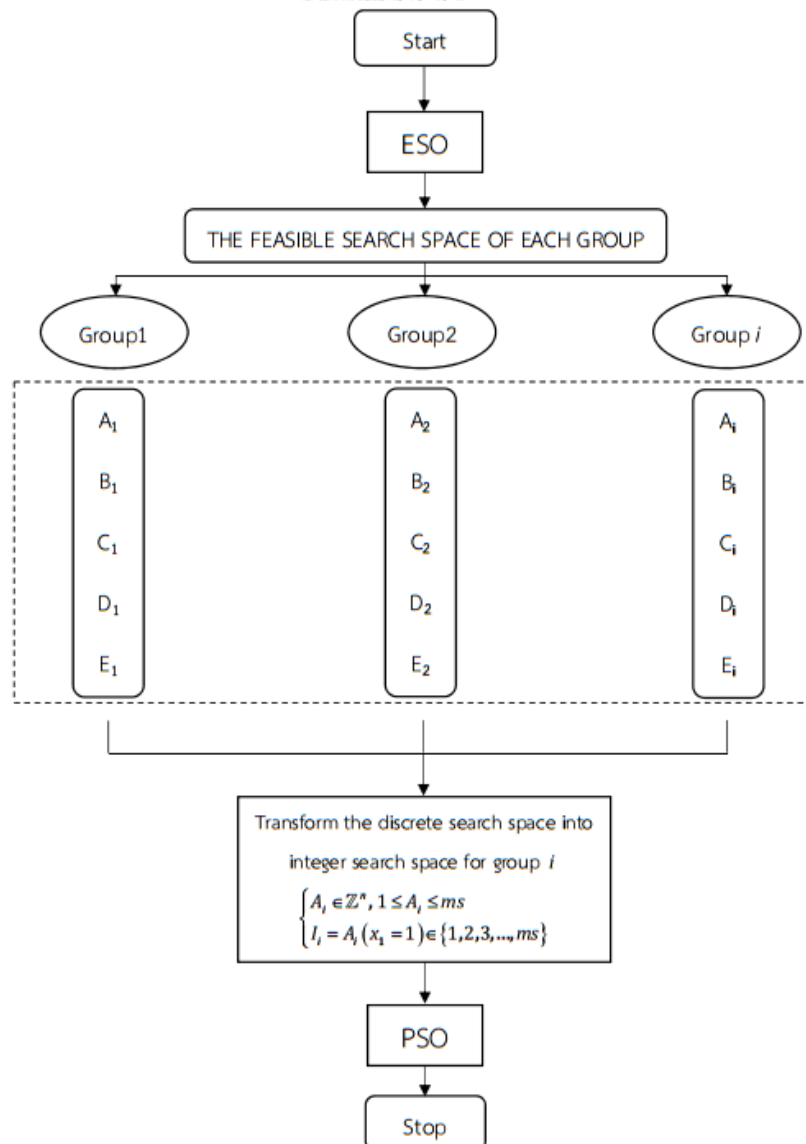


Fig . 4.20 Flowchart of the mixed ESO-PSO approach.

The proposed algorithm is divided into two separate phases. During the first phase, the ESO algorithm explores the search space thoroughly and detects the neighborhoods by eliminating ineffective design variables or even infeasible design domains. As a result, the sizes of discrete variable entries prior is accordingly reduced. When the ESO process terminates, the design search space is narrowed down to a relatively small search space. However, an enumerative search is significantly slow to find an optimum solution. This results in enormously time-consuming structural analyses. Hence the PSO algorithm is applied in the second phase as a global search to discover reasonable quality solutions. The second phase starts from the best estimate of the ESO algorithm. The PSO helps the ESO process not only to accelerate the speed of convergence but also to efficiently reach the optimum or near optimum solution.

4.3.2 Test on BenchMark Steel Frame

The effectiveness of the mixed ESO-PSO approach is tested on the same as benchmark steel frame, which is applied by using the ESO algorithm in section 4.1.4.1. The results confirm the validity and provide a comparison between the performance of the proposed algorithm and the other meta-heuristic optimization in the literature.

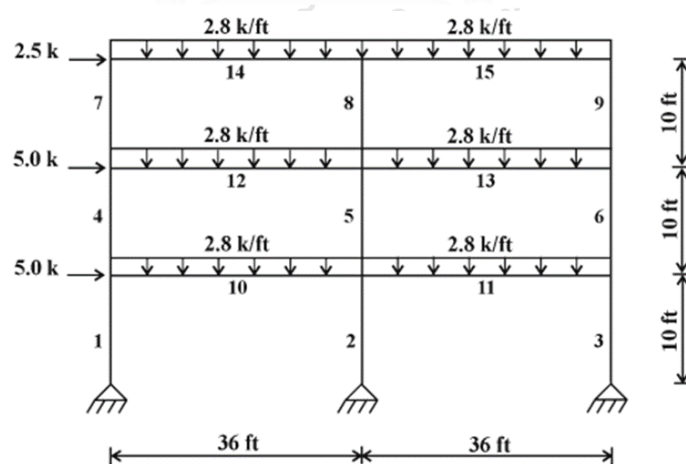


Fig . 4.21 Two-bay, three storey planar steel frame (Degertekin, 2008)

Two cases are only considered. In Cases 1 and 2, members of the steel frame are divided into two groups. The imposed fabrication conditions require that all six

beams be of the same group with a set of the entire 274 W-sections from AISC database. The column group section of Case 1 is limited to W10 sections resulting in 18 W-sections. The size of the resulting search space has an exhaustive search of 4,932 structural analyses. However, the column group sections in Case 2 are chosen from all 274 W-sections. The resulting search space has an exhaustive search of 75,076 structural analyses.

Table 4.5 and Figure 4.22 summarize the optimization results and the convergence history developed and compared with applying different algorithms for the two-bay, three-storey steel frame problem. The algorithm took only couple of minutes to converge the optimum solution. In this study, the optimum weight of Case 1 has the same optimization results with the other algorithms as 18,792 lb. The mixed ESO-PSO method excellent obtained within the modest 14 analyses for both cases, which is significantly less than 1800 frame analyses for the GA, 3000 analyses for the ACO, 200 analyses for the DDHS, and 100 analyses for the SGA. However, The lowest weight in Case 2 yielded approximately 1.2% lighter than Case 1 and all other reported results.

Table 4.5 Optimization results obtained for the two-bay, three storey steel frame

Algorithm	Case	1. Beam	2. Inner columns	3. Outer columns	Number of analyses	Weight (lb)
GA	1	W24X62	W10X60		1,800	18,792
ACO	1	W24X62	W10X60		3000	18,792
DDHS	1	W24X62	W10X60		200	18,792
SGA	1	W24X62	W10X60		100	18,792
ESO	1	W24X62	W10X60		16	18,792
	2	W24X62	W12X58		41	18,624
	3	W24X62	W12X53	W14X53	84	18,192
ESO-PSO	1	W24X62	W10X60		14	18,792
	2	W24X62	W16X57		14	18,561

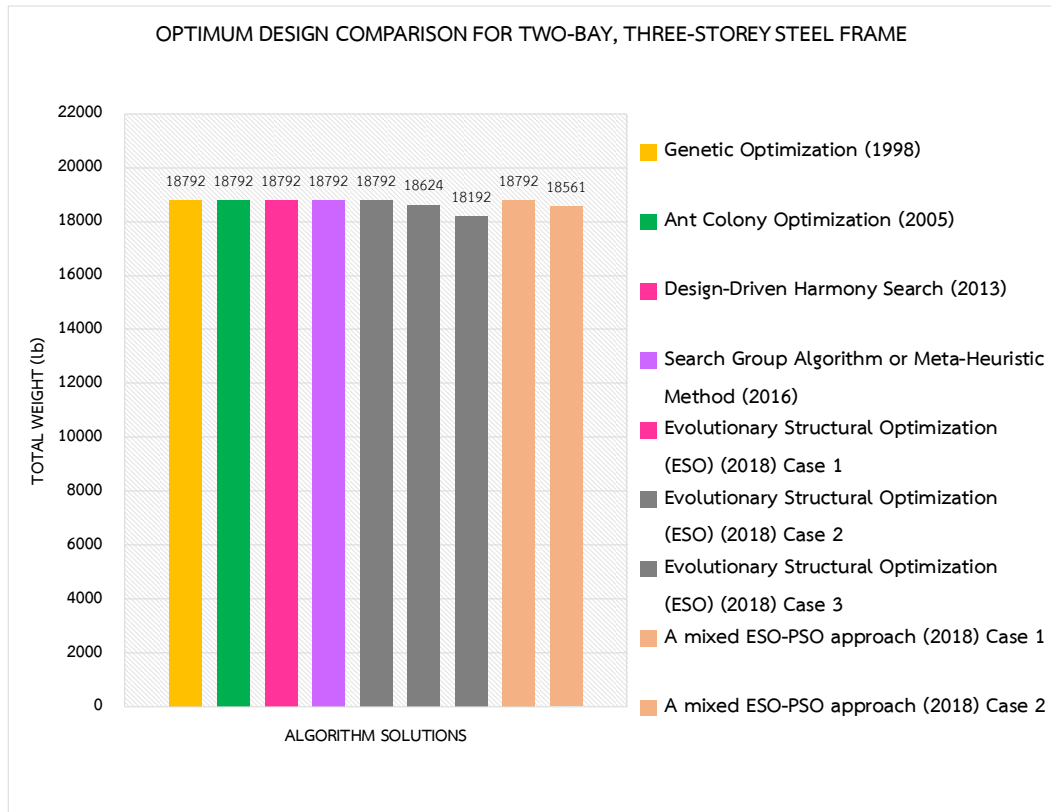


Fig . 4.22 Optimum design coMParison for the two-bay, three-storey steel frame

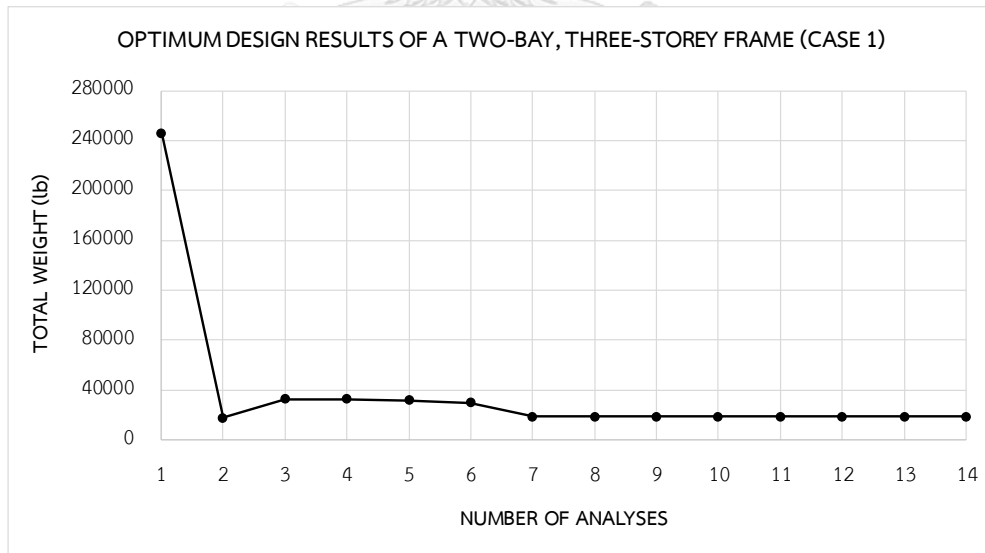


Fig . 4.23 Convergence history of two-bay three-storey frame design (Case 1)

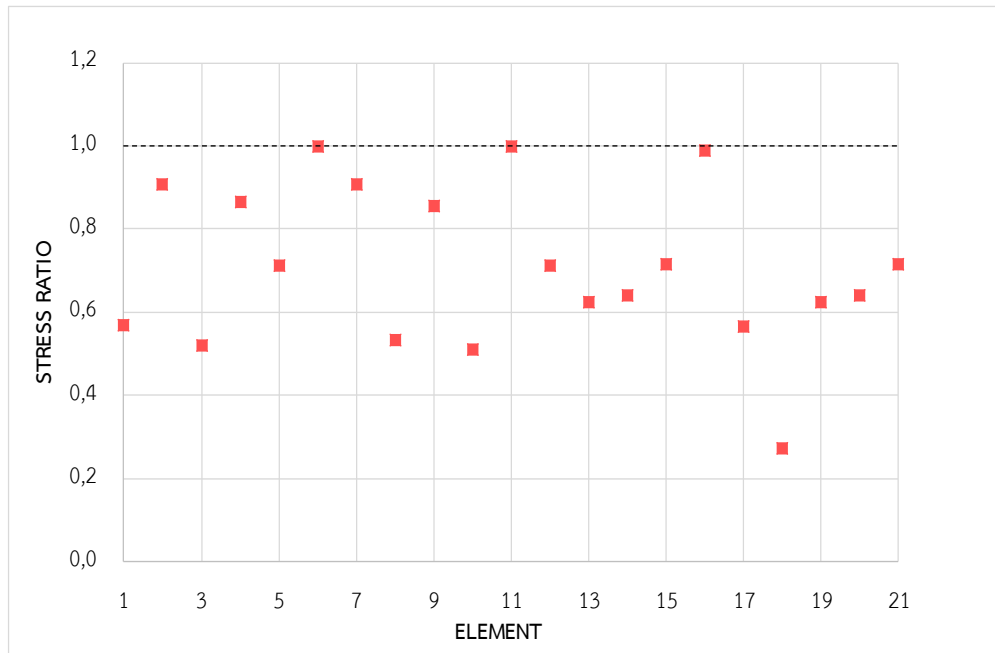


Fig . 4.24 Stress ratio for members of two-bay three storey frame (Case 1)

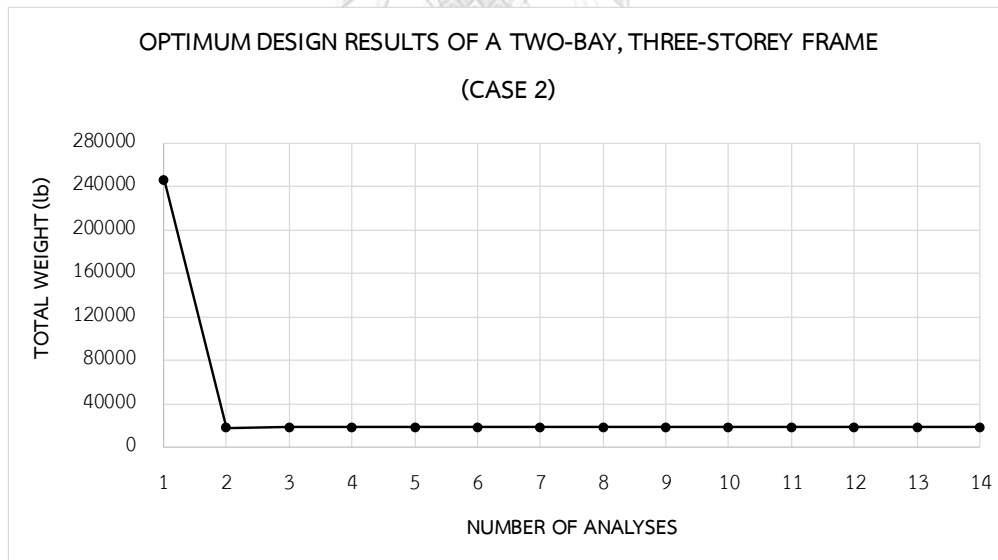


Fig . 4.25 Convergence history of two-bay three-storey frame design (Case 2)

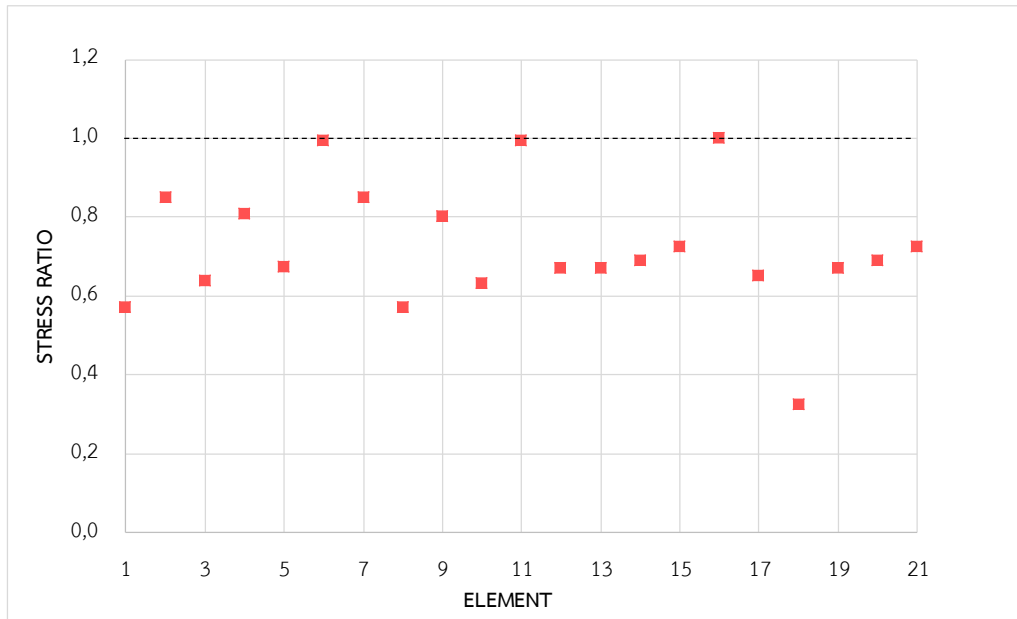


Fig . 4.26 Stress ratio for members of two-bay three storey frame (Case 2)

The convergence history and the critical scaling factor ratios obtained by the mixed ESO-PSO algorithm are shown in Figures 4.18-4.21. The algorithm took only couple of minutes to converge the optimum solutions. All the critical scaling ratios of the maximum stress in three cases were under the upper limit. For all cases, the critical scaling ratio of maximum stress ratio within 100% at the best solution. This indicate that the optimum solution satisfied its given constraints.

CHAPTER 5

OPTIMUM DESIGN OF COLD-FORMED STEEL ARCH WAREHOUSE STRUCTURES

5.1 Optimization Scheme of Arch Steel Warehouse Structures

In the optimization scheme, the procedure is automatically performed as an iterative process. The mixed ESO-PSO procedure and various constraints are coded directly using a post-processing Microsoft Visual Basic Application environment, whilst the response of a structure with assigned specific material cross-sections is computed using a commercial analysis software (SAP2000). The transparent interface between the two computer programming environment is enabled through a so-called Open Application Programming Interface (OAPI). The OAPI functions can help to access the model and control all of the analysis and design from SAP2000 software easily as shows in Figure 5.1.

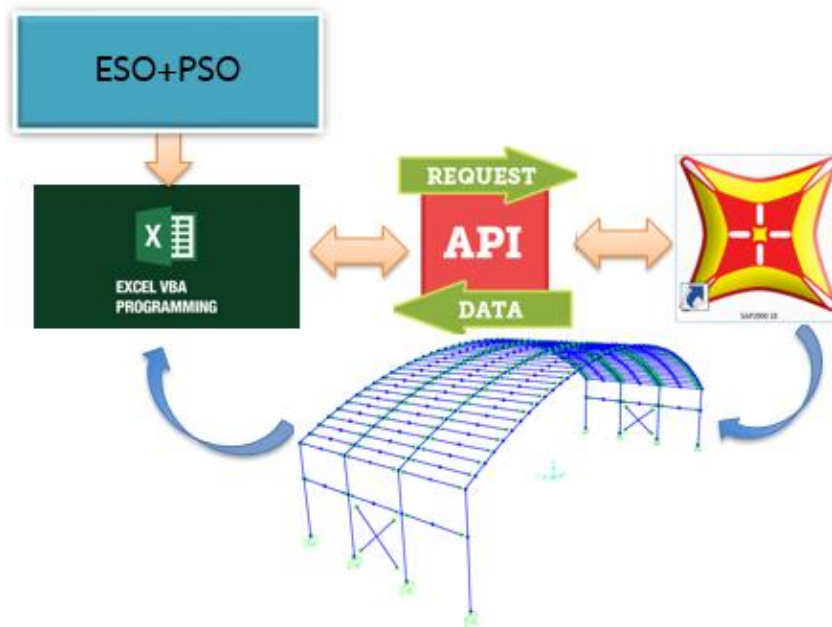


Fig . 5.1 Optimization scheme of arch steel warehouse structures

5.2 Optimization Results and Discussion

Figure 5.2 shows the layout as well as the main components of optimum design arch steel warehouse structures. The structure is divided into five member groups including arched roofs (G1), columns (G2), purlins (G3), column bracings (G4) and roof beams (G5). The loading conditions and material properties are discussed in section 3.1. The advanced analyses of 3D arch steel warehouse structures are directly performed in SAP2000 software under non-linear static conditions.

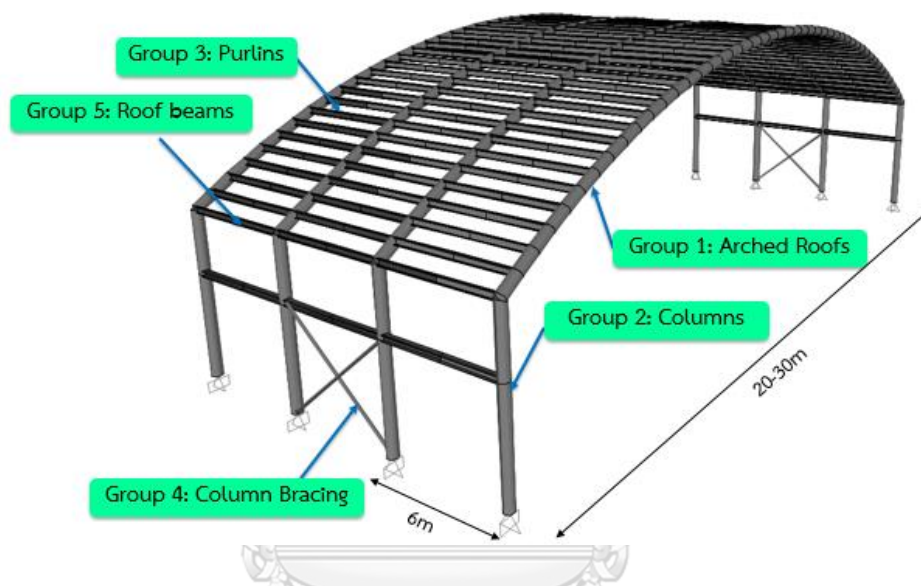


Fig . 5.2 The main components of optimum design arch warehouse structures

The aim of work is to minimize the total weight of material distributed over an arch steel warehouse structure considering simultaneously ultimate strength and serviceability conditions complying with AISC-LRFD and AISI-LRFD specifications. All constraints are checked by SAP2000. The mixed ESO-PSO approach is proposed to deal with discrete design variables. In this thesis, an available steel table of cold-formed steel hollow sections and C-sections are provided from manufacturers with a set of 192 HS-sections and 13 C-sections. The column group and arched roof group are chosen from all 192 HS-sections. However, the column bracing group and roof beam group are limited to CHS sections resulting in 69 CHS-sections. While the purlin group is only chosen from 13 C-sections. The size of the exhaustive search is approximately 2.28×10^9 structural analyses. The member effective length are assumed as $K_x=1$ and $K_y=1$.

Optimum design of arch warehouse structures are performed with roof spans ranging from 20 m to 30 m, bay length of 6 m, and eave height of 8 m. Optimization results of each span length are shown in the following tables and figures.

a) Optimization results of arch warehouse structures with a 20-m span

Table 5.1 Optimum sections obtained for arch warehouse structure with a 20-m span

Group	Name of Section	Ratio	Displacement X (m)	Displacement Z (m)	S_s	$S_{d(x)}$	$S_{d(z)}$	S_{Max} Group
G1	RHS350x150x6	0.9	0.0000	0.0374	0.9	0.0	0.4	0.9
G2	CHS355,6(14")x6	1.0	0.0125	0.0001	1.0	0.8	0.0	1.0
G3	CC250X25	0.5	0.0000	0.0052	0.5	0.0	0.2	0.5
G4	CHS89,1(3")x2,8	0.8	0.0000	0,0001	0.8	0.0	0.0	0.8
G5	CHS101,6(3.1/2")x3,2	0.6	0.0000	0.0202	0.6	0.0	0.8	0.8

The deflection limits: $H/100=0.08$ m; $L/240=0.08$ m

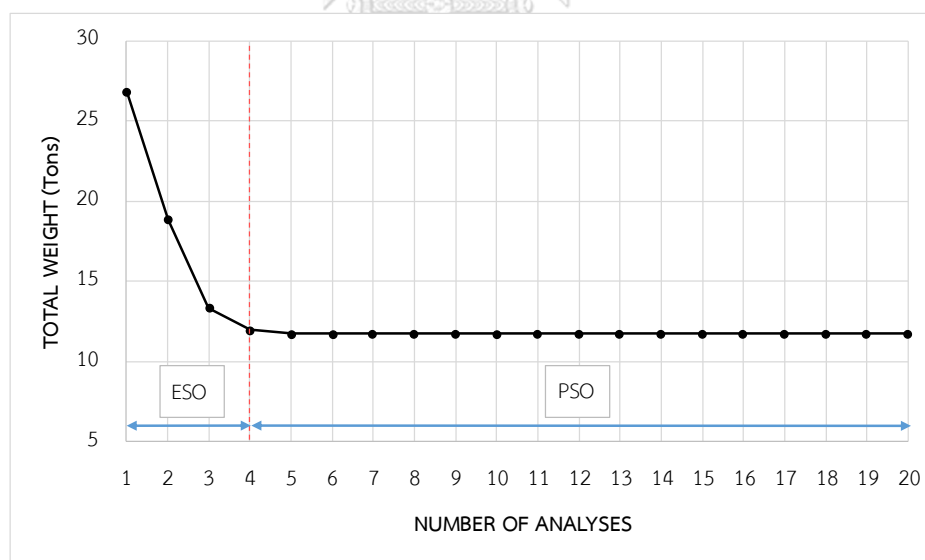


Fig . 5.3 Convergence history with a 20-m span

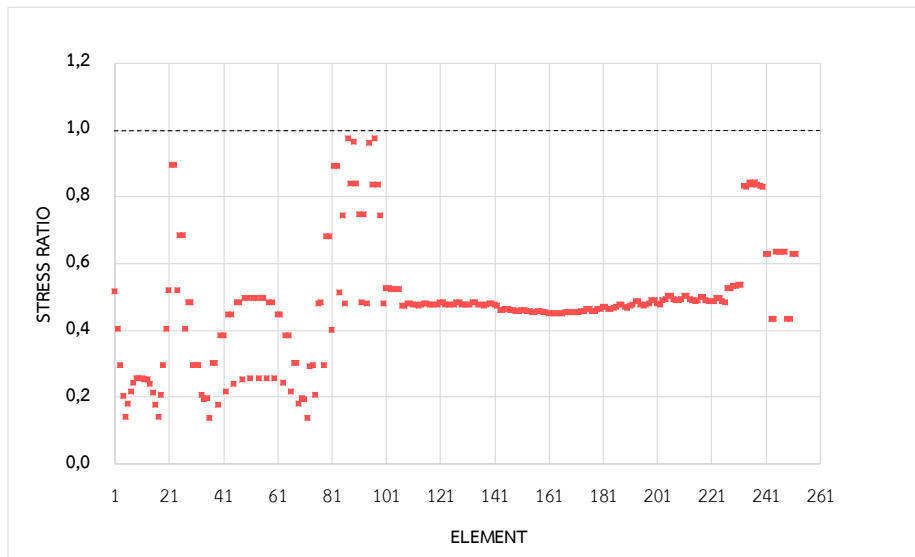


Fig . 5.4 Stress ratio for members with a 20-m span

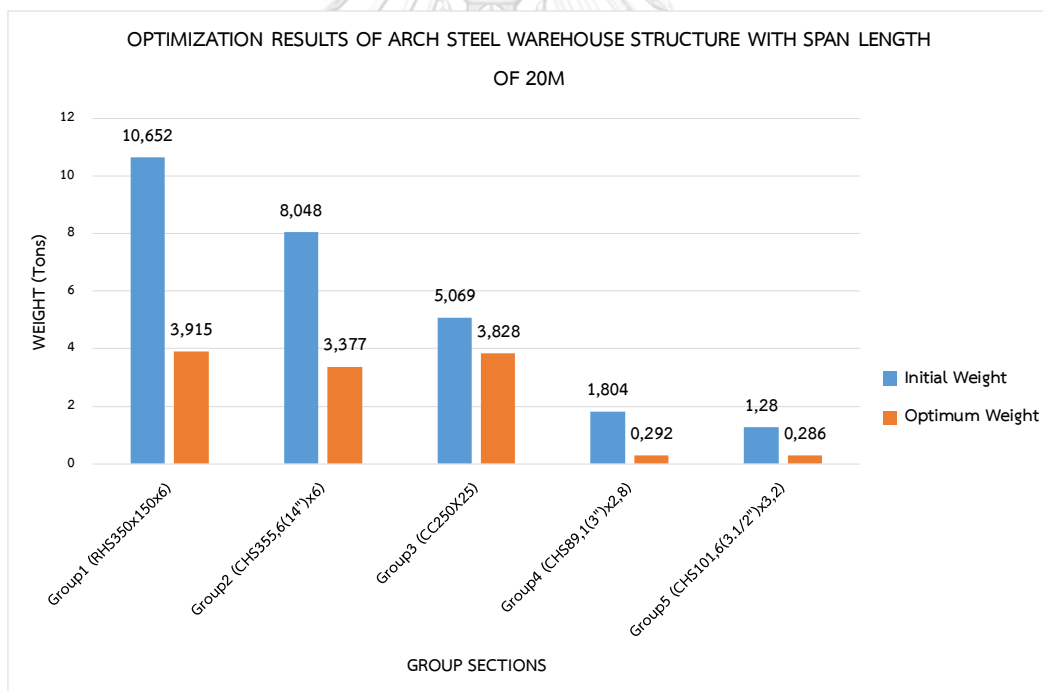


Fig . 5.5 Material distributed over an arch warehouse structure with a 20-m span

b) Optimization results of arch warehouse structures with a 25-m span

Table 5.2 Optimum sections obtained for arch warehouse structure with a 25-m span

Group	Name of Section	Ratio	Displacement X (m)	Displacement Z (m)	S_s	$S_{d(x)}$	$S_{d(z)}$	S_{Max} Group
G1	RHS400x200x6	0.9	0.0000	0.0462	0.9	0.0	0.4	0.9
G2	RHS350x150x9	1.0	0.0161	0.0001	1.0	1.0	0.0	1.0
G3	CC250X25	0.5	0.0000	0.0052	0.5	0.0	0.2	0.5
G4	CHS89,1(3")x2,8	0.8	0.0000	0,0001	0.8	0.0	0.0	0.8
G5	CHS101,6(3.1/2")x3,2	0.7	0.0000	0.0202	0.7	0.0	0.8	0.8

The deflection limits: $H/100=0.08$ m; $L/240=0.104$ m

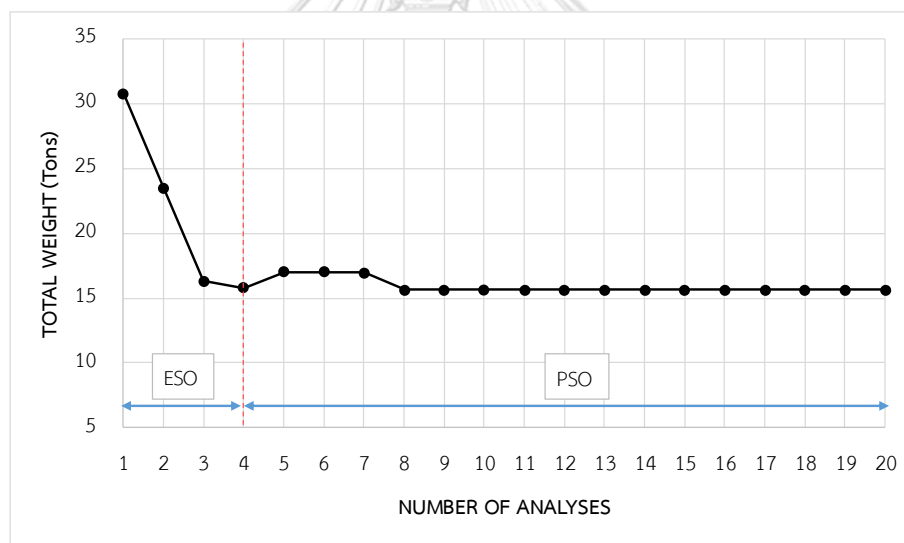


Fig . 5.6 Convergence history of arch warehouse structure with a 25-m span

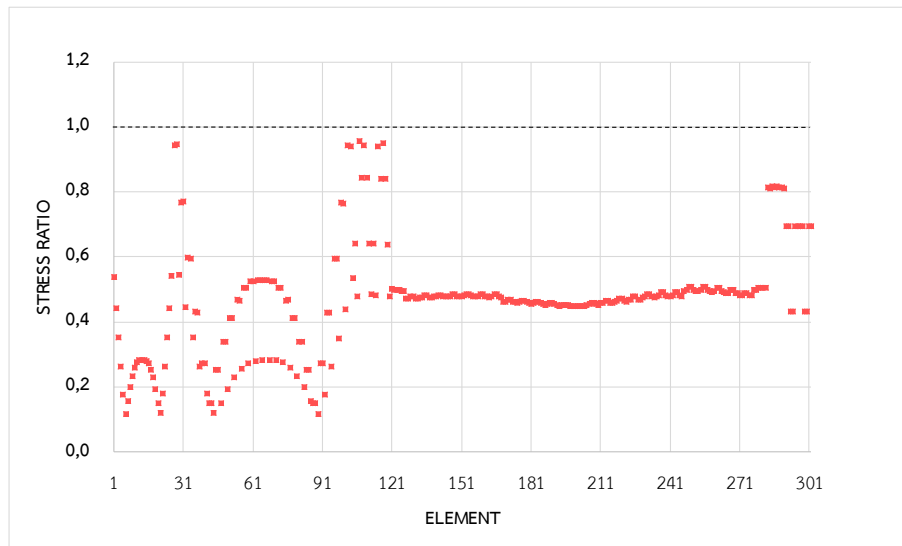


Fig . 5.7 Stress ratio for members with a 25-m span

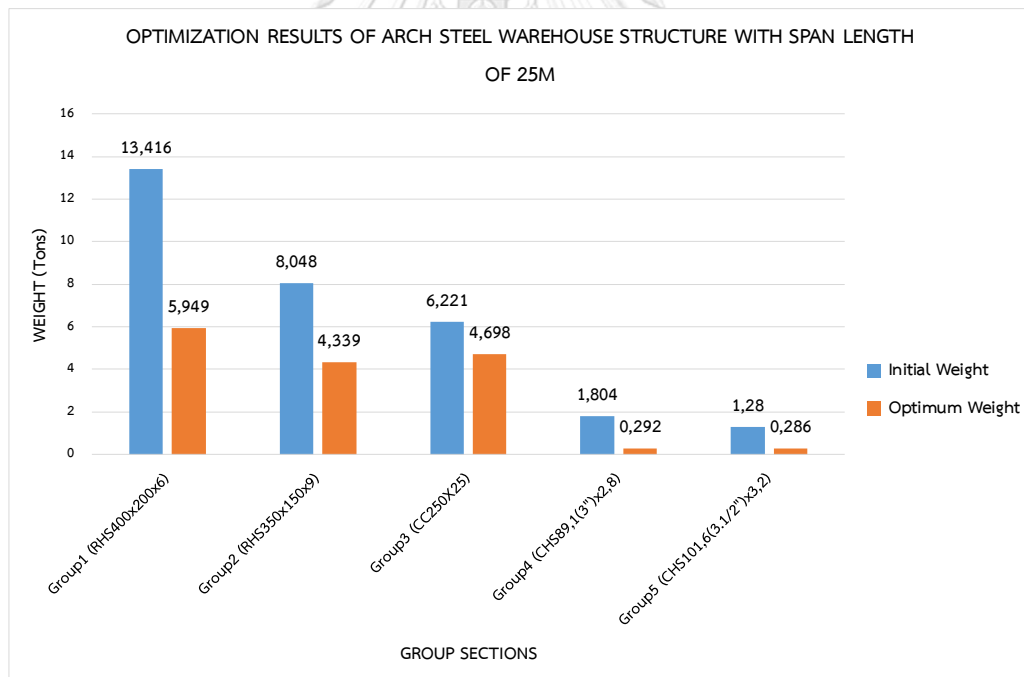


Fig . 5.8 Material distributed over an arch warehouse structure with a 25-m span

c) Optimization results of arch warehouse structures with a 30-m span

Table 5.3 Optimum sections obtained for arch steel warehouse with a 30-m span

Group	Name of Section	Ratio	Displacement X (m)	Displacement Z (m)	S_s	$S_{d(x)}$	$S_{d(z)}$	S_{Max} Group
G1	CHS406,4(16")x7,9	0.9	0.0000	0.0550	0.9	0.0	0.4	0.9
G2	RHS400x200x9	1.0	0.0190	0.0001	1.0	0.95	0.0	1.0
G3	CC250X25	0.5	0.0000	0.0052	0.5	0.0	0.2	0.5
G4	CHS76,3(2.1/2")x4	1.0	0.0000	0,0001	1.0	0.0	0.0	1.0
G5	CHS101,6(3.1/2")x3,2	0.7	0.0000	0.0202	0.7	0.0	0.8	0.8

Note: The deflection limits: $H/100=0.08$ m; $L/240=0.125$ m

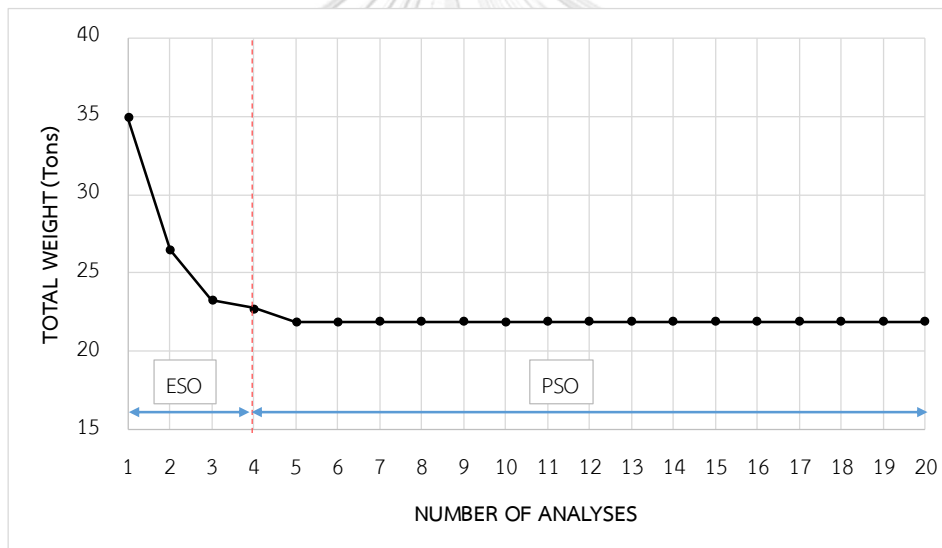


Fig . 5.9 Convergence history of arch steel warehouse with a 30-m span

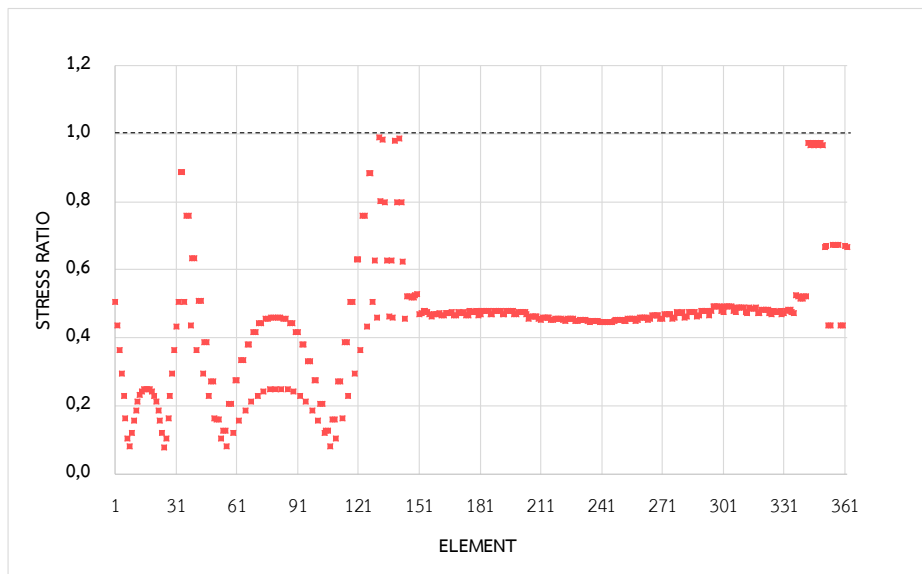


Fig . 5.10 Stress ratio for members with a 30-m span

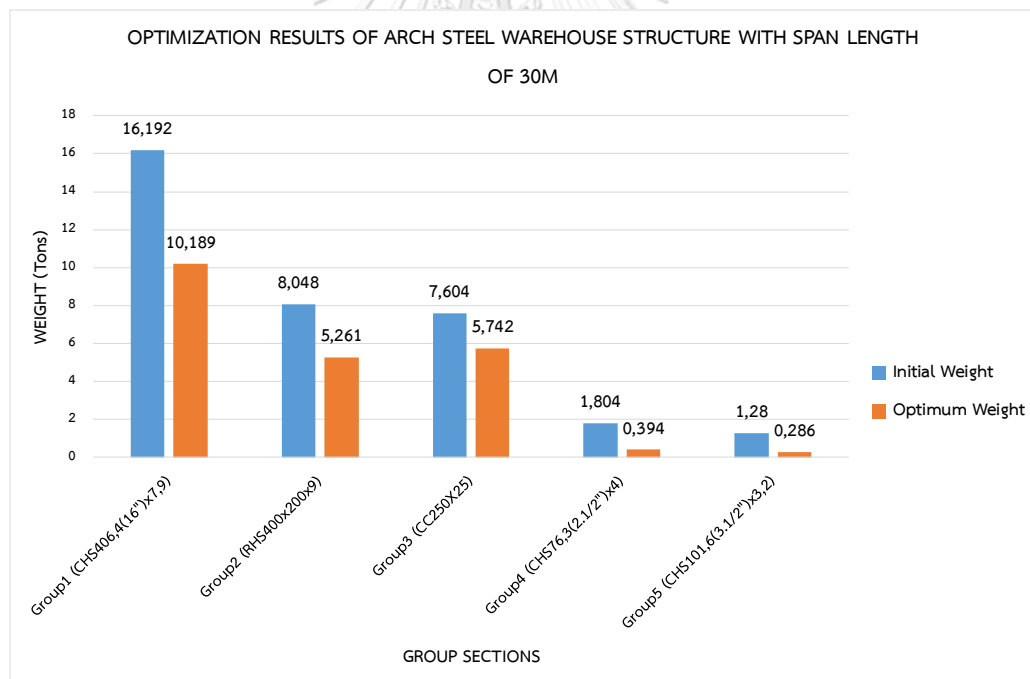


Fig . 5.11 Material distributed over an arch warehouse structure with a 30-m span

As already discussed in section 4.3.1, the proposed algorithm is divided into two separate phases. We can see that the convergence history of all three span lengths obtain the optimum solution after 20 iterations. The total weight of the optimum

solution is significantly less than 56% of the initial design weight for a 20-m span, 49% of the initial design weight for a 25-m span, 38% of the initial design weight for a 30-m span. All the maximum stress and the maximum displacement of each group were under the upper limit at the best solution. This indicates that the optimum design satisfied its given constraints.



CHAPTER 6

CONCLUSIONS AND FUTURE RESEARCH

6.1 Conclusions

A number of conclusions can be drawn from this research effort as follows

1. The novel algorithm adopts two-step optimization processes. The first step is the preliminary design using the ESO algorithm. The ESO provides good initial points by eliminating those infeasible design domains, and hence reduces the sizes of discrete variable entries prior to performing the PSO search in the final step. The PSO as an enhancement helps the ESO process not only to accelerate the speed of convergence but also to efficiently reach the optimum or near optimum solution.
2. The procedure of the mixed ESO-PSO is very simple to program via the interaction between computational languages and finite element analysis (FEA) packages by direct OAPI communication. The OAPI functions can help to access the model and control all of the analysis and design from (FEA) packages easily as well as input data and output data at each iteration.
3. Both of the ESO and mixed ESO-PSO algorithms were separately demonstrated the accuracy in finding the optimum design by testing on a benchmark steel frame. Therein, the ESO has a larger computational time than the mixed ESO-PSO which exhibited in general performance in terms of convergence speed. In addition, the optimization results are compared to those of some well-known meta-heuristics. The results obtained by the present algorithms is the same or lighter than all other reported results.
4. In the mixed ESO-PSO approach, the param of the PSO algorithm have to be fine-tuned carefully, based on the experience of the designers. The selection of the PSO algorithm plays an important role. In general, a bad selection of these param can lead to a poor result as well as easily entrap into near-optimum solutions (local solutions), especially in case of high nonlinearity and widely separated allowable discrete values.

5. The optimum design of arch steel warehouse structures obtained after a few iterations with considering simultaneously strength and serviceability conditions comply with AISC-LRFD and AISI-LRFD specifications under applied forces. The mixed ESO-PSO approach is incorporated with the advanced analysis, namely large (i.e., second-order nonlinear geometry) deformations. As already observed, the total weight of the optimum solution is significantly less than the initial design weight. To sum up, the optimization results showed that the mixed ESO-PSO is an efficient and robust technique for discrete structural optimizations.

6.2 Future Researchs

In addition to the work carried out in this thesis, recommendations for future research include the following:

1. The “Direct analysis method” may also need to apply for all range of second-order effects without restrictions. This method especially ignores the need for calculation of the effective length factor, K , to avoid confusion for practical design of complex steel structures.
2. A hybrid version of the proposed algorithm can be developed to enhance the accuracy and the speed of convergence.
3. Application of the proposed method to topology and sizing optimization such as optimum design of strut and tie models should be conducted.
4. A dynamic analysis can be included in design optimization for high-rise building subjected to seismic loads, for example, optimum design of bracing systems for multistorey steel frames under earthquake loads.
5. For the structures with semi-rigid connections, an optimization process can be carried out on different types of connections to find the best param, such as plate dimensions and the bolt diam.

REFERENCES



จุฬาลงกรณ์มหาวิทยาลัย
CHULALONGKORN UNIVERSITY

REFERENCES

- American Institute of Steel Construction, 2016. Specification for Structural Steel Buildings. American National Standard ANSI/AISC 360-16, 620 pages.
- AISC, L. (2001). Manual of steel construction, load and resistance factor design: American Institute of Steel Construction Chicago, IL.
- AISI S100-2016 North American Specification for Design of Cold-Formed Steel Structural Members, American Iron and Steel Institute, 2016 Edition.
- Al-Bermani, F. G., & Kitipornchai, S. (1990). Nonlinear analysis of thin-walled structures using least element/member. *Journal of Structural Engineering*, 116(1), 215-234.
- American Iron and Steel Institute "AISI Manual Cold-Formed Steel Design 2002 Edition.
- Arora, J. S. (2000). Methods for discrete variable structural optimization *Advanced Technology in Structural Engineering* (pp. 1-8).
- ASCE/SEI 7-10 Minimum Design Loads for Buildings and Other Structures, Structural Engineering Institute.
- Bathe, K. J., & Bolourchi, S. (1979). Large displacement analysis of three-dimensional beam structures. *International Journal for Numerical Methods in Engineering*, 14(7), 961-986.
- Bathe, K. J., Ramm, E., & Wilson, E. L. (1975). Finite element formulations for large deformation dynamic analysis. *International Journal for Numerical Methods in Engineering*, 9(2), 353-386.
- Camp, C., Pezeshk, S., & Cao, G. (1998). Optimized design of two-dimensional structures using a genetic algorithm. *Journal of Structural Engineering*, 124(5), 551-559.
- Camp, C. V., Bichon, B. J., & Stovall, S. P. (2005). Design of steel frames using ant colony optimization. *Journal of Structural Engineering*, 131(3), 369-379.
- Carbas, S. (2016). Design optimization of steel frames using an enhanced firefly algorithm. *Engineering Optimization*, 48(12), 2007-2025.

- Carraro, F., Lopez, R. H., & Miguel, L. F. F. (2017). Optimum design of planar steel frames using the Search Group Algorithm. *Journal of the Brazilian Society of Mechanical Sciences and Engineering*, 39(4), 1405-1418.
- Coello, C. A. C. (2002). Theoretical and numerical constraint-handling techniques used with evolutionary algorithms: a survey of the state of the art. *Computer methods in applied mechanics and engineering*, 191(11-12), 1245-1287.
- Conci, A. (1992). Stiffness matrix for nonlinear analysis of thin-walled frames. *Journal of engineering mechanics*, 118(9), 1859-1875.
- Chu, D. N., Xie, Y., Hira, A., & Steven, G. (1996). Evolutionary structural optimization for problems with stiffness constraints. *Finite Elements in Analysis and Design*, 21(4), 239-251.
- Degertekin, S. (2008). Optimum design of steel frames using harmony search algorithm. *Structural and multidisciplinary optimization*, 36(4), 393-401.
- Degertekin, S. (2012). Improved harmony search algorithms for sizing optimization of truss structures. *Computers & structures*, 92, 229-241.
- Doğan, E., & Saka, M. P. (2012). Optimum design of unbraced steel frames to LRFD-AISC using particle swarm optimization. *Advances in Engineering Software*, 46(1), 27-34.
- Dumonteil, P. (1992). Simple equations for effective length factors. *Eng J AISC*, 29(3), 111-115.
- Eberhart, R., & Kennedy, J. (1995). Particle swarm optimization, proceeding of IEEE International Conference on Neural Network. *Perth, Australia*, 1942-1948.
- Farreyre, A., & Journot, J.-B. (2005). Timber trussed arch for long span.
- Farshchin, M., Maniat, M., Camp, C. V., & Pezeshk, S. (2018). School based optimization algorithm for design of steel frames. *Engineering Structures*, 171, 326-335.
- Fourie, P., & Groenwold, A. A. (2002). The particle swarm optimization algorithm in size and shape optimization. *Structural and multidisciplinary optimization*, 23(4), 259-267.

- Gandomi, A. H., Yang, X.-S., & Alavi, A. H. (2013). Cuckoo search algorithm: a metaheuristic approach to solve structural optimization problems. *Engineering with computers*, 29(1), 17-35.
- Hasançebi, O., & Azad, S. K. (2012). An exponential big bang-big crunch algorithm for discrete design optimization of steel frames. *Computers & structures*, 110, 167-179.
- Hasançebi, O., Erdal, F., & Saka, M. P. (2009). Adaptive harmony search method for structural optimization. *Journal of Structural Engineering*, 136(4), 419-431.
- He, S., Prempain, E., & Wu, Q. (2004). An improved particle swarm optimizer for mechanical design optimization problems. *Engineering Optimization*, 36(5), 585-605.
- Kang, Y. J., & Yoo, C. H. (1994). Thin-walled curved beams. II: analytical solutions for buckling of arches. *Journal of engineering mechanics*, 120(10), 2102-2125.
- Kaveh, A., & Bakhshpoori, T. (2013). Optimum design of steel frames using Cuckoo Search algorithm with Lévy flights. *The Structural Design of Tall and Special Buildings*, 22(13), 1023-1036.
- Kaveh, A., & Ghazaan, M. I. (2017). Optimum design of skeletal structures using PSO-Based algorithms. *Periodica Polytechnica Civil Engineering*, 61(2), 184-195.
- Kaveh, A., & Shojaee, S. (2007). Optimal design of skeletal structures using ant colony optimization. *International Journal for Numerical Methods in Engineering*, 70(5), 563-581.
- Kaveh, A., & Talatahari, S. (2009). A particle swarm ant colony optimization for truss structures with discrete variables. *Journal of Constructional Steel Research*, 65(8-9), 1558-1568.
- Kaveh, A., & Talatahari, S. (2010). An improved ant colony optimization for the design of planar steel frames. *Engineering Structures*, 32(3), 864-873.
- Kaveh, A., & Talatahari, S. (2012). Charged system search for optimal design of frame structures. *Applied Soft Computing*, 12(1), 382-393.
- King, W. (1990). Simplified second-order inelastic analysis for frame design.
- Kostina, E. (2017). Constructive solutions of a sport complex roof structure.

- Li, Qing Steven, & Grant P Xie, Y. (2000). Evolutionary structural optimization for stress minimization problems by discrete thickness design. *Computers & structures*, 78(6), 769-780.
- Li, L., Huang, Z., & Liu, F. (2009). A heuristic particle swarm optimization method for truss structures with discrete variables. *Computers & structures*, 87(7-8), 435-443.
- Li, L., Huang, Z., Liu, F., & Wu, Q. (2007). A heuristic particle swarm optimizer for optimization of pin connected structures. *Computers & structures*, 85(7-8), 340-349.
- MBMA-2012 Metal building Manufacturers Association, Base on the 2012 IBC and ASCE 7-10.
- MacCrimmon, R. (2005). *Guide for the Design of Crane Supporting Steel Structures*: Quadratone Graphics.
- Manickarajah, D., Xie, Y., & Steven, G. (2000). Optimum design of frames with multiple constraints using an evolutionary method. *Computers & structures*, 74(6), 731-741.
- Marini, F., & Walczak, B. (2015). Particle swarm optimization (PSO). A tutorial. *Chemometrics and Intelligent Laboratory Systems*, 149, 153-165.
- Murren, P., & Khandelwal, K. (2014). Design-driven harmony search (DDHS) in steel frame optimization. *Engineering Structures*, 59, 798-808.
- Nha, C. D., Xie, Y., & Steven, G. (1998). An evolutionary structural optimization method for sizing problems with discrete design variables. *Computers & structures*, 68(4), 419-431.
- Perez, R. L., & Behdinan, K. (2007). Particle swarm approach for structural design optimization. *Computers & structures*, 85(19-20), 1579-1588.
- Pezeshk, S., Camp, C., & Chen, D. (2000). Design of nonlinear framed structures using genetic optimization. *Journal of Structural Engineering*, 126(3), 382-388.
- Plevris, V., Batavanis, A., & Papadrakakis, M. (2011). Optimum design of steel structures with the Particle Swarm Optimization method based on EC3. *Computational Methods in Structural Dynamics and Earthquake Engineering*.

- Plevris, V., & Papadrakakis, M. (2011). A hybrid particle swarm—gradient algorithm for global structural optimization. *Computer-Aided Civil and Infrastructure Engineering*, 26(1), 48-68.
- Phan, D. T., Lim, J. B., Tanyimboh, T. T., & Sha, W. (2017). Optimum design of cold-formed steel portal frame buildings including joint effects and secondary members. *International Journal of Steel Structures*, 17(2), 427-442.
- Saka, M. P., & Geem, Z. W. (2013). Mathematical and metaheuristic applications in design optimization of steel frame structures: an extensive review. *Mathematical problems in engineering*, 2013.
- SAP, V. 19 (2017). CSI analysis reference manual. *Computers and Structures Inc., Berkeley, California, USA*.
- Schutte, J., & Groenwold, A. (2003). Sizing design of truss structures using particle swarms. *Structural and multidisciplinary optimization*, 25(4), 261-269.
- Shi, Y., & Eberhart, R. (1998). *A modified particle swarm optimizer*. Paper presented at the Evolutionary Computation Proceedings, 1998. IEEE World Congress on Computational Intelligence., The 1998 IEEE International Conference on.
- Shi, Y., & Eberhart, R. C. (1998). *Parameter selection in particle swarm optimization*. Paper presented at the International conference on evolutionary programming.
- Steven, G., Querin, O., & Xie, M. (2000). Evolutionary structural optimisation (ESO) for combined topology and size optimisation of discrete structures. *Computer methods in applied mechanics and engineering*, 188(4), 743-754.
- Tanskanen, P. (2006). A multiobjective and fixed elements based modification of the evolutionary structural optimization method. *Computer methods in applied mechanics and engineering*, 196(1-3), 76-90.
- Tangaramvong, S., & Tin-Loi, F. (2013). Automatic identification of the worst load combination for structural safety assessment using an optimization approach. *Engineering Structures*, 56, 2287-2298.
- Tangaramvong, S., & Tin-Loi, F. (2015). Optimal performance-based rehabilitation of steel frames using braces. *Journal of Structural Engineering*, 141(10), 04015015.

- Toğan, V. (2012). Design of planar steel frames using teaching–learning based optimization. *Engineering Structures*, 34, 225-232.
- Thompson, G. (2007). *Best practice of crane support structures design: an expert survey*. Stellenbosch: University of Stellenbosch.
- Venter, G., & Sobieszczanski-Sobieski, J. (2003). Particle swarm optimization. *AIAA journal*, 41(8), 1583-1589.
- White, D. W., & Hajjar, J. F. (1991). Application of second-order elastic analysis in LRFD: research to practice. *Engineering Journal*, 28(4), 133-148.
- Xie, Y. M., & Steven, G. P. (1993). A simple evolutionary procedure for structural optimization. *Computers & structures*, 49(5), 885-896.
- Xie, Y. M., & Steven, G. P. (1997). Basic evolutionary structural optimization *Evolutionary Structural Optimization* (pp. 12-29): Springer.
- Yang, Y.-B., & Chiou, H.-T. (1987). Rigid body motion test for nonlinear analysis with beam elements. *Journal of engineering mechanics*, 113(9), 1404-1419.
- Yang, Y.-B., & Kuo, S.-R. (1994). Theory and analysis of nonlinear framed structures.
- Yang, Y.-B., Kuo, S.-R., & Yau, J.-D. (1991). Use of straight-beam approach to study buckling of curved beams. *Journal of Structural Engineering*, 117(7), 1963-1978.
- Yang, Y.-B., & McGuire, W. (1986). Stiffness matrix for geometric nonlinear analysis. *Journal of Structural Engineering*, 112(4), 853-877.
- Yang, Y.-B., Yau, J.-D., & Leu, L.-J. (2003). Recent developments in geometrically nonlinear and postbuckling analysis of framed structures. *Applied Mechanics Reviews*, 56(4), 431-449.
- Ziemian, R. D. (2010). *Guide to stability design criteria for metal structures*: John Wiley & Sons.

VITA

NAME Thu Huynh Van

DATE OF BIRTH 6 July 1992

PLACE OF BIRTH Binh Dinh Province, Viet Nam

INSTITUTIONS ATTENDED University of Architecture Ho Chi Minh City, Vietnam
Chulalongkorn University, Thailand

HOME ADDRESS Binh Dinh Province, Viet Nam

PUBLICATION Thu H. V. and Sawekchai T. (2018). "An ESO-based approach for optimal design of steel structures", The AUN/SEED-Net Regional Conference in Civil Engineering (RCCE) 2018 in conjunction with The 4th International Conference on Sustainable Civil Engineering Structures and Construction Materials (SCESCM), Indonesia.

Thu H. V. and Sawekchai T. (2018). "A mixed ESO-PSO Approach for Optimal AISC-LRFD Design of Steel Structures", The Thirty-First KKHTCNN Symposium on Civil Engineering, November 22-24, 2018, Kyoto, Japan